Doctoral Dissertation

Study of Integrated Magnetic Components in Resonant DC-DC Converters

共振型 DC-DC コンバータの統合磁気部品に関する研究

DISSERTATION SUBMITTED TO DEPARTMENT OF ELECTRICAL ENGINEERING
AND COMPUTER SCIENCE SCHOOL OF ENGINEERING
NAGOYA UNIVERSITY
IN PARTIAL FULFILLMENT OF THE REQUIRMENTS FOR THE DEGREE OF
DOCTOR OF PHILOSOPHY
IN
ELECTRICAL ENGINEERING

MOSTAFA SALAHELDIN AHMED ABDALAZIZ NOAH
モスタファ サライデイン アハメド アブドウアラシズ ノア

August, 2019

In dedication to my mother and father

Acknowledgment

Getting a Ph.D. degree in electrical engineering is a milestone in my life and completing this thesis is the most significant academic challenge I have ever faced till now. Specifically, this Ph.D. degree is being pursued from a Japanese university. Moving from Egypt to Japan and being a Ph.D. student came along with moments of joy, uncertainty, challenges, and difficulties. It is hard to forget those who helped me to overcome these difficulties, those who gave me so much to remember. It is to them I owe my deepest gratitude.

I would like to thank Prof. Masayoshi Yamamoto for giving me the opportunity to join his lab and study under his supervision. He provided me with unlimited guidance and support whenever I needed throughout my Ph.D. program. Thanks for giving me the opportunity to work on interesting projects and collaborate with companies. Many thanks for making me a better researcher. Thanks for motivating me, for being very supportive, and for encouraging me the moments I was down. I'm truly indebted to him my whole life.

Prof. Jun Imaoka, words cannot express the favors that I owe to him. Thanks for all technical discussions, for the collaborative research that we conducted together, for supporting my life in Japan inside and outside the campus. Many thanks for being a close friend of mine.

Prof. Kazuhiro Umetani, I would like to thank him for the collaborative research that we conducted together. Thanks for discussing interesting research ideas together at Okayama University and during several international conferences. Thanks for encouraging and motivating me.

I would like to thank the examining committee Prof. Kazuo Shiokawa, Prof. Takeyoshi Kato, and Prof. Eiji Hiraki. I would like to thank them for the insightful comments they provided me to improve the quality of this thesis.

I would like to thank Shiori Idaka for giving me the opportunity to visit Mitsubishi Electric Europe during my Ph.D. course, and many thanks for providing me with many pieces of advice and supporting my future career.

I would like to thank the secretaries in our Lab. Megumi Yasuda, thank you for taking care the administrative process of my graduation, for handling all my business trips, for speaking to me in Japanese, intentionally, to help me improve my language skills. Also, I would like to express my gratitude to Sayuri Yamamoto, Tomomi Natsume, Ikuyo Miyake many thanks for helping and supporting me. Furthermore, I would like to thank assistant researcher Takashi Sawada who welcomed me in Nagoya and taught me a lot of aspects in the Japanese culture.

I would like to thank all my friends and Lab. Colleagues in Shimane and Nagoya. Special thanks to Prof. Wilmar Martinez, Prof. Kimihiro Nanamori, Dr. Hirokatsu Umegami, Fumiya Hattori, Yasuki Kanazawa, Dr. Shota Kimura, Prof. Taichi Kawakami, Tengfei Ou, Toshihiro Iwaki, Yuki Ishikura, Daisaku Mukaiyama, Dr. Koichi Shigematsu, Dr. Thilak Senanayake, Hongjing Zhang, Mamoru Sasaki, Yusuke Sugihara, Shun Endo, Freddy Velandia, Tomohide Shirakawa, Masataka Ishihara, Daigoro Ebisumoto, Toshikazu Harada, Hiroki Ishibashi, and Tatsuya Aoki.

This thesis is dedicated to my mother and father, still I would like to thank them again, also many thanks to my brother and sisters Mohamed, Dalia, Dina, Miral and my lifelong friends Haitham and Hossam for their unconditional love and support.

Abstract

The importance of isolated DC-DC power converters is growing along with the growth of the market of “transportation electrification”, such as More Electric Aircraft (MEA) and Electric Vehicles (EV). Within various topologies of isolated DC-DC converter, the LLC resonant converter is widely popular due to its merits, such as: The capability of the primary switches to achieve zero voltage switching (ZVS) and the feasibility of integrating one transformer and one inductor into a single magnetic core. Nonetheless, adapting single phase LLC resonant converter in high power applications comes with some drawbacks. Since the current ripple stress on the output capacitor becomes severely high to handle, and hence, a large size output smoothing capacitor is needed to compensate the high output current ripples. In this regard, three-phase topologies have gained more attention, since they possess many advantages over the single phase ones. For instance, the three-phase configuration lessens circuit current per phase to 1/3 of the total current in an equivalent single-phase topology. Therefore, the output current ripples can be reduced. Nevertheless, the three-phase topology might present some drawbacks due to the need of adapting three magnetic cores, in which, adding to the power converter more weight, size (footprint) and cost. In the development of the power conversion circuits, designers tend to adapt the techniques which downsize the circuit and improve its efficiency.

The research conducted in this thesis is concerned about keeping the converter with high-power density and high-efficiency. Integrated magnetics was used as an approach to increase the converter power density, especially in the three-phase LLC resonant converter, by integrating the resonant and magnetizing inductances of the three phases into a single core.

Another drawback regarding the three-phase LLC converter is the current unbalance between the paralleled phases, which arises because the values of the parameters are never exactly the same. The sources of the unbalance are well-investigated and a simple solution is proposed to tackle the unbalanced current which deteriorates the converter efficiency.

Another issue had been investigated is that in the literature it was always assumed that the transformer primary leakage inductance equals the secondary leakage inductance. In this thesis, it had been disclosed that this assumption is not accurate. Furthermore, the effects of the secondary leakage inductance on the operation of the LLC resonant converter had been investigated.

The discussion presented in this thesis proposes a novel three-phase integrated transformer which allow for a mass downsizing of 28% and an approximate cost reduction of %16 have been attained by utilizing the integrated transformer, in comparison to its three-discrete counterparts presented in the state of the art (as in the three-phase DC-DC converter of TESLA Model 3). Another contribution in this thesis is proposing current balancing transformer to tackle the current unbalance. The proposed technique is very simple and easy to be implemented compared with the complicated active control techniques exist in the literature (as in the three-phase DC-DC converter of TESLA Model 3).

Furthermore, it has been revealed for the first time in this thesis that unbalanced magnetic leakage distribution in the transformer primary and secondary sides can be realized by allocating the primary winding in the vicinity of the air gap and placing the secondary winding in a close contact with the magnetic core to minimize the magnetic leakage flux originated from the primary winding and maximize the leakage flux originated from the secondary. The value of the secondary leakage inductance was intentionally controlled to investigate its influence on the converter efficiency and frequency control bandwidth. Compared with the existing LLC converter presented in the literature, a transformer with concentrated secondary leakage inductance has a better efficiency and a wider frequency control bandwidth.

With the constant increase in the EV auxiliary system electric loads, the future direction is to realize high power isolated DC-DC converter (more than 3kW) and to realize high power density to keep more space for human and to keep the vehicle light to enhance the efficiency of the fuel consumption.

To summarize, this thesis addresses the challenges of magnetics in the LLC resonant converter. With the academic contribution in this thesis, the cost and footprints of the magnetics of the three-phase converter can be reduced by applying the proposed three-phase integrated transformer, and the balancing transformer to tackle the current unbalance. Furthermore, the efficiency can be improved with proper design of the secondary leakage inductance. This thesis will help the industry engineers and power electronics researchers to design an LLC resonant converter with high efficiency, high-power density and reduce the cost for the converter used in EVs and MEA.

Chapter 1 : Introduction

1.1 Social Background 1

1.2 Transportation Electrification 1

1.3 LLC Resonant Converter 3

1.4 Thesis Contents 6

References 8

Chapter 2 : Lagrangian Dynamics of the Three-phase Integrated Transformer in Three-phase LLC Resonant Converter 9

2.1 Introduction 9

2.1.1 Research Motivation : Lagrangian Dynamics 9

2.1.2 Lagrangian Dynamics- Literature review 9

2.1.3 Chapter contents 11

2.2 Developing the Lagrangian Models 11

2.2.1 Lagrangian Example: Basic Transformer 12

2.2.2 Lagrangian Model of the Proposed Integrated Transformer 13

2.3 Energy Equivalency 15

2.4 Theoretical Discussion 17

2.5 Practical Implementation of Transformer 18

2.5.1 System Description 18

2.5.2 Volume and weight comparison 19

2.5.3 Cost 19

2.5.3 Simulation and Experimental Results 19

2.6 Summary 22

References 23

Chapter 3 : Magnetic Design and Experimental Evaluation of Three-phase Integrated transformer in Three-phase LLC Resonant Converter 24

3.1 Introduction 24

3.1.1 Research Motivation : Integrated Transformer 24

3.1.2 Challenges of implementing multi-phase LLC resonant topologies 25

3.1.3 Magnetic integration in LLC converter- Literature review 26

3.1.4 Chapter contents 27

3.2 Three-phase LLC Integrated Transformer 28

3.2.1 Magnetic Analysis 28

3.2.2 Flux Density Equations 30

3.3 Design Example 34

3.4 Simulation Tests, Experimental Evaluation and Power Losses Distribution 37

3.4.1 FEA Simulation 37

3.4.2 Experimental Environment and Results 38

3.4.3 Efficiency 39

3.4.4 Thermal Performance 40
3.4.5 Volume, weight and Cost Comparison between integrated and discrete transformers 42
3.4.5 Power loss distribution 42
3.5 Summary 44
3.6 Appendix 44
References 46
Chapter 4 : Current Balance Mechanism in Three-phase LLC Resonant Converter 49
4.1 Introduction 49
4.1.1 Research Motivation : Current Balance Mechanism 49
4.1.2 Current Unbalance in Three-phase LLC Resonant converter- Literature Review 50
4.1.3 Chapter contents 52
4.2 Three-phase LLC with Spatial Integrated Transformer 53
4.3 Current Balance Evaluation Using Single Balancing Transformer 55
4.4 Equivalent Circuits of Different Topologies 58
4.4.1 Paralleled non-coupled three transformers 58
4.4.2 Parallel connection integrated transformer 58
4.4.3 Star connected non-coupled three transformers 59
4.4.4 Integrated transformer with a current balance transformer 59
4.5 Simulation and Experimental Evaluation 61
4.5.1 Evaluation Considering Uneven Leakage and Magnetizing Inductances 61
4.5.2 Conventional parallel connection for the transformer 62
4.5.3 Utilizing the balancing transformer 62
4.5.4 Connecting the transformer in star 64
4.5.5 Further Evaluation Considering Other Sources of Unbalance 66
4.5.6 Design Procedures 67
4.6 Summary 67
4.7 Appendix 70
References 71
Chapter 5 : Effects of Secondary Leakage Inductance on the LLC Resonant Converter 73
5.1 Introduction 73
5.1.1 Research Motivation : Secondary Leakage Inductance 73
5.1.2 Secondary Leakage Inductance - Literature Review 74
5.1.3 Chapter contents 76
5.2 Transformer Structure with Concentrated Leakage on Secondary-side 76
5.3 Extracting the Transformer Parameters and Calculating the Coupling Factor 79
5.4 T-Model and Voltage Gain of Gapped Transformer 82
5.4.1 Equivalent circuit and voltage equations 83
5.4.2 Transformer Voltage Gain 84
5.5 Frequency Control Bandwidth with respect to Load Variation 85

5.6 Experimental and Simulation Evaluation 87
5.6.1 Experimental set-up 88
5.6.2 Transformer voltage Gain and LLC converter 89
5.6.3 Efficiency of LLC converter and power loss analysis 89
5.6.4 Maximum flux density 92
5.6.5 Frequency Control Bandwidth- experimental waveforms 94
5.7 Summary 94
5.8 Appendix 95
5.8.1 Interleaving and high frequency operations on leakage inductance 96
5.8.2 Effects of core size on the leakage inductance 96
5.8.3 Measurement of Self-Resonant Frequency (SRF) of the Primary Winding 97
References 98
Chapter 6 : Conclusion 100
6.1 Summary of each Chapter 100
6.2 Overall Contribution of Thesis 101
6.3 Future Challenges 101
List of Publications 103

Chapter 1: Introduction

1.1 Social Background

Worldwide transportation consumes about 66% of oil supply and produces a lot of carbon dioxide emissions [1]-[4]. It is predicted that by 2050 the energy budget and emissions of Carbon dioxide (CO_2) of the transportation industry will increase by 80% [2]. In order to address global environmental concerns, the Intergovernmental Panel on Climate Change has targeted a reduction in CO_2 emissions of at least 50% by 2050 [2].

On the other hand, air pollution is another concern in a developing country like Egypt, where there has been continuous public concern related to the degradation of air quality in the major cities and, in particular, in Cairo. This concern was sparked by the occurrence of a "Black Cloud" appearing in the skies of the capital around 1999. in Cairo, the capital of Egypt, where more than 12 million people live. Cairo has a very poor factor because of lack of rain and its layout of tall buildings and narrow streets, which create a bowl effect (bad ventilation and consequent trapping of pollutants). The most notable sources of the CO_2 in streets is due to the excess amount of cars exhaust [5]-[8]. The typical sources of pollution in Egypt is shown in Fig.1.1.

Transportation Electrification is an alternative option to deal with these environmental problems not only in Egypt but all around the world, because a substantial cut in emissions from transportation, including the cars and aircrafts, is necessary to reduce carbon dioxide emissions and thereby to prevent the global warming. Recently, there has been a lot of efforts had been done to develop Electric-based technologies in the transportation. Including both Electric vehicles (EV) and More Electric Aircraft (MEA).

1.2 Transportation Electrification

Electric vehicles are becoming more popular and now several manufacturing companies are competing to provide the best model for the customers. For instance, now there are three different electric-based technologies as follow: (i) Pure EVs such "Nissan LEAF" and "Mitsubishi i-MiEV". (ii) Hybrid Electric Vehicles (HEVs) such as "Toyota Prius" and "Ford Escape Hybrid". (iii)

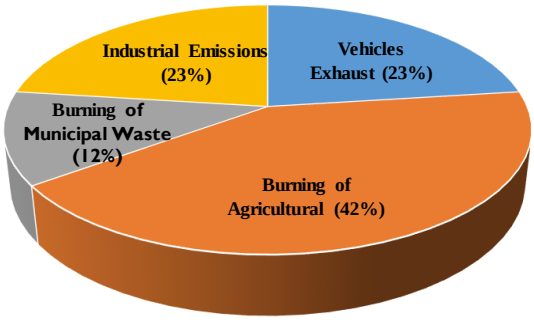

Fig. 1.1 Typical sources of air pollution in Egypt [5].

Plug-in Hybrid Vehicles (PHEVs) such as “Chevrolet Volt” and “Ford C-Max”. Furthermore, based on the charging/discharging capability of EVs and the requirement of power grid, the vehicle-to-home (V2H) and vehicle-to-grid (V2G) concepts have become more and more attractive in recent years and will turn into reality in the near future [9]. Actually, V2H and V2G enable EVs to not only serve as a transportation tool but also to act as controllable loads and distributed sources for the power grid, as shown in Fig.1.2 These new technologies involve power electronics converters to interface the grid with the vehicle’s battery.

On the other hand, from one manufacture to another, the power train of the vehicle configuration varies. Within the power train, DC-DC converter is required to step-up the voltage level to provide power to Electric Power Steering (EPS) drive system. Furthermore, another isolated DC-DC converter is implemented to step down the battery voltage to a lower voltage suitable for the auxiliary systems (usually 12V or 48V). For the keeping human living space and high fuel efficiency, the isolated dc-dc converter has to obtain compact and light weight performance in the EV and HEV applications. As an example, the power train of Toyota Prius is depicted in Fig.1.3.

At the same way, the aviation sector is responsible for approximately 20% of global transport emissions [2].

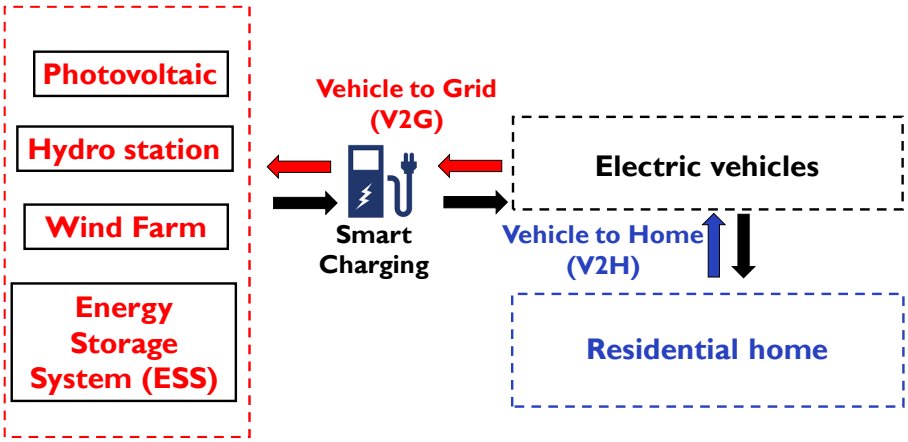

Fig. 1.2 Integration of the EV in grid.

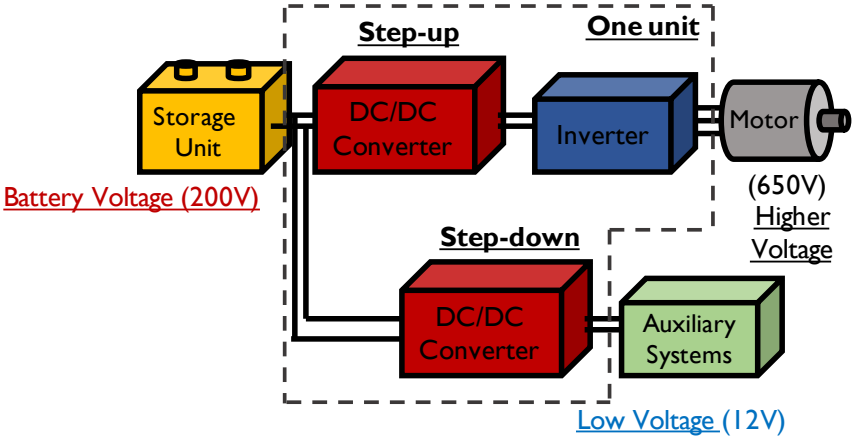

Fig. 1.3 Power train of Toyota Prius 3rd generation.

In order to reduce this impact and to improve fuel consumption efficiency, big aviation corporations such as Airbus and Boeing have been investing significant money and efforts in the direction of MEA [4]. In the MEA, the purpose is to eliminate the use of pneumatic, hydraulic, and mechanical systems and replace them with electrical systems. The main motivations behind this move to electrical power can be summarized as follows [4]:

1. Reduced system weight. Electrical systems are often much lighter than hydraulic systems due to the absence of hydraulic fluids.
2. Ease of maintenance. About 75% of late flights are due to system faults. Electrical systems are much faster and easier to be replaced than most pneumatic, hydraulic, and mechanical systems.
3. Increased engine efficiency.
4. Reduction of engine use on ground. When used to maneuver the aircraft on-ground, aircraft engines are incredibly inefficient due to low airflow and power demands vastly below their design point.

In that direction, Boeing made the MEA's first commercial flight known as “Boeing 787 Dreamliner”. However, Boeing batteries suffered from overheating as reported in [10]. As a result, Boeing has recently come-up with a comprehensive set of solutions that can result in a safer battery powered system [11]. Airbus has also produced the all-electric E-Fan 1.0 and hybrid E-Fan 1.2, which combined a 60 kW motor with a combustion engine. Their next mission is to develop E-Fan X. The E-Fan X will be a comparatively huge step forward to replace one of four gas turbines on a flying testbed with a 2 MW electric motor [12].
The generation and distribution voltage in these advanced aircraft is mainly ±270V DC with 230V variable frequency AC and 28V DC distribution for low power loads [13]- [16]. Hence, the electric source not only supplies the energy storage system, avionics and auxiliary loads, but also the actuators for flight control surface, landing gear, de-icing systems and the engines’ starter/generator [17]- [18]. All these devices are connected through power converters: Inverters, rectifiers and DC-DC converters. In this kind of power electronic systems specific features are needed such as: electromagnetic compatibility (EMC), efficiency, size, weight, harsh environment and isolation [10]. The latter characteristic is necessary for safety and reduction of EMC current [19]. This isolation function is usually made with high frequency transformer, included in power electronic converter.

1.3 LLC Resonant Converter

As mentioned in the previous section, it is very important to realize high-efficiency and high-power density in a converter used in EV or MEA. In order to achieve high-efficiency, it is recommended to implement a resonant topology to reduce the switching losses, because hard-switching converters suffers from a deteriorated efficiency, especially at high frequency. Fig.1.4 shows several approaches to realize high power density, such as magnetic integration, operating the converter at high-frequency (to downsize the energy storage components), and to select a suitable circuit topology. One of the most popular isolated DC-DC circuit topologies suitable for such applications is the LLC resonant converter and it is the converter under study in this thesis.

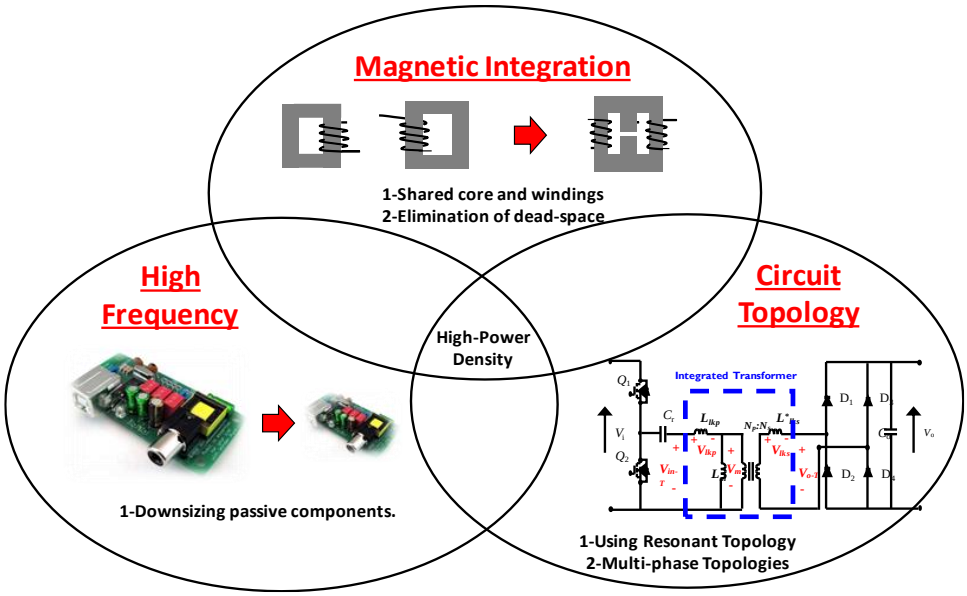

Fig. 1.4 Several approaches to realize high-power density.

Resonant converters are a type of electric power converter that contains a network of inductors and capacitors called a "resonant tank", tuned to resonate at a specific frequency. The resonant converters are able to work at high frequency operation because of their low switching losses. They all operate in essentially the same way: A square pulse of voltage or current generated by the power switches is applied to a resonant circuit. These resonant converters regulate their output voltage by changing the frequency of the driving voltage such that the impedance of the resonant circuit changes.

Among resonant converters, the LLC resonant converter has many additional benefits over conventional resonant converters. For example, it can regulate the output over wide line and load variations with a relatively small variation of switching frequency, while maintaining excellent efficiency. It can also achieve zero voltage switching (ZVS) over the entire operating range [20]. The circuit configuration of the LLC resonant converter is shown in Fig.1.5.

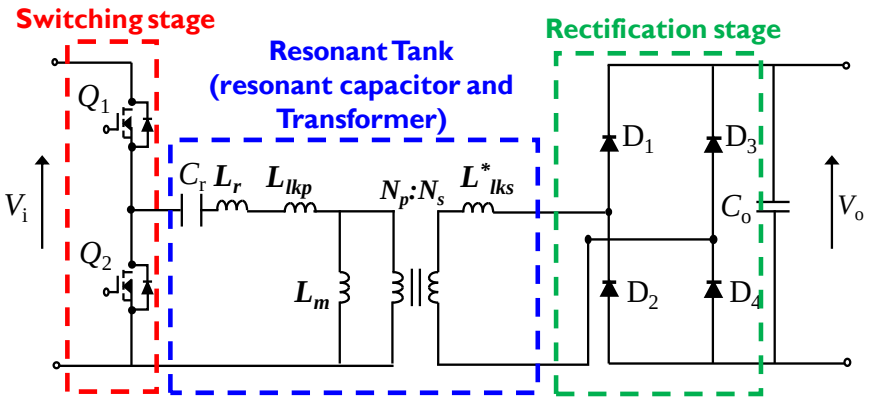

Fig. 1.5 LLC resonant converter.

The LLC resonant converter consists of three stages:

1. Switching bridge: usually MOSFETs are used to form a square wave generator. The driving switches Q_1 and Q_2, operate with alternating 50% duty cycles for each switch. A small dead time is needed between the transitions, both to prevent the possibility of cross-conduction and to allow for zero voltage switching (ZVS) operation.
2. The resonant tank: consists of the resonant capacitance (C_r), the series resonant inductance (L_r) and the transformer's magnetizing inductance (L_m). The transformer's leakage and magnetizing inductance is usually utilized in the resonant tank. Furthermore, the transformer provides both electrical isolation and the proper turns ratio to deliver the required voltage level to the output.
3. Rectification stage: to convert AC input to DC output and supply the load. The output capacitor smooths the rectified voltage and current.

Recently many companies are developing the LLC resonant converter to realize both of high-efficiency and high-power density. For example, one of the converters available in the market is a 200kHz, 340V-170V/200W LLC resonant converter. The converter is shown in Fig.1.6. This converter is developed to provide power to the sockets under seats and the entertainment system in the aircraft, as shown in Fig.1.7.

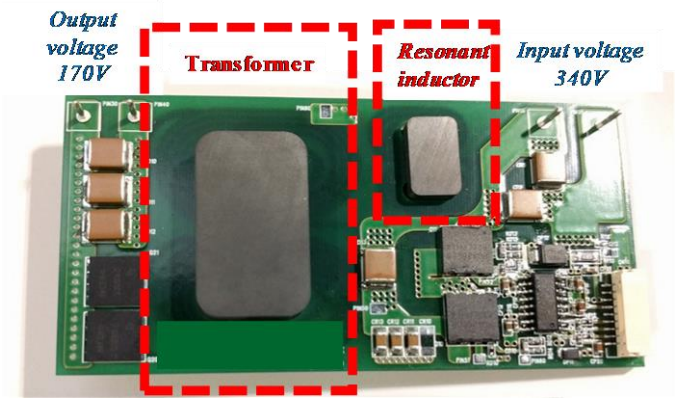

Fig. 1.6 Commercialized LLC resonant converter.

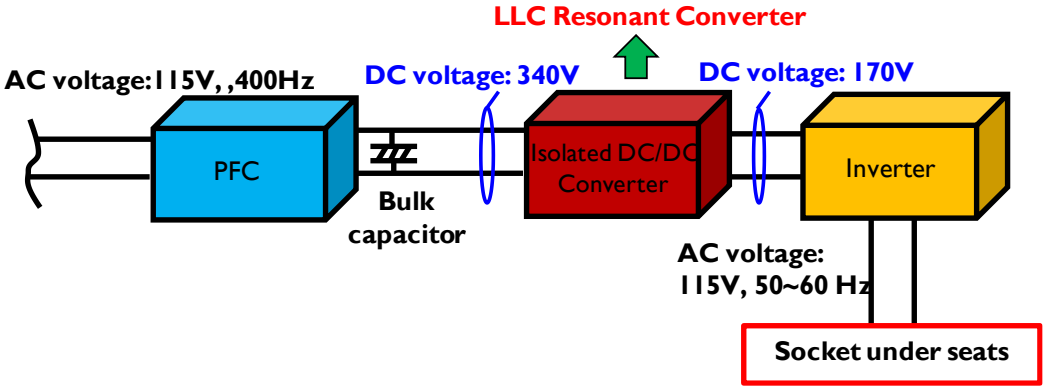

Fig. 1.7 One of the applications of LLC resonant converter in the aircraft system.

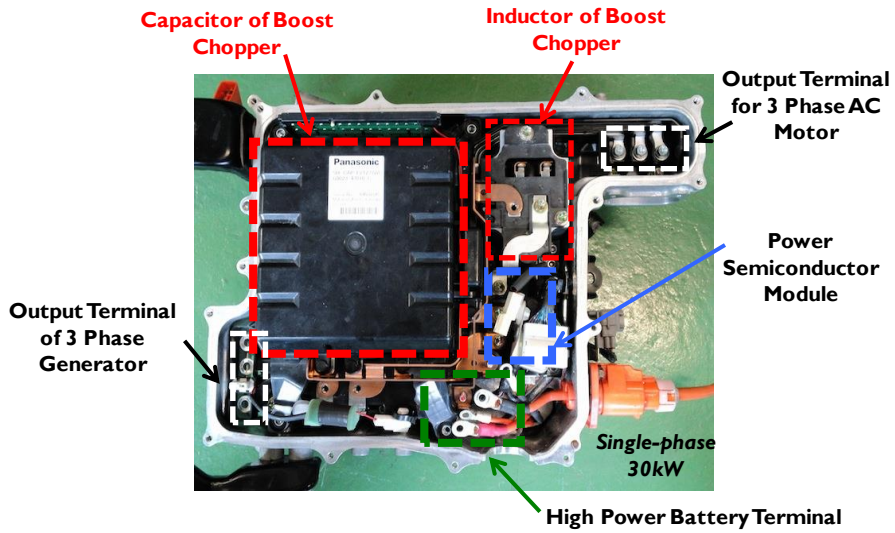

Fig. 1.8 Power control unit PCU for Toyota Prius 2nd Generation.

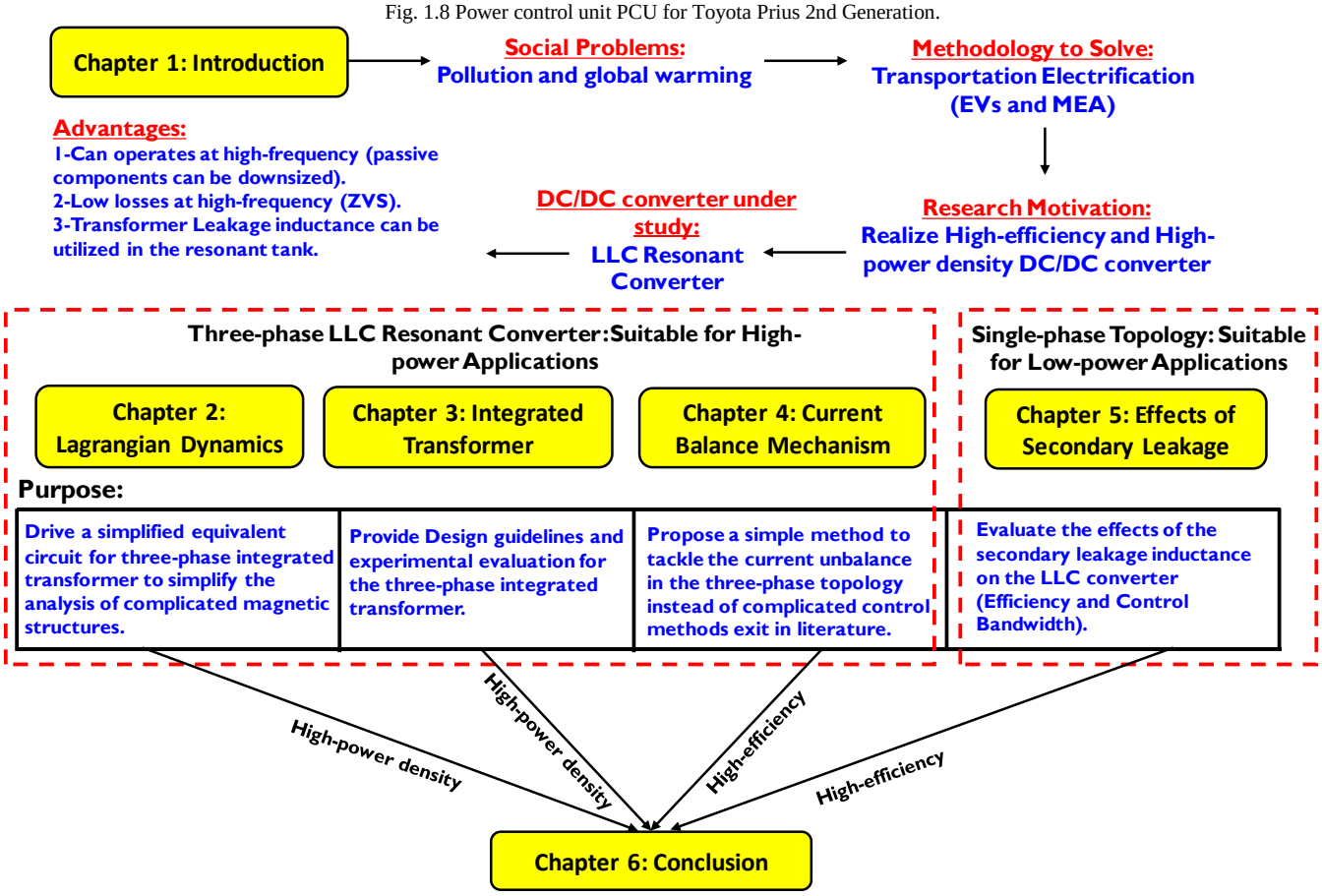

Fig. 1.9 Conceptual diagram showing the purpose and contents of the thesis.

1.4 Thesis Contents

The research done in this thesis is concerned about realizing high-power density and high-efficiency. It is well-known that the passive components (energy storage components) of the converter usually occupy large size (footprint). This can be noticed in the Power Control Unit (PCU) of Toyota Prius 2nd Generation, as shown in Fig.1.8 and marked by red color.

It can also be noticed that the magnetics (transformer and inductor) of the LLC resonant converter contribute with large size (footprint), as shown in the LLC converter in Fig.1.6.

A conceptual figure showing the purpose and contents of this thesis are summarized in Fig.1.9. Multi-phase topologies are preferably employed in power conversion systems to lessen the per phase circuit current, conduction losses, devices thermal stresses, and to reduce the output current ripples to reduce the output capacitor. However, the three-phase LLC resonant DC-DC converter usually possess a number of magnetic cores equal to the number of phases. Therefore, integrated magnetics is applied to integrating the three transformers into a single magnetic core to reduce the volume, weight, and cost of the power converter. Lagrangian dynamics is used as a tool to simplify the complicated integrated magnetic structure and the theory is presented in Chapter 2. A design method and intensive experimental evaluation are carried out in Chapter 3. Another concern in the three-phase topology is the unbalanced current that arises among the paralleled phases. This unbalanced current deteriorates the converter efficiency. The sources of the current unbalance are studied, discussed, and a simple solution is proposed in Chapter 4. The effects of the secondary leakage inductance are not well-discussed in the relevant literature. Nonetheless, it shall be considered in integrated magnetic structure, because the transformer leakage inductance does not exist only on the primary side but also on the secondary side. The effects of the secondary leakage inductance are presented in details in Chapter 5. The conclusion is shown in Chapter 6.

REFERENCES

[1] L. Chapman. J. Transp. Geogr. pp 354–367, 2007.

[2] OECD. Transport Energy and CO_2: Moving Towards Sustainability, OECD/IEA Publishing, 2009.

[3] Department for Transport. Low Carbon Transport: A Greener Future, a Carbon Reduction Strategy for transport. TSO, 2009.

[4] S. Bozhko, C. Ian Hill, T. Yang "More-Electric Aircraft: Systems and Modeling", Wiley Encyclopedia of Electrical and Electronics Engineering, 2018.

[5] M. Moussa and A. Abdelkhalek, "Meteorological Analysis for Black Cloud (Episodes) Formation and its Monitoring by Remote Sensing" Journal of Applied Sciences Research, 3(2): 147-154, 2007.

Available online: https://pdfs.semanticscholar.org/e162/fcbb8cfd1a3af763fd0e0dbbdd85fbd5fc4f.pdf

[6] H. Marey, J. Gille, ElAskary, E. Shalaby, M. ElRaey, "Study of the formation of the "black cloud" and its dynamics over Cairo, Egypt, using MODIS and MISR sensors" Journal of Geophysical Research, pp.1-10, Nov. 2010

[7] Available online: https://www.env.go.jp/earth/coop/coop/c_report/egypt_h16/english/pdf/016.pdf

[8] Available online: https://www.env.go.jp/earth/coop/coop/c_report/egypt_h16/english/pdf/018.pdf

[9] C. Liu, K. Chau, D. Wu, and S. Gao "Opportunities and Challenges of Vehicle-to-Home, Vehicle-to-Vehicle, and Vehicle-to-Grid Technologies" in Proc. IEEE, July, 2013.

[10] R. Naayagi, "A review of more electric aircraft technology," in Proc. 2013 International Conference on Energy Efficient Technologies for Sustainability (ICEETS), pp. 750–753, April, 2013.

[11] S. Musil, "Boeing: Here's our plan to nix 787 battery fire risk",

Available online: http://news.cnet.com/8301-11386_3-57574484-76/boeingheres-our-plan-to-nix-787-battery-fire-risk/, Last accessed: March 2013.

[12] Available online: https://www.airbus.com/newsroom/news/en/2018/07/the-future-is-electric.html

[13] M. Rinaldi, S. Jones, "Aircraft Electrical system architectures to support more electric aircraft", in Proc. Society of Aerospace Engineers Conference, pp. 10.1-10.7, April, 2004.

[14] E. Pallet, Aircraft Electrical Systems, Longman Scientific & Technical, Third edition, 1987.

[15] J. Weimer, "Electric power technology for the more electric aircraft", in Proc. IEEE Digital Avionics Systems Conference, pp.445-450, October, 1993.

[16] J. Weimer, "The role of electrical machines and drivers in the more electric aircraft", in Proc. IEEE Electrical Machines and Drives Conference, pp. 11-15, June, 2003.

[17] M. Maldonado, N. Shah, K. Cleek, P. Walia, G. Korba, "Power Management and Distribution System for a More Electric Aircraft (MADMEL) Program status", in Proc. Energy Conversion Engineering Conference, pp.274-279, Aug. 1997.

[18] H. Zhang, C. Saudemont, B. Robyns, M. Petit, "Comparison of Technical Features between a More Electric Aircraft and a Hybrid Electric Vehicle", in Proc. IEEE Vehicle Power and Propulsion Conference, pp.1-6, Sep. 2008.

[19] M. Taha, "Power electronics for aircraft application," in IEE Colloquium on Power Electronics for Demanding Applications (Ref. No. 1999/059), pp. 7/1–7/4, 1999.

[20] H. Huang "Designing an LLC Resonant Half-Bridge Power Converter". Available online: https://www.ti.com/seclit/ml/slup263/slup263.pdf.

Chapter 2: Lagrangian Dynamics of the Three-phase Integrated Transformer in Three-phase LLC Resonant Converter

2.1 Introduction

2.1.1 Research Motivation: Lagrangian dynamics

In conventional arrangements of three-phase LLC converters, there are at least three magnetic components that occupy a considerable volume and mass of the power converter. Although, the three-phase LLC topology has many advantages over the single-phase one, circuit designers tend to select the single-phase topology because it has the minimal number of magnetic components. The purpose of this study is to reduce the number of the magnetic components of the three-phase topology, by integrating the three-discrete transformers into a single magnetic core, based on a theoretical framework. Lagrangian dynamics is applied to theoretically prove that it is possible to replace the three-discrete transformers by a single integrated transformer. The Lagrangian dynamics theory allowed us to derive a physically motivated model for the integrated transformer, in which each component of the integrated transformer has its own Lagrangian parameter. The remarkable result to emerge from the Lagrangian model is that in a symmetrical design, there is no interphase coupling due to the flux cancellation. This implies that there is no return path for the three ac fluxes, and as a result the magnetic components can be downsized. Along with the theoretical discussion, the practical merits of implementing the integrated transformer is reported. Furthermore, the experimental tests are conducted utilizing 500W 390V/12V, 200kHz, power converter.

2.1.2 Lagrangian dynamics- Literature review:

One of the most popular advantages of the LLC resonant converter topology is the feasibility of integrating one transformer and one inductor into a single magnetic core. Nonetheless, adapting single phase LLC resonant converter in high power applications comes with some drawbacks. Since the current ripple stress on the output capacitor becomes severely high to handle, and hence, a large size output smoothing capacitor is needed to compensate the high output current ripples.

Three-phase topologies have been gaining more attention, since they possess many advantages over the single phase ones. For instance, the three-phase configuration lessens circuit current per phase to 1/3 of the total current in an equivalent single-phase topology. Therefore, the output current ripples can be reduced. Nevertheless, the three-phase topology might bring some drawbacks due to the need of adapting three magnetic cores, in which, adding to the power converter more weight, volume and

cost. In the development of the power conversion circuits, designers tend to adapt the techniques which downsize the circuit and realizes high efficiency.

Integrated magnetics is one of the effective techniques to increase the converter's power density, in which multiple inductors and transformers are advantageously combined into a single magnetic core. In the literature, several studies have adapted the concept of integrated magnetics for both isolated and non-isolated DC-DC converters [1]-[5]. The basic concept of the magnetic integration for the three-phase LLC resonant converter is to replace the three discrete transformers, presented in Fig.2.1, by a single integrated transformer. In this discussion, a generic EE core is utilized as shown in Fig.2.2. In this case, multiple windings are distributed among the legs of the integrated transformer. Utilizing the integrated transformer has two main merits [4]-[5]: i) In a well-designed integrated transformer, the *ac* flux cancellation can be realized. Therefore, the total amount of magnetic core in the circuit is reduced, and hence a higher power density can be attained. ii) The dead space between the discrete transformers is completely eliminated. However, in case of a secondary center-tapped topology of three-phase LLC resonant converter, the magnetic circuit of the integrated transformer becomes difficult to comprehend. Since, in this case, the integrated transformer has one primary winding and two secondary windings for each phase, and considering mutual coupling between them leads the

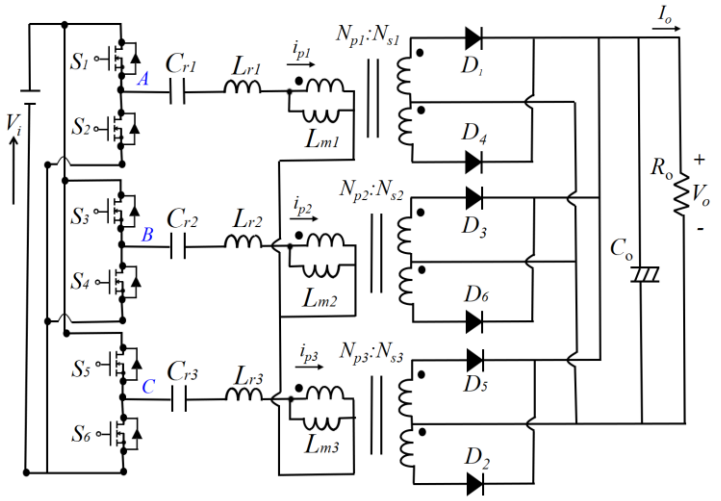

Fig.2.1 Three-phase LLC resonant converter with three-discrete transformers.

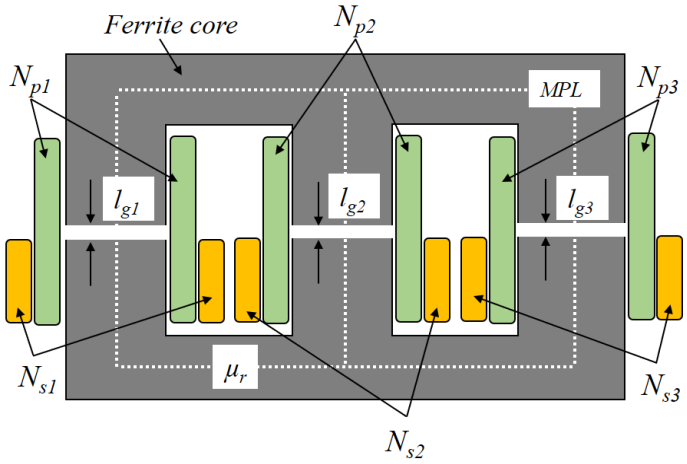

Fig.2.2 Proposed core structure of the integrated transformer.

number of independent parameters to be 45. Therefore, a conventional inductance matrix representing the integrated transformer would yield to a (9x9) dimensional matrix representing 36 mutual-inductances and 9 self-inductances. The inductance matrix is an effective solution to be applied for a basic transformer with a single flux path. However, as for more complicated magnetic circuits, determining the inductance matrix becomes generally difficult because of its great dimension.

On the other hand, in the literature, the Lagrangian dynamics have been proven to be effective to derive simplified equivalent models from many complicated magnetic structures and electric systems, through a straightforward and systematic procedure [6]-[7]. For example, in [8]-[9], Lagrangian dynamics has been utilized to develop a simplified equivalent circuits for the basic topologies of electric field wireless power transfer systems. In [10], a Lagrangian based derivation for a sliding-mode control for the synchronous converter has been proposed. In [11] Lagrangian dynamics based model has been proposed to simplify the integrated magnetic components of a coupled inductor in interleaved boost converter. In [12] Lagrangian model has been proposed to simplify the nonlinearity of the concentrated-winding switched reluctance motors.

The purpose of this chapter is to provide a theoretical framework to integrate the three-discrete transformer into a single core, which has never been presented before in the literature. Lagrangian dynamics theory is applied to simplify the integrated transformer by obtaining a novel circuit. The Lagrangian based model of the integrated transformer leads to an equivalency of three-discrete transformers. Experimental tests have been conducted to validate the proposed analysis. The experimental tests have utilized two prototypes of the LLC converter, one employing the integrated transformer and other utilizes three-discrete transformers.

2.1.3 Chapter contents:

Chapter 2 is divided as follows: In section 2.2, first, as an example the Lagrangian formula of a basic transformer is presented. Second, the Lagrangian dynamics based model of the integrated transformer is developed. On the basis of the energy equivalency, section 2.3 shows that the equivalent circuit obtained from the Lagrangian is consistent with the magnetic circuit of the integrated transformer. In section 2.4, the striking results emerged from the Lagrangian model is reported. Since, the derived circuit has no interphase coupling, which agrees with the flux cancellation concept, and indicates that there is no return path for the *ac* fluxes and hence, the magnetic component can be downsized. The practical merits of implementing the integrated transformer is reported in section 2.5. The summary is presented in section 2.6. Furthermore, experimental results are presented to validate the analysis and to show the analogy between the integrated transformer and its three-discrete counter parts.

2.2 Developing the Lagrangian Models

It is well known that the basic laws of dynamics can be mathematically formulated in several ways such as: a) D' Alembert's principle b) Lagrange's equations c) Hamilton's principle. However, as a means of treating a wide range of problems (theoretical

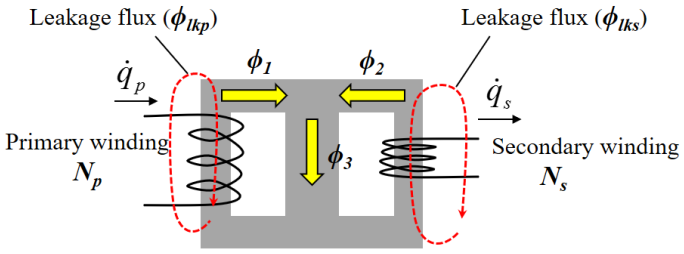

Fig.2.3 Basic transformer, proposed here as an example.

as well as practical) involving mechanical, electrical, electro-mechanical and other systems, the Lagrangian method is outstandingly powerful and remarkably simple to apply [13]-[14].

In this section, the Lagrangian model for both a basic transformer and for the proposed integrated transformer are developed; where the following approximations are made: i) There is no electric field neither magnetic field outside the circuit components. ii) There is no charge nor current outside the circuit components. The Lagrangian describing any magnetic component is reducible into

a) Lagrangian component for the magnetic core (L_M).

$$L_M = -\frac{R.\phi^2}{2} \qquad (2.1)$$

b) Lagrangian component for the windings (L_W).

$$L_W = \sum_n N_n \phi_n \dot{q}_n \qquad (2.2)$$

Where n is the total number of the turns; R is the reluctance of the magnetic core in which the flux ϕ passes; N is the winding number of turns; and the current flowing through a winding is regarded as the time derivative of the cumulative charge q which is the time integration of the current i, and the dot over the variable is its time derivative. Essentially, the Lagrangian multiplier (λ) is needed to describe the transformer's core geometry by considering the flux continuity in the core.

2.2.1 Lagrangian example: Basic transformer

In this subsection, as an example, the Lagrangian of a basic transformer shown in Fig.2.3 is derived. The transformer has a primary winding with number of turns (N_p), and a secondary winding with number of turns (N_s). The Lagrangian expression for the basic transformer can be obtained easily, and it can be expressed as

$$L = N_p(\phi_1 + \phi_{lkp})\dot{q}_p + N_s(\phi_2 + \phi_{lks})\dot{q}_s - \frac{R_1.\phi_1^2}{2} - \frac{R_{lkp}.\phi_{lkp}^2}{2} - \frac{R_2.\phi_2^2}{2} - \frac{R_{lk2}.\phi_{lk2}^2}{2} - \frac{R_3.\phi_3^2}{2} + \lambda(\phi_1 + \phi_2 - \phi_3) \qquad (2.3)$$

Where R_i is the magnetic reluctance that dissipates the magnetic energy due to the flux ϕ_i.

2.2.2 Lagrangian Model of the proposed Integrated transformer

The integrated transformer can be implemented with different magnetic core structures; in this discussion we utilize a generic EE magnetic core. The proposed core structure is shown in Fig.2.2 The core has three legs, in which each pair of primary and secondary windings is placed on one leg. Air gaps are inserted in the three legs to store magnetic energy, in order to realize a soft switching operation for the LLC resonant converter. All primary windings have the same number of turns; and all secondary windings have the same number of turns as well. The Lagrangian formula for the proposed integrated transformer can be expressed as follows

$$L=\left\{\sum_{i=1}^{3}N_{pi}\phi_i\dot{q}_i+\sum_{i=1}^{3}N_{si}\phi_i\dot{q}_i-\sum_{k=1}^{3}\frac{R_k\phi_k^2}{2}+\sum_{i=1}^{3}N_{pi}\phi_{lkpi}\dot{q}_i\ \sum_{i=1}^{3}N_{si}\phi_{lksi}\dot{q}_i+\lambda(\phi_1+\phi_2+\phi_3)-\sum_{n=1}^{6}\frac{R_{lkn}\phi_{lkn}^2}{2}\right. \quad (2.4)$$

The Lagrangian multiplier λ is function of the constraint parameters of the core, in this case the flux constraint is ($\phi_1 + \phi_2 + \phi_3 = 0$). From (2.4), the Lagrangian expression can be expressed as

$$L=\left\{\left(N_{p1}\phi_1\dot{q}_{p1}+N_{s1}\phi_1\dot{q}_{s1}-\frac{R_{lkp1}\phi_{lkp1}^2}{2}-\frac{R_{lks1}\phi_{lks1}^2}{2}+N_{p1}\phi_{lkp1}\dot{q}_{p1}+N_{s1}\phi_{lks1}\dot{q}_{s1}\right)+\left(N_{p2}\phi_2\dot{q}_{p2}+N_{s2}\phi_2\dot{q}_{s2}-\frac{R_{lkp2}\phi_{lkp2}^2}{2}\right.\right.$$

$$\left.-\frac{R_{lks2}\phi_{lks2}^2}{2}+N_{p2}\phi_{lkp2}\dot{q}_{p2}+N_{s2}\phi_{lks2}\dot{q}_{s2}\right)+\left(N_{p3}\phi_3\dot{q}_{p3}+N_{s3}\phi_3\dot{q}_{s3}-\frac{R_{lkp3}\phi_{lkp3}^2}{2}-\frac{R_{lks3}\phi_{lks3}^2}{2}+N_{p3}\phi_{lkp3}\dot{q}_{p3}+N_{s3}\phi_{lks3}\dot{q}_{s3}\right)+$$

$$\left.\lambda(\phi_1+\phi_2+\phi_3)-\frac{R_1\phi_1^2}{2}-\frac{R_2\phi_2^2}{2}-\frac{R_3\phi_3^2}{2}\right\} \quad (2.5)$$

The Lagrangian multiplier λ can be replaced by a virtual winding that has a number of turns = N_v, in which a virtual current q_v flows in this winding. The Lagrangian expression of (2.5) can be reconstructed into

$$L=\left\{\left((N_{p1}\dot{q}_{p1}+N_{s1}\dot{q}_{s1}+N_v\dot{q}_v)\phi_1-\frac{R_1\phi_1^2}{2}+N_{p1}\phi_{lkp1}\dot{q}_{p1}+N_{s1}\phi_{lks1}\dot{q}_{s1}-\frac{R_{lkp1}\phi_{lkp1}^2}{2}-\frac{R_{lks1}\phi_{lks1}^2}{2}\right)\right.$$

$$+\left((N_{p2}\dot{q}_{p2}+N_{s2}\dot{q}_{s2}+N_v\dot{q}_v)\phi_2-\frac{R_2\phi_2^2}{2}+N_{p2}\phi_{lkp2}\dot{q}_{p2}+N_{s2}\phi_{lks2}\dot{q}_{s2}-\frac{R_{lkp2}\phi_{lkp2}^2}{2}-\frac{R_{lks2}\phi_{lks2}^2}{2}\right)$$

$$\left.+\left((N_{p3}\dot{q}_{p3}+N_{s3}\dot{q}_{s3}+N_v\dot{q}_v)\phi_3-\frac{R_3\phi_3^2}{2}+N_{p3}\phi_{lkp3}\dot{q}_{p3}+N_{s3}\phi_{lks3}\dot{q}_{s3}-\frac{R_{lkp3}\phi_{lkp3}^2}{2}-\frac{R_{lks3}\phi_{lks3}^2}{2}\right)\right. \quad (2.6)$$

This Lagrangian expression can be translated into physical magnetic core structures, in which the expression corresponds to equivalent core geometries of three discrete ideal transformers, and six cores representing the primary and secondary leakage inductances, as shown in Fig.2.4.

Based on the circuit theory, Maxwell's equations can be applied on the magnetic components shown in Fig.2.4, which have been obtained from the Lagrangian formula. The following equations (2.7)-(2.9) have been obtained by integrating Ampere's law around *Loop 1*, *Loop 2*, and *Loop 3*, respectively.

$$N_{p1}i_{p1} + N_s i_{s1} + N_v i_v = R_1 \phi_1 \tag{2.7}$$

$$N_{p2}i_{p2} + N_s i_{s2} + N_v i_v = R_2 \phi_2 \tag{2.8}$$

$$N_{p3}i_{p3} + N_s i_{s3} + N_v i_v = R_3 \phi_3 \tag{2.9}$$

Under balanced conditions, and as the transformer is star connected. Therefore, the sum of the three-phase currents equals zero. On the other hand, Faraday's law can be applied on the electrical terminal 1 and 2 shown in Fig.2.4, and since the virtual winding is short circuited, the following equation can be obtained

$$N_v \left(\frac{d\phi_1}{dt} + \frac{d\phi_2}{dt} + \frac{d\phi_3}{dt} \right) = 0 \tag{2.10}$$

Therefore, the sum of the three fluxes goes to zero.

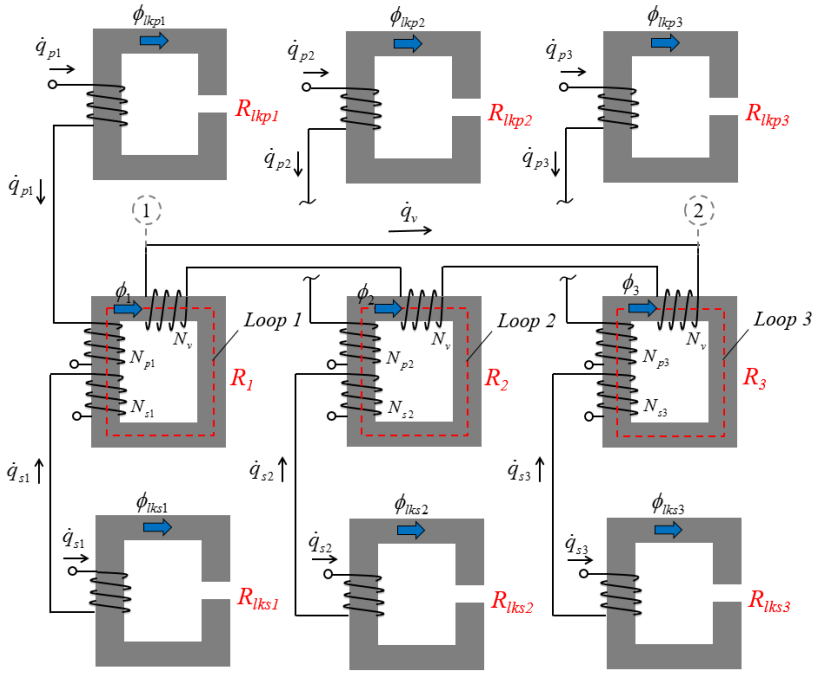

Fig.2.4 Equivalent magnetic components translated from the Lagrangian formula.

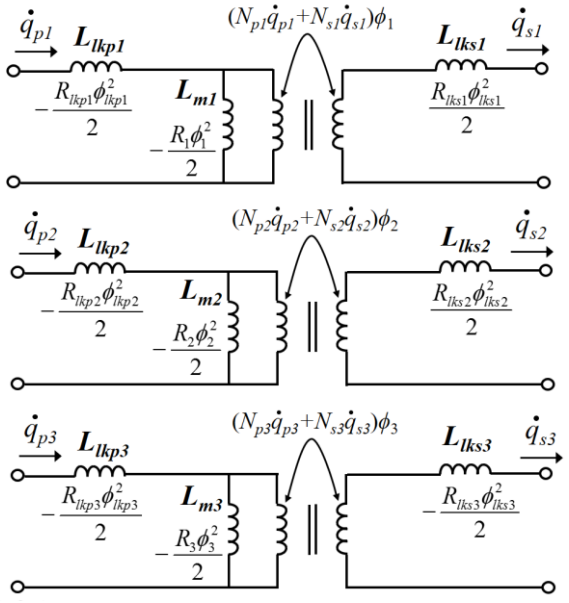

Fig.2.5 Equivalent electric circuit model obtained from the Lagrangian formula.

$$\phi_1+\phi_2+\phi_3=0 \qquad (2.11)$$

Considering a similar values of the magnetic reluctances, therefore, the sum of (2.7), (2.8) and (2.9) leads to

$$3N_v i_v = R_1\phi_1 + R_2\phi_2 + R_3\phi_3 = R\left(\phi_1+\phi_2+\phi_3\right)=0 \qquad (2.12)$$

It can be deduced from (2.12) that i_v =0. As a result, the equivalent circuit of the integrated transformer can be translated into a simplified equivalent circuit shown in Fig.2.5. Fig.2.5 implies that the magnetic behavior of the integrated transformer is consistent with three-discrete independent transformers.

2.3 Energy Equivalency

This section confirms that the equivalent circuit obtained from the Lagrangian model has the same electric functions as the original magnetic circuit of the integrated transformer. For this purpose, the aim is to prove that Fig.2.5 is functionally equivalent to the original magnetic circuit shown in Fig.2.6 In order to discuss the functional equivalence, we derive the energy expressions for the two circuits. The energy expression of the equivalent circuit shown in Fig.2.5, which had been developed from the Lagrangian dynamics theory can be expressed as

$$E = 3\times\left\{\frac{1}{2}L_{lkp}i_p^2+\frac{1}{2}L_{lkp}i_p^2+\frac{1}{2}L_m\left(i_p-\frac{N_s}{N_p}i_s\right)^2\right\} \qquad (2.13)$$

The energy expression of the magnetic circuit, shown in Fig.2.6, can be expressed as the sum of the external leakage energy due to the primary side, external leakage on the secondary side, and the energy stored in the magnetic core, as follows

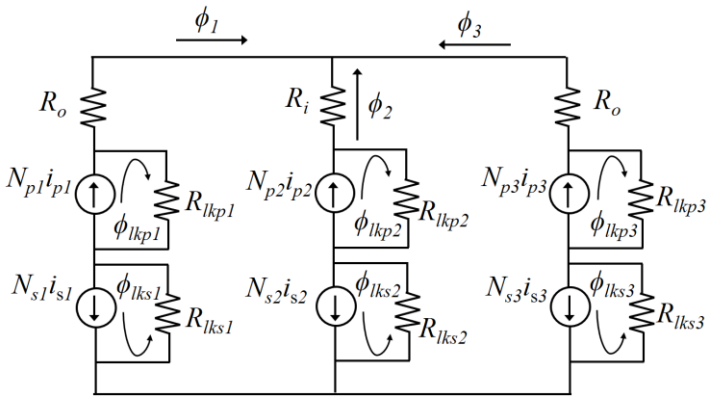

Fig.2.6 The magnetic circuit of the three-leg integrated transformer.

$$E = E_{lkp} + E_{lks} + E_m \tag{2.14}$$

Equation (2.14) can be rewritten as

$$E = \sum_{i=1}^{3} \frac{1}{2} R_{lkpi} \phi_{lkpi}^2 + \sum_{i=1}^{3} \frac{1}{2} R_{lksi} \phi_{lksi}^2 + \sum_{i=1}^{3} \frac{1}{2} R_i \phi_i^2 \tag{2.15}$$

The first term of the right hand side of this formula expresses the external leakage energy due to the primary current, as follow

$$E_{lkp} = \sum_{i=1}^{3} \frac{1}{2} R_{lkpi} \phi_{lkpi}^2 = \frac{3}{2} \left(\frac{N_p^2}{L_{lkp}} \right) \left(\frac{L_{lkp} i_p}{N_p} \right)^2 = \frac{3}{2} L_{lkp} i_p^2 \tag{2.16}$$

The second term of the right hand side of (2.15) expresses the external leakage energy due to the secondary current, as follow

$$E_{lks} = \sum_{i=1}^{3} \frac{1}{2} R_{lksi} \phi_{lksi}^2 = \frac{3}{2} \left(\frac{N_s^2}{L_{lks}} \right) \left(\frac{L_{lks} i_s}{N_s} \right)^2 = \frac{3}{2} L_{lks} i_s^2 \tag{2.17}$$

The third term of the right hand side of (2.15) expresses the energy stored in the magnetic core, as follow

$$E_{\acute{s}} = \sum_{i=1}^{3} \frac{1}{2} R_i \phi_i^2 = \frac{3}{2} \left(\frac{N_p^2}{L_m} \right) \left(\frac{L_m i_m}{N_p} \right)^2 = \frac{3}{2} L_m i_m^2 \tag{2.18}$$

The sum of (2.16), (2.17) and (2.18) gives the same energy expression of (2.13). Consequently, Fig.2.6 and Fig.2.4 are shown to be equivalent.

2.4 Theoretical Discussion

Designing a three-phase integrated transformer is considered to be a challenge, because in order to realize a proper operation of the integrated transformer the three-phases shall be symmetric. It is important to keep the symmetry of the leakage and magnetizing inductances. Otherwise, a mismatch between the phase components would lead the three phases to exhibit different voltage conversion ratios, causing one phase or even two phases to totally reduce their delivered power, that would badly affect the efficiency of the power converter. Therefore, it is important to design the integrated transformer carefully, to avoid the unbalanced power sharing between the paralleled phases. It worth mentioning here that the equivalent circuit, shown in Fig.2.5, translated from the Lagrangian has been obtained under the assumption of a complete symmetry between the three-phases. If all phases of the integrated transformer are designed in symmetry; the number of primary turns of all phases are equal, similarly; the secondary winding turns are equal; the reluctance of three outer legs are equal ($R_1 = R_2 = R_3 = R$); which can be achieved by adjusting the air-gap lengths in the three outer limbs to the same value. This would lead to an *ac* flux cancellation. The *ac* flux cancelation would be realized since all the flux of the three-phases are equal in magnitude and 120^o phase shifted. Therefore, there is no return path for the *ac* fluxes, and therefore, the magnetic components can be downsized.

TABLE 2.I
DESIGN SPECIFICATIONS FOR THE LLC RESONANT CONVERTER

Symbol	Quantity	Value
P_o	Output power	500 W
f_{sw}	Switching frequency	200 kHz
V_i	Input voltage	390 V
V_o	Output voltage	12 V
L_{m1}, L_{m2}, L_{m3}	Magnetization inductances	132 µH
L_{r1}, L_{r2}, L_{r3}	Resonant inductances	23 µH
C_{r1}, C_{r2}, C_{r3}	Resonant capacitance	22 *n*F
L_n	Inductance ratio	5.7
Q_e	Quality factor	0.338
N	Turns ratio	16

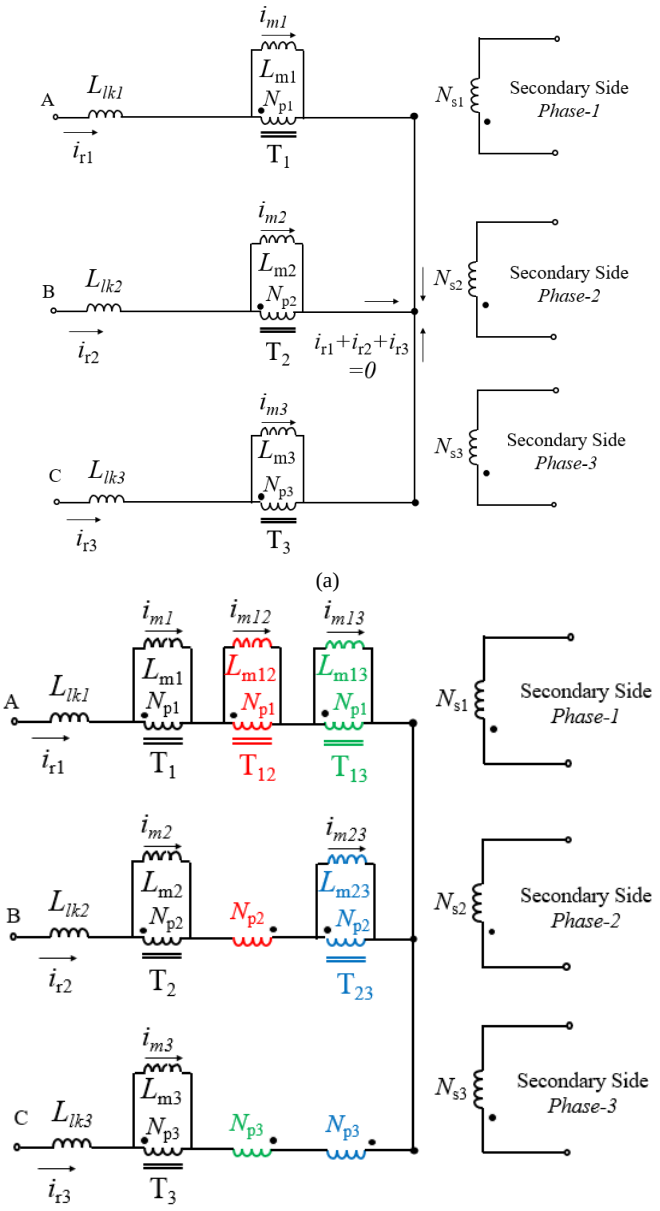

Fig.2.7 Equivalent circuit (a) Three non-coupled transformers. (b) The integrated transformer.

The equivalent circuits of the three discrete transformers and the integrated transformer are depicted in Fig.2.7 In an integrated transformer, since the three phases are placed on the same core, there are three transformer actions (T_{12}, T_{13}, and T_{23}), beside the transformer action between the primary-secondary of each phase (T_1, T_3, and T_3). Nonetheless, since there is no coupling between the phases, as implied from the Lagrangian model, therefore L_{m12}, L_{m13}, L_{m23} goes to zero (i.e becomes short circuit). In this case, the equivalent circuit of Fig.2.7 (b) yields to the equivalent circuit of the three discrete transformers of Fig.2.7 (a). Consequently, the waveforms of the two prototypes are expected to be analogous. However, in practice, the values of L_{m12}, L_{m13}, L_{m23} are a little bit higher than zero. Therefore, the rate of change in the current becomes a little bit lower in case of the integrated transformer, than its counterpart of the three discrete transformers. Since ($V = L\ di/dt$), and the applied voltage is the same in the two prototypes.

TABLE 2.II
MEASURED VALUES OF THE THREE-DISCRETE TRANSFORMERS

Parameters	Transformer No.1	Transformer No.2	Transformer No.3
Magnetic core	3 cores (PC40 EER42/42/20-Z)		
Resonance inductance L_r	19.2 µH	24 µH	21.5 µH
Magnetizing inductance L_m	134.4 µH	130 µH	128.7 µH
Number of Turns	32:2:2	32:2:2	32:2:2

TABLE 2.III
MEASURED VALUES OF THE INTEGRATED TRANSFORMER

Parameters	Phase No.1	Phase No.2	Phase No.3
Magnetic core	1 core (PC40 EC70x69x16)		
Resonance inductance L_r	24.8 µH	23.2 µH	24.3 µH
Magnetizing inductance L_m	137.3 µH	128.5 µH	133.4 µH
Number of Turns	32:2:2	32:2:2	32:2:2

The most striking result to emerge from the Lagrangian model of the integrated transformer is that it theoretically proves that it is equivalent to the three-discrete transformers, with no interphase coupling which agrees with the *ac* flux cancellation concept. A simulation case study has been conducted using PLECS software (Plexim Inc.) to show the transformer voltage and the flux waveforms. The simulation tests have been done employing the paratmeters listed in Tables 2.I., Table 2.II, and Table 2.III. And the simulation results are compared side by side along with the experimental results in the next section for the two prototypes.

2.5 Practical Implementation of Transformer

In this section, the practical merits of employing the integrated transformer in a three-phase LLC resonant converter is reported. The discussion in this section includes a comparison between the integrated transformer and the three-discrete transformers on the basis of volume, weight, and cost. Furthermore, experimental results are presented. The purpose of the experimental test is to validate the proper operation of the integrated transformer utilized in the three-phase LLC converter. In addition, in order to validate the Lagrangian based equivalent circuit, two prototypes were tested to show the analogy between the integrated transformer and the three-discrete transformers.

2.5.1 System Description

In order to evaluate the proper operation of the three-phase integrated transformer the LLC converter was constructed and experimentally tested. The experimental evaluation is conducted utilizing two prototypes. The first prototype employs

three-discrete transformers, and the second prototype employs the integrated transformer. The three-phase LLC converter's specifications are listed in Table 2.I. Fig.2.8 shows the experimental prototype using the three discrete transformers, while Fig.2.9 presents the integrated transformer's prototype. These prototypes use Schottky diodes (VS-100BGQ100), primary Mosfets (Toshiba, TK20E60W). Litz wires with low ESRs are used to reduce the skin effect and proximity effect losses in the transformer's windings, and their cross-section area is 0.628 mm^2, 3.297 mm^2 for the primary and secondary windings, respectively. Texas Instruments DSP is used to drive the primary switches. The three-legged integrated transformer can be implemented with different magnetic core structures, in this discussion we utilized ferrite core, PC40 EC70x69x16. The measured parameters of the three discrete transformers are listed in Table 2.II, where three magnetic cores of PC40EER42/42/20-Z are utilized. The measured parameters of the integrated transformer are listed in Table 2.III.

2.5.2 Volume and weight comparison

Referring to the product catalog of TDK [15], the magnetic core's volume and weight of the integrated transformer are 40.42 cm^3 and 250g. Referring to [16], the total volume and weight of the discrete transformers are 3x23.7 = 71.1 cm^3 and 3x116=348g. In other words, for the same LLC resonant converter, the integrated transformer enables an approximate 43% transformer volume reduction as compared with the three discrete transformer, and a weight reduction of 28%. Moreover, the dead spaces between the discrete transformers are no longer required in case of utilizing the integrated transformer.

2.5.3 Cost

From the website of Allied Electronics [17], the estimated cost of magnetic core for the integrated transformer is 7.06 USD/unit. However, the total cost for the three discrete magnetic cores is 3x2.8 = 8.4 USD/unit. The windings cost is out of comparison. Therefore, employing the magnetic integrated transformer would achieve a cost reduction of 16%.

2.5.4 Simulation and Experimental Results

Simulation and experimental tests have been conducted for the three-phase LLC resonant converter considering the two transformer prototypes. The operating conditions are as follows: This LLC converter is a 390V - 12V step-down converter, and its operating frequency is 200kHz, the power rating is 500W. The secondary rectifier bridge is center tapped and the transformers number of turns are 32:2:2 to satisfy a turns ratio of 16:1.

Fig.2.10 shows the resonant currents and drain-source voltage waveforms for the three discrete transformers prototype. The simulation waveforms are presented in Fig.2.10 (a), and the experimental waveforms are shown in Fig.2.10 (b). On the other hand, Fig.2.11 shows the resonant currents and drain-source voltage waveforms for the integrated transformer prototype. Likewise, the simulation waveforms of the integrated transformer are shown in Fig.2.11 (a), and the experimental waveforms are shown in Fig.2.11 (b). The switching transition has been zoomed in, and depicted in Fig.2.12. Soft switching is obtained within

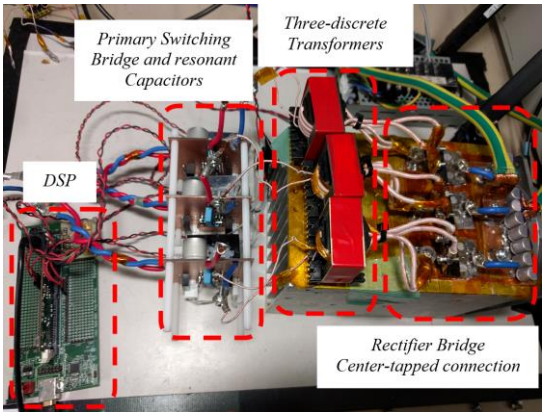

Fig.2.8 Prototype utilizing three-discrete transformer.

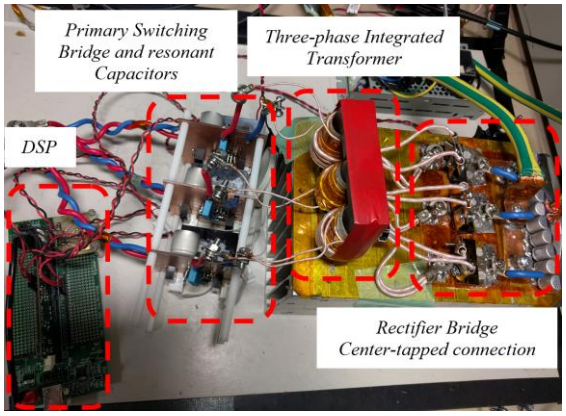

Fig.2.9 Prototype utilizing one Integrated transformer.

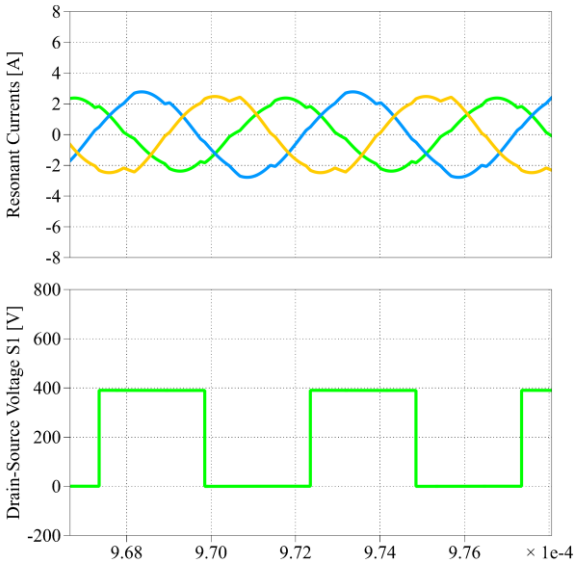

(a)

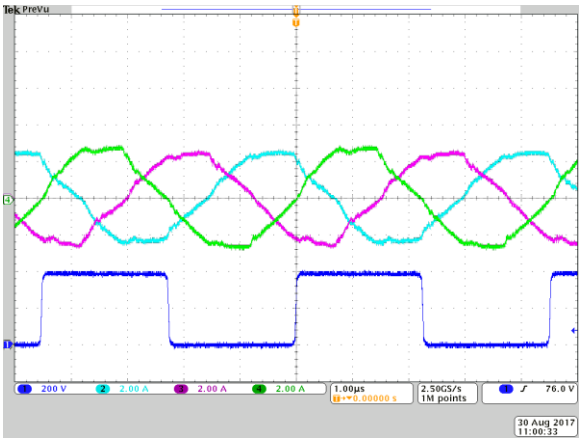

(b)

Fig.2.10 Resonant current and drain-source voltage waveforms for the three discrete transformers. (a) Simulation waveforms. (b) Experimental waveforms.

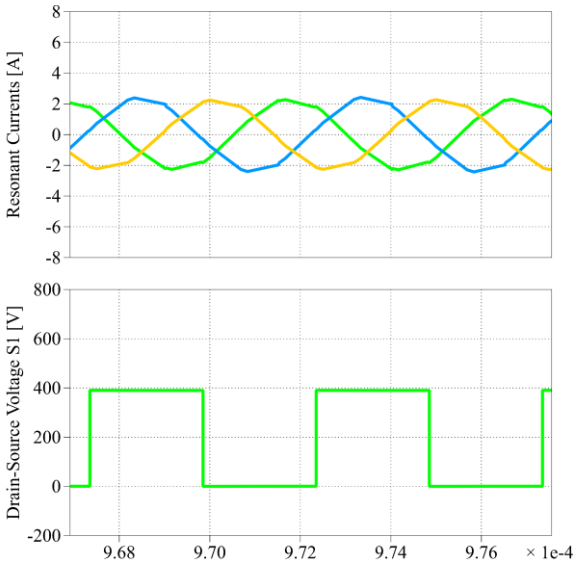

(a)

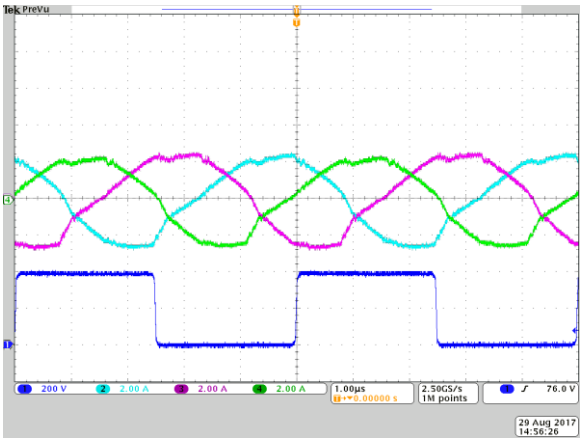

(b)

Fig.2.11 Resonant current and drain-source voltage waveforms for the integrated transformer. (a) Simulation waveforms. (b) Experimental waveforms.

the two prototypes. It is clear that the waveforms obtained from the two prototypes are analogous, except the fact that the resonant current rate of change is a little bit lower in case of the integrated transformer.

The simulation waveform of the output voltage is shown in Fig.2.13 (a), and the experimental waveform is shown in Fig.2.13 (b).

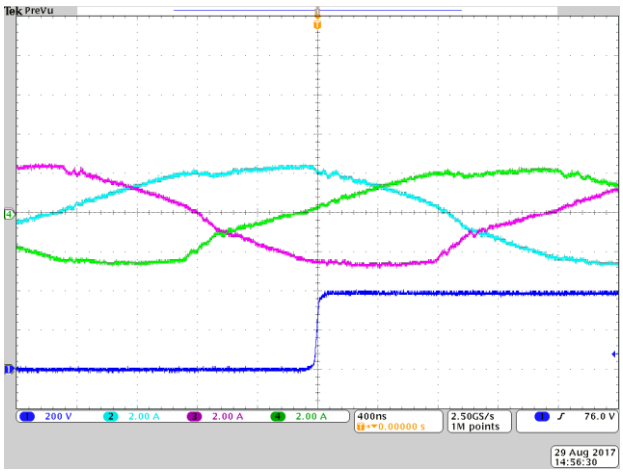

Fig.2.12 Zoomed-in on the switching transition waveform.

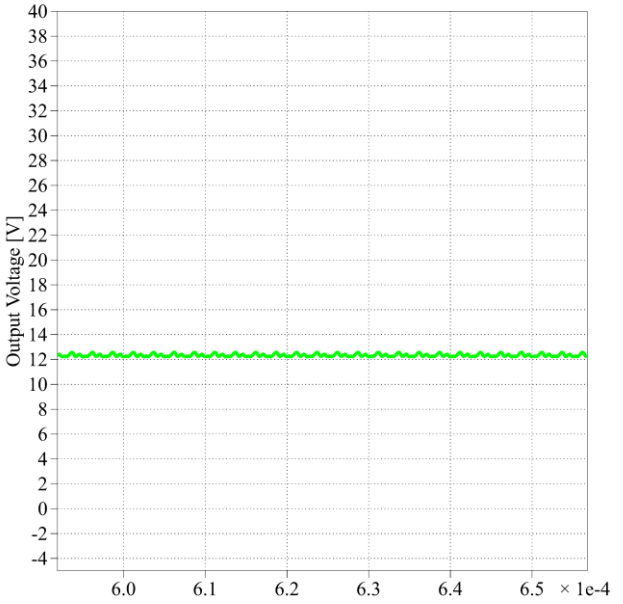

(a)

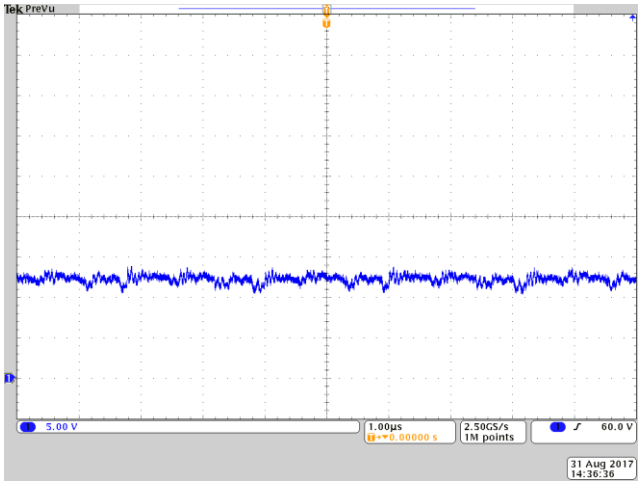

(b)

Fig.2.13 Output voltage waveform. (a) Simulation waveform. (b) Experimental waveform.

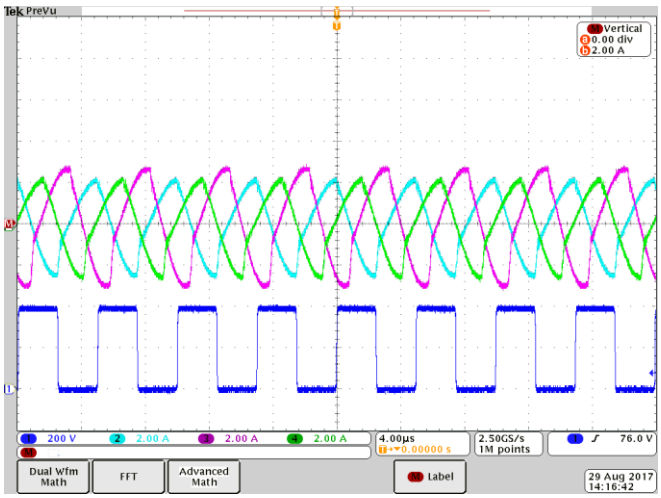

(a)

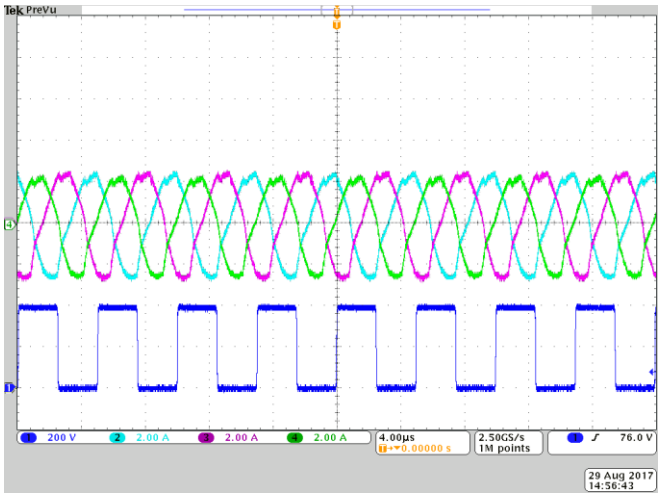

(b)

Fig.2.14 Experimental waveforms of the integrated transformer. (a) Conventional parallel connection. (b) Star connection.

It worth mentioning here that The transformer parameters discrepancy would directly affect the voltage gain of the LLC converter. Since, the three resonant inductances are not identical, which is practically difficult to realize. Therefore, each phase of the LLC converter is encountering a voltage gain different than the other, leading to unbalanced current sharing between the phases, as shown in Fig.2.14 (a).

In this chapter, the unbalance was tackled by connecting the integrated transformer's primary in Star, as shown in Fig.2.1 (not conventional parallel connection). The positive balancing effect

of the connecting the transformer primary in star is shown in Fig.2.14 (b). This current balancing approach has been previously reported in the literature, in [18]-[19].

2.6 Summary

In order to simplify the complicated magnetic structure of the three-phase integrated transformer, a Lagrangian dynamics based model of the integrated transformer incorporated in three-phase LLC converter is proposed. The Lagrangian formulation leads to an equivalent model of a three-discrete transformers, with three independent magnetic cores. The remarkable result to emerge from the Lagrangian model is that in a symmetrical design, there is no interphase coupling. The proposed Lagrangian model can be implemented on various integrated magnetic structures, however in this thesis, a three-phase integrated transformer structure incorporated in three-phase LLC converter was proposed as an example. The proper operation of the integrated transformer incorporated in a three-phase LLC resonant converter is validated through experimental tests. The discussion presented in this chapter would promote implementing three-phase integrated transformer in DC-DC converters to realize high power density in several industrial applications.

References

[1] M. Pavlovsky´, G. Guidi, and Atsuo Kawamura, “Assessment of Coupled and Independent Phase Designs of Interleaved Multiphase Buck/Boost DC-DC Converter for EV Power Train”, IEEE Trans. on Power Electron., Vol. 29, No. 6, pp. 2693-2704, June, 2014.

[2] L. Wong, Y. Lee, D. K. Cheng, and M. H. L. Chow, “Two-Phase Forward Converter using an Integrated Magnetic Component”, IEEE Trans. on Aerospace and Electron. Sys., Vol. 40, No.4, pp.1294-1310 Sep. 2004.

[3] K. J. Hartnett, J. G. Hayes, M. G. Egan and M. S. Rylko, “CCTT-Core Split-Winding Integrated Magnetic for High-power DC-DC Converters”, IEEE Trans. on Power Electron., Vol. 28, pp. 4970-4984, Nov. 2013.

[4] M. Noah, S. Kimura, S. Endo, M. Yamamoto, J. Imaoka, K. Umetani, W. Martinez “A Novel Three-phase LLC Resonant Converter with Integrated Magnetics for Lower Turn-off losses and Higher Power Density,” in Proc. IEEE Appl. Power Electron. Conf. Expo. (APEC), pp. 1–8, March, 2017.

[5] W. Martinez, M. Noah, S. Endo, K. Nanamori, S. Kimura, M. Yamamoto, J. Imaoka and K. Umetani, “Three-phase LLC Converter with Integrated Magnetics,” in Proc. IEEE Energy Conver. Cong. and Expo. (ECCE), pp. 1-8, Sep. 2016.

[6] K. Umetani, “A generalized method for Lagrangian modelling of power conversion circuit with integrated magnetic components”, IEEJ Trans. On Electrical and Electronic Engineering, vol. 7, pp. 146-152 Nov. 2012.

[7] K. Umetani, “Lagrangian method for deriving electrically dual power converters applicable to nonplanar circuit topologies”, IEEJ Trans. On Electrical and Electronic Engineering, Vol. 11, pp. 521-530. 2016.

[8] M. Ishihara, K. Umetani, H. Umegani, M. Yamamoto, and E. Hiraki, “Quasi-duality between SS and SP topologies of basic electric field coupling wireless power transfer system”, IET Electronics Letters, Vol. 52, No.25, pp. 2057-2059, 2016.

[9] H. Umegami, K. Umetani, M. Yamamoto, and E. Hiraki, “Lagrangian-based equivalent circuit of basic electric field coupling wireless power transfer system”, IEEJ Trans. On Electrical and Electronic Engineering, Vol. 10, pp. S168-S170, 2015.

[10] K. Umetani, M. Yamamoto, and E. Hiraki, “Lagrangian-based derivation of a novel sliding-mode control for synchronous buck converters”, IEEJ Trans. On Industry Applications, Vol. 4, No.6, pp. 728-729, April, 2015.

[11] K. Umetani, J. Imaoka, M. Yamamoto, S. Arimura, and T. Hirano, “Evaluation of the Lagrangian Method for Deriving Equivalent Circuits of Integrated Magnetic Components: a Case Study Using the Integrated Winding Coupled Inductor”, IEEE Trans. Ind. Appl., vol. 51, no. 1, pp. 547-555 Jan. 2015.

[12] K. Umetani, M. Yamamoto, and E. Hiraki, “Simple flux-based Lagrangian formulation to model nonlinearity of concentrated winding switched reluctance motors”, IET Electronics Letters, Vol. 51, No.24, pp. 1984-1986, 2015.

[13] C. Lanczos “The Variation Principle of Mechanics”, Dover: Mineola, NY, 125-128, 1970,

[14] K. Kawamura “Electromagnetism” Iwanami: Tokyo, Japan; pp. 218-223, 1994, (In Japanese).

[15] Large size ferrite cores for high power, TDK. Available online: https://product.tdk.com/info/en/catalog/datasheets/ferrite_mz_large_e_en.pdf.

[16] Ferrite core for switching power supplies, TDK. Available online:product.tdk.com/info/en/catalog/datasheets/ferrite_mz_sw_e_en.pdf.

[17] Allied Electronics Co. Ltd, USA, “Passive components”. Available online: http://www.alliedelec.com/passive-components/

[18] E. Orietti, P. Mattavelli, G. Spiazzi, C. Adragna, and G. Gattavari, “Current sharing in three phase LLC interleaved resonant converter,” in Proc. IEEE Energy Convers. Congr. Expo. (ECCE), pp. 1145–1152, Sep. 2009.

[19] E. Orietti, P. Mattavelli, G. Spiazzi, C. Adragna, and G. Gattavari, “Analysis of multi-phase LLC resonate converter,” in Brazilian Power Electronics Conference, Dec. 2009.

Chapter 3: Magnetic Design and Experimental Evaluation of Three-phase Integrated transformer in Three-phase LLC Resonant Converter

3.1 Introduction

3.1.1 Research Motivation: Integrated Transformer

Multi-phase topologies are preferably employed in power conversion systems to lessen the per phase circuit current, conduction losses, devices thermal stresses, and to reduce the output current ripples. Multi-phase LLC resonant DC-DC converter usually possess a number of magnetic cores equal to the number of phases. These magnetic cores are the major contributors to supply weight, and size (footprint). For these reasons, circuit designers tend to select the topologies that have a minimal number of magnetic cores. The purpose of this chapter is to promote the industrial applications of the three-phase LLC resonant converter shown in Fig.3.1 by integrating three transformers into a single, commercially available, magnetic core to reduce the volume, weight, and cost of the power converter. A comprehensive magnetic analysis for the three-phase integrated transformer is conducted. FEM Simulation and experimental tests are carried out to validate the proper operation of the integrated transformer utilized in a 390/12V-500W prototype. Furthermore, the power losses distribution has been presented. The proposed integrated transformer has been proven efficient, and it realized a uniform thermal distribution along the core compared to the three discrete transformers.

Passive components are usually the biggest contributor to the power converter's volume, weight and cost. Driving the power devices with high switching frequency is one of the successful ways to downsize the magnetic components, especially with the

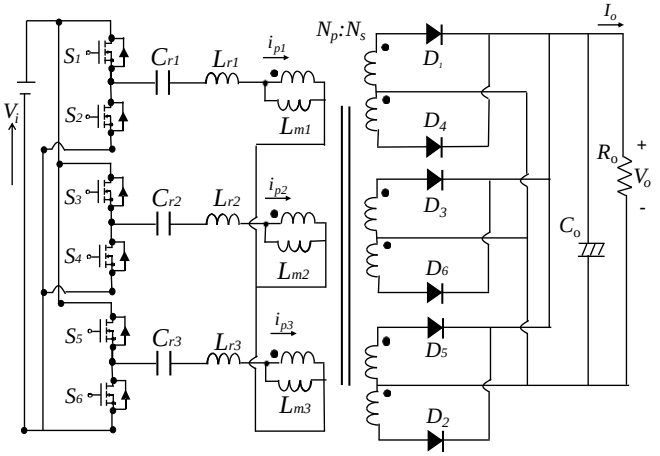

Fig.3.1 Three-phase LLC resonant converter.

advanced development of semiconductor devices such as: SiC and GaN, which are capable of operating at high frequencies [1]-[3]. However, operating at high frequencies are limited to a certain range, where the converter overall losses are not dominated by switching losses. Moreover, higher frequencies lead to an increase in EMI/RFI noise which badly affects the converter operation.

As an alternative, designers are now turning towards integrating the magnetics, as another solution to reduce the footprint of the passive components. The expression “integrated magnetics” is used to describe a magnetic design whereby various inductive elements of a power converter are combined on a single magnetic core structure, and it has been applied to non-isolated buck and boost converters [4]-[9], and isolated DC-DC topologies such as Flyback and Forward converters [10]-[13].

LLC resonant converter is a popular topology among other power conversion circuits. However, adapting single phase LLC topology in high power applications comes with drawbacks. Since the current ripple stress on the output capacitor becomes severely high to handle, a large size output smoothing capacitor is needed to compensate the high output current ripples.

3.1.2 Challenges of implementing multi-phase LLC resonant converter topologies

There are two main drawbacks related to the footprint of the passive components, usually arise whilst employing multi-phase LLC resonant topologies. The first one is that the values of the resonant tank parameters are never exactly identical among the phases, thus each phase encounters a gain characteristic different than other phases, aggravating the output current ripples and hence, a larger output capacitor is needed to compensate the current imbalance [14]. The second drawback is that multi-phase LLC converter requires many magnetic components, which increase the volume, weight and cost of the converter. For a three-phase topology depicted in Fig.3.1, the former problem has been widely discussed in the literature. The authors of [15] have proposed a control scheme to compensate the gain difference between the phases by controlling the PFC's output voltage, and based on that adjusting the input voltage for each converter according to the peak value of the rectifier current. In [16] the current imbalance in the interleaved LLC converter has been tackled by phase-shift modulation (PSM). In [17], The three half-bridge LLC converter with a star connected primary transformer is presented, to reduce the output current ripples with the aid of a phase-shift control technique. However, applying control schemes tend to make the system more complex. Therefore, many studies have proposed other methods without employing control schemes. In [18] three current balancing transformers have been utilized in the three-phase LLC converter to equalize the currents between the phases. The primary side of the balancing transformer is connected in series with the resonant capacitor, while the secondary side is paralleled with the other phases. Nonetheless, adding three additional magnetic components costs the circuit additional power losses, adding extra volume, weight and cost to the converter. In [19]-[21] common passive components current sharing methods have been proposed to realize an equalized current between the phases. In the common inductor method, the resonant inductors of each phase are connected in parallel to form a common inductor, taking the current of each phase and redistributing it equally. However, having discrete resonant inductors is inevitably required in this

method, integrating them in the transformer is not feasible. The aforementioned methods can minimize the output current ripples, and hence the output capacitor size can be effectively reduced.

3.1.3 Magnetic integration in LLC converter- Literature review:

Integrated magnetics is one of the effective ways to downsize the magnetic components, in which multiple windings are placed on the same magnetic core. In a single-phase LLC converter, it is popular to employ the leakage inductance between the primary and secondary winding of a transformer as a resonant tank inductance. In other words, to integrate the resonant inductor and the magnetizing inductance into the transformer structure. The magnetic integration within the single-phase topology is well documented in the literature [22]-[27]. For instance, in [22]-[26] an integrated magnetic design is proposed to integrate the magnetic components of the converter (Lr, Lm) into one magnetic core. In [27], to improve the power density of the LLC converter, a further passive integration is proposed to integrate all passive components within the resonant tank, including the resonant capacitor Cr, into one single component – an integrated L-L-C-T. However, there is a drawback usually arises while applying magnetic integration techniques. For instance, it is difficult to control the value of the leakage inductance, which is extremely important to be designed precisely because it directly affects the converter gain curve. In [28], it has been revealed that in asymmetric core structures the primary and secondary leakage inductance may not be equal due to their location with respect to air gap.

On the other hand, recently some studies have been proposed to integrate the magnetics of the three phases of multi-phase LLC topologies. For instance, in [29], a customized four limbs core has been utilized, where the air-gap was inserted in the center leg as shown in Fig.3.2 (a). As a result, this converter encountered in-phase triple frequency resonant currents, as shown in Fig.3.3 (a). Inserting air gap in the center leg has led to an increment in the center leg reluctance, and hence a strong coupling between the three-phases occurred. In [30]-[31], Lagrangian dynamics has been employed to mathematically prove that it is possible to integrate the three-discrete transformers into a single core. The purpose of [32], is to propose a magnetic-based current balancing technique to improve the current sharing between the paralleled phases of three-phase LLC transformer with spatial core transformer. The proposed spatial core in this study is shown in Fig.3.2 (b). It has been reported in this study that when the air gaps are inserted in the outer leg, a similar performance to the three-discrete transformers can be realized using the spatial core, as shown in the resonant current waveforms of Fig.3.3 (b). Nonetheless the spatial core has three main drawbacks: i) The core is customized, and not suitable for mass production. ii) It may not be suitable to implement in industrial applications, as it is hard to package a spatial transformer. iii) The center leg unnecessarily utilizes additional magnetic material.

The problem aimed to be tackled is the usage of three-discrete transformers which deteriorate the power density. The novelty of this chapter is integrating the three-transformers into a single magnetic core, which is available in the market and easy to be

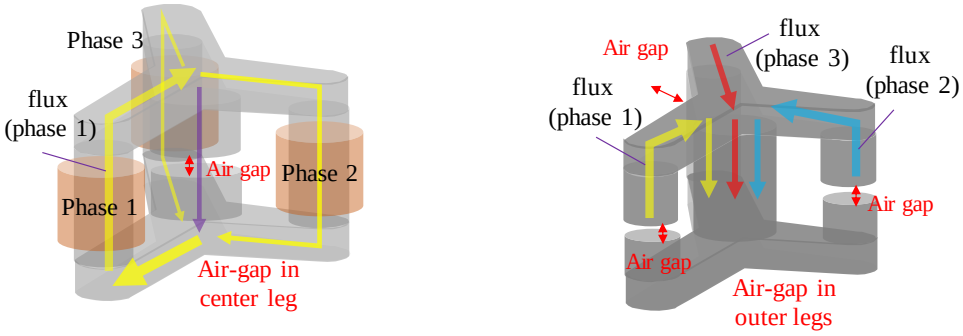

Fig.3.2 Spatial core integrated transformer (a) air-gap in the center leg reported in [29] (b) air-gap in three outer leg reported in [32]

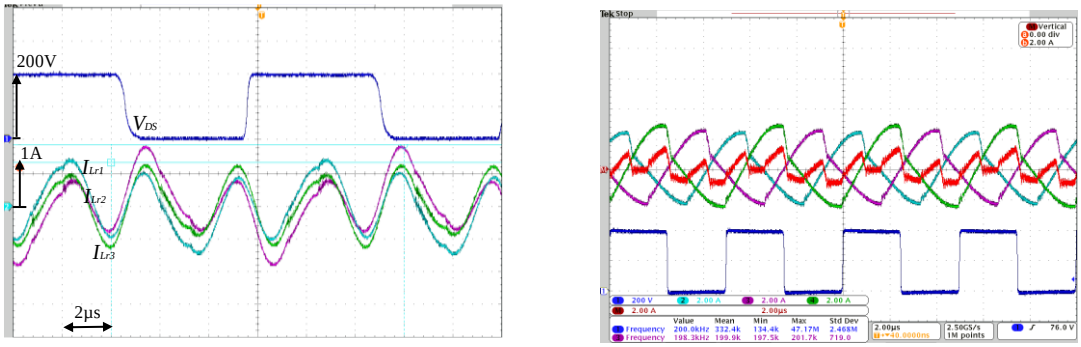

Fig.3.3 Resonant currents (a) In-phase resonant currents due to mutual induction reported in [29] (b) Resonant current and the unbalanced current (red waveform) reported in [32].

implemented by industry engineers and researchers. Furthermore, magnetic design guidelines are provided and a comprehensive magnetic analysis had been done to guide the engineers to have a better understanding of the magnetic behavior of the proposed integrated transformer, supported by a design example and FEA simulations. Moreover, additional experimental tests have been carried out to evaluate the proposed integrated transformer. Implementing the integrated transformer allows for a mass and footprint reduction of the magnetics. Furthermore, it has been proven that using the integrated transformer is efficient and it enables a uniform thermal distribution along the core.

3.1.4 Chapter contents

The following discussion is divided into five sections. Section 3.2 presents the magnetic analysis of the integrated transformer, where the transformer is functioning as resonant and magnetizing inductors of the three-phases utilizing a single magnetic core. Section 3.3 presents a magnetic design example. The proper operation of the proposed integrated transformer is supported by various simulation and experimental tests in section 3.4. In the same section, efficiency and thermal tests have been conducted. Furthermore, the practical merits of employing the integrated transformer over the three-discrete transformers are reported. The summary is presented in section 3.5. Finally, the appendix section is shown in section 3.6.

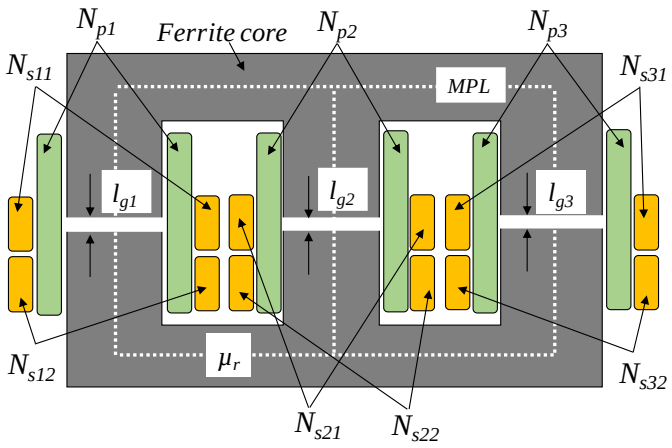

Fig.3.4. Core structure of proposed integrated transformer.

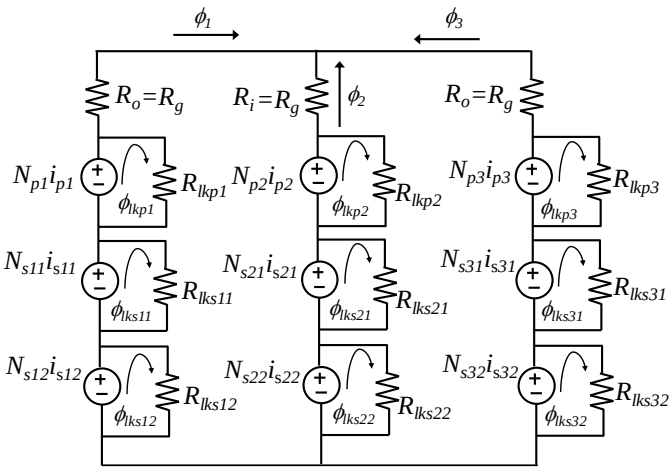

Fig.3.5 Magnetic circuit model for the three-leg integrated transformer.

3.2 Three-phase LLC Integrated Transformer

3.2.1 Magnetic Analysis

Magnetic integration is a technique whereby various inductive and transformer elements are advantageously combined on a single core. In this discussion, the windings of the three phases are advantageously combined into a single magnetic core. The designed magnetizing inductance is achieved, by placing air gaps in the three legs. The leakage inductance can be controlled by varying the distance between the primary and secondary winding on the same leg. An alternative way to alter the leakage is presented in Appendix 3.6.1. The structure of the proposed integrated transformer is shown in Fig.3.4. The primary number of turns of the three phases are N_{p1}, N_{p2}, N_{p3}; and the secondary turns are N_{s11}, N_{s12}, N_{s21}, N_{s22}, N_{s31} and N_{s32}. The magnetic circuit model of the three-leg transformer core is depicted in Fig.3.5. The reluctances of the outer and inner legs are denoted as R_o and R_i, respectively.

The next step is to solve the magnetic circuit, and in order to simplify the analysis, the following assumptions have been made:

a) The external leakage fluxes are ignored. b) For each phase, the two secondary center-tapped windings are assumed to be one winding with number of turns $N_{s1} = N_{s11} = N_{s12}$, $N_{s2} = N_{s21} = N_{s22}$ and $N_{s3} = N_{s31} = N_{s32}$. And currents $i_{s1} = i_{s11} + i_{s12}$, $i_{s2} = i_{s21} + i_{s22}$ and $i_{s3} = i_{s31} + i_{s32}$ for phases one, two and three; respectively. The simplified magnetic circuit model is shown in Table 3.I. The magneto-motive forces follow Kirchhoff's voltage law and the fluxes follow Kirchhoff's current law; therefore, the following expressions can be obtained

$$R_o\phi_1 - R_i\phi_2 = N_{p1}i_{p1} - N_{s1}i_{s1} - N_{p2}i_{p2} + N_{s2}i_{s2} \tag{3.1}$$

$$R_o\phi_1 - R_o\phi_3 = N_{p1}i_{p1} - N_{s1}i_{s1} - N_{p3}i_{p3} + N_{s3}i_{s3} \tag{3.2}$$

$$\phi_1 + \phi_2 + \phi_3 = 0 \tag{3.3}$$

Solving the preceding equations with respect to the fluxes, we obtain

$$\phi_1 = \frac{\left(N_{p1}i_{p1} - N_{s1}i_{s1} - N_{p2}i_{p2} + N_{s2}i_{s2}\right)}{R_o} + \frac{R_i}{R_o}\phi_2 \tag{3.4}$$

$$\phi_3 = \frac{\left(N_{p3}i_{p3} - N_{s3}i_{s3} - N_{p2}i_{p2} + N_{s2}i_{s2}\right)}{R_o} + \frac{R_i}{R_o}\phi_2 \tag{3.5}$$

$$\phi_2 = -\phi_1 - \phi_3 \tag{3.6}$$

Substituting (3.6) in (3.4), (3.5), we obtain

$$\phi_1 = \left[\left(\frac{1+\alpha}{1+2\alpha}\right)\frac{N_{p1}i_{p1} - N_{s1}i_{s1}}{R_o} - \left(\frac{1}{1+2\alpha}\right)\frac{N_{p2}i_{p2} - N_{s2}i_{s2}}{R_o} - \left(\frac{\alpha}{1+2\alpha}\right)\frac{N_{p3}i_{p3} - N_{s3}i_{s3}}{R_o}\right] \tag{3.7}$$

$$\phi_2 = \left[\left(\frac{2}{1+2\alpha}\right)\frac{N_{p2}i_{p2} - N_{s2}i_{s2}}{R_o} - \left(\frac{1}{1+2\alpha}\right)\frac{N_{p1}i_{p1} - N_{s1}i_{s1}}{R_o} - \left(\frac{1}{1+2\alpha}\right)\frac{N_{p3}i_{p3} - N_{s3}i_{s3}}{R_o}\right] \tag{3.8}$$

$$\phi_3 = \left[\left(\frac{1+\alpha}{1+2\alpha}\right)\frac{N_{p3}i_{p3} - N_{s3}i_{s3}}{R_o} - \left(\frac{1}{1+2\alpha}\right)\frac{N_{p2}i_{p2} - N_{s2}i_{s2}}{R_o} - \left(\frac{\alpha}{1+2\alpha}\right)\frac{N_{p1}i_{p1} - N_{s1}i_{s1}}{R_o}\right] \tag{3.9}$$

Where α is a reluctance ratio factor $\alpha = \left(R_i / R_o\right)$. We propose a relevant coupling factors k_1, k_2 and k_3, where:

$$k_1 = \left(\frac{1+\alpha}{1+2\alpha}\right) \tag{3.10}$$

$$k_2 = \left(\frac{1}{1+2\alpha}\right) \tag{3.11}$$

$$k_3 = \left(\frac{\alpha}{1+2\alpha}\right) \tag{3.12}$$

Thereby (3.7), (3.8) and (3.9) can be rewritten as

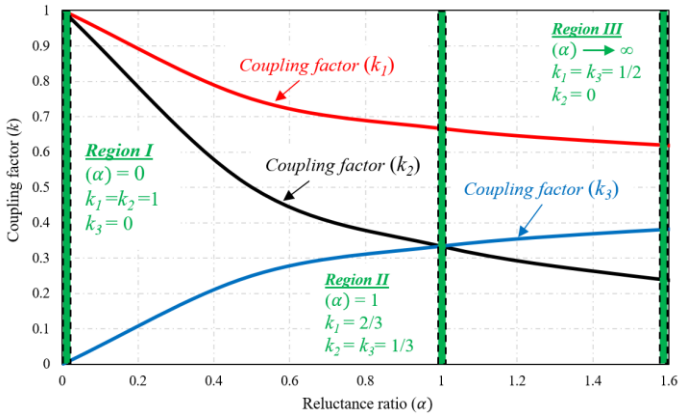

Fig.3.6 Relationship between coupling factors and reluctance ratio α.

$$\phi_1 = \left[k_1 \frac{N_{p1} i_{p1} - N_{s1} i_{s1}}{R_o} - k_2 \frac{N_{p2} i_{p2} - N_{s2} i_{s2}}{R_o} - k_3 \frac{N_{p3} i_{p3} - N_{s3} i_{s3}}{R_o} \right] \quad (3.13)$$

$$\phi_2 = \left[2k_2 \frac{N_{p2} i_{p2} - N_{s2} i_{s2}}{R_o} - k_2 \frac{N_{p1} i_{p1} - N_{s1} i_{s1}}{R_o} - k_2 \frac{N_{p3} i_{p3} - N_{s3} i_{s3}}{R_o} \right] (3.14)$$

$$\phi_3 = \left[k_1 \frac{N_{p3} i_{p3} - N_{s3} i_{s3}}{R_o} - k_2 \frac{N_{p2} i_{p2} - N_{s2} i_{s2}}{R_o} - k_3 \frac{N_{p1} i_{p1} - N_{s1} i_{s1}}{R_o} \right] (3.15)$$

The proposed relevant coupling factors (k_1, k_2 and k_3) have a direct relationship with the reluctance ratio (α). This relationship is shown in Fig.3.6. This chart represents three important regions, in which the reluctance ratio varies from a small to higher values. The three regions are well described in Table 3.I. The equations describing the magnetic behavior of the integrated transformer in the three regions are listed in details in Table 3.I.

In this discussion, the design is based on region II, this is to realize a symmetry between the three-phases, and therefore, *ac* flux cancellation can be obtained. Moreover, in region II, a similar number of turns among the phases can be realized, since the reluctance of the three legs are equal. This is to achieve an equalized value of magnetizing inductance among the phases, which is necessary for the ZVS operation for the three-phase LLC resonant converter.

3.2.2 Flux Density Equations

The design methodology of a transformer incorporated in LLC resonant converter is different from conventional transformer. In the conventional transformer the leakage inductance is unavoidable and undesirable. However, in LLC resonant cconverter, the transformer's leakage inductance is unavoidable but desirable, and in many designs the leakage is intentionally increased, since it functions as a resonant inductance and it shall be precisely designed for a proper operation for the converter. The value of the leakage inductance is controlled by changing the distance between the primary and secondary windings. On the other hand, the transformer's magnetizing inductance shall be designed carefully to achieve ZVS for the LLC converter. In this regards, the magnetizing inductance is controlled by placing air gaps in the transformer legs.

Usually, the transformer is designed to operate below the saturation, the maximum flux density can be obtained from Faraday's law as follows

$$V_{inT-i} = N_{pi} \frac{\phi_i}{T_{on}} \tag{3.16}$$

Where V_{inT}, N_p, ϕ_i and T_{on} are the applied voltage on the transformer primary winding, primary number of turns, peak-to-peak flux and switching on-time, respectively. i = [1, 2, 3] and it denotes for the phase number. Since the generated flux is only *ac* flux, the maximum flux can be expressed as half the peak-to-peak flux as follows

$$\phi_{m-i} = \frac{1}{2} \frac{V_{inT-i}.d.T_s}{N_{pi}} \tag{3.17}$$

Where ϕ_m, d, and T_s are the maximum flux, switching devices duty cycle and cycle time, respectively. The maximum flux density can be expressed as

TABLE 3.I
THE MAGNETIC BEHAVIOR OF THE INTEGRATED TRANSFORMER

	Region I	Region II	Region III
Simplified magnetic circuit model	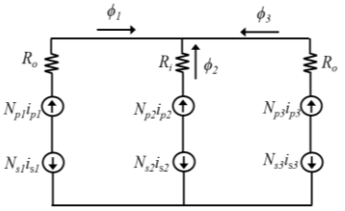		
Reluctance ratio	$R_o \rangle\rangle R_i$	$R_o = R_i = R$	$R_o \langle\langle R_i$
α	0	1	HIGH
k_1 ,k_2 ,k_3	1, 1, 0	2/3, 1/3, 2/3	0.5, 0, 0.5
Peak-to-peak flux in outer leg (phase 1)	$\phi_1 = \left[\frac{N_{p1}i_{p1} - N_{s1}i_{s1}}{R_o} - \frac{N_{p2}i_{p2} - N_{s2}i_{s2}}{R_o} \right]$	$\phi_1 = \left[\frac{2}{3}\frac{N_{p1}i_{p1} - N_{s1}i_{s1}}{R_o} - \frac{1}{3}\frac{N_{p2}i_{p2} - N_{s2}i_{s2}}{R_o} - \frac{1}{3}\frac{N_{p3}i_{p3} - N_{s3}i_{s3}}{R_o} \right]$	$\phi_1 = \left[\frac{1}{2}\frac{N_{p1}i_{p1} - N_{s1}i_{s1}}{R_o} - \frac{1}{2}\frac{N_{p3}i_{p3} - N_{s3}i_{s3}}{R_o} \right]$
Peak-to-peak flux in inner leg (phase 2)	$\phi_2 = \left[2\frac{N_{p2}i_{p2} - N_{s2}i_{s2}}{R_o} - \frac{N_{p1}i_{p1} - N_{s1}i_{s1}}{R_o} - \frac{N_{p3}i_{p3} - N_{s3}i_{s3}}{R_o} \right]$	$\phi_2 = \left[\frac{2}{3}\frac{N_{p2}i_{p2} - N_{s2}i_{s2}}{R_o} - \frac{1}{3}\frac{N_{p1}i_{p1} - N_{s1}i_{s1}}{R_o} - \frac{1}{3}\frac{N_{p3}i_{p3} - N_{s3}i_{s3}}{R_o} \right]$	$\phi_2 = 0$
Peak-to-peak flux in outer leg (phase 3)	$\phi_3 = \left[\frac{N_{p3}i_{p3} - N_{s3}i_{s3}}{R_o} - \frac{N_{p2}i_{p2} - N_{s2}i_{s2}}{R_o} \right]$	$\phi_3 = \left[\frac{2}{3}\frac{N_{p3}i_{p3} - N_{s3}i_{s3}}{R_o} - \frac{1}{3}\frac{N_{p2}i_{p2} - N_{s2}i_{s2}}{R_o} - \frac{1}{3}\frac{N_{p1}i_{p1} - N_{s1}i_{s1}}{R_o} \right]$	$\phi_3 = \left[\frac{1}{2}\frac{N_{p3}i_{p3} - N_{s3}i_{s3}}{R_o} - \frac{1}{2}\frac{N_{p1}i_{p1} - N_{s1}i_{s1}}{R_o} \right]$
Equivalent reluctance (phase 1)	$R_{eq1} = R_o + \frac{R_i.R_o}{R_i. + R_o} \approx R_o$	$R_{eq1} = R + \frac{R.R}{R+R} = \frac{3}{2}R$	$R_{eq1} = R_o + \frac{R_i.R_o}{R_i. + R_o} \approx 2R_o$
Equivalent reluctance (phase 2)	$R_{eq2} = \frac{R_o}{2} + R_i \approx \frac{R_o}{2}$	$R_{eq2} = R + \frac{R.R}{R+R} = \frac{3}{2}R$	$R_{eq2} = \frac{R_o}{2} + R_i \approx R_i$
Equivalent reluctance (phase 3)	$R_{eq3} = R_o + \frac{R_i.R_o}{R_i. + R_o} \approx R_o$	$R_{eq3} = R + \frac{R.R}{R+R} = \frac{3}{2}R$	$R_{eq3} = R_o + \frac{R_i.R_o}{R_i. + R_o} \approx 2R_o$

$$B_{m-i} = \frac{\phi_{m-i}}{A_{c-i}} = \frac{1}{2}\left[\frac{V_{inT-i}.d}{N_{pi}.f_s.A_{c-i}}\right] \quad (3.18)$$

Where B_m, A_c and f_s are the maximum flux density, the core cross section area and switching frequency. The primary switches operate with a fixed duty cycle (d = 0.5). It worth mentioning that the switching duty cycle shall be replaced by an effective duty cycle "d_{eff}" when it comes to relating the maximum flux density with the reflected secondary voltage and the secondary number of turns, in LLC converter working below resonance. The effective duty cycle equals the switching duty cycle ($d_{eff} = d_s = 0.5$) when the converter operates at the normalized frequency $f_n = 1$ (i.e the switching frequency = resonance frequency), in which the secondary diodes are continuously conducting and the secondary voltage is clamped to the magnetizing inductance. Nonetheless, for operation below the resonant frequency, which is the case in this discussion, the secondary devices stop conducting before the end of the switching half-cycle, therefore, the voltage across the magnetizing inductance is no longer clamped to the primary reflected output voltage. The maximum flux density in each leg of the integrated transformer can be expressed as

$$B_{m-1} = \frac{1}{2}\left[\frac{V_o.d_{eff}}{N_{s1}.f_s.A_o}\right] \quad (3.19)$$

$$B_{m-2} = \frac{1}{2}\left[\frac{V_o.d_{eff}}{N_{s2}.f_s.A_i}\right] \quad (3.20)$$

$$B_{m-3} = \frac{1}{2}\left[\frac{V_o.d_{eff}}{N_{s3}.f_s.A_o}\right] \quad (3.21)$$

Where A_o, A_i and d_{eff} are the cross section area of the outer leg, inner leg of the magnetic core and the effective duty cycle, respectively. The derivation of the effective duty cycle can be obtained as follows:

When the LLC converter operates below resonance, each half of the switching cycle contains a power delivery operation, at which the magnetizing current is lower than the resonant current, this period can be estimated as (T_r/2), as shown in Fig.3.7. As the resonant current equals the magnetizing current the secondary diodes stop to conduct, and the primary reflected secondary voltage is no longer clamped to the magnetizing inductance. The effective duty cycle can be expressed as

$$d_{eff} = d_s - d_{nc} \quad (3.22)$$

Where d_{eff}, d_s, and d_{nc} are the effective duty cycle, the switching duty cycle (d_s = 0.5), and the duty cycle at which there is no conduction through the secondary rectifiers.

The time where there is no conduction through the secondary rectifiers for each half-cycle can be determined as

$$T_{nc} = \frac{T_s}{2} - \frac{T_r}{2} = \frac{1}{2}\left(\frac{1}{f_s} - \frac{1}{f_r}\right) \quad (3.23)$$

The duty cycle d_{nc} can be denoted as

$$d_{nc} = d_s \frac{\frac{1}{2}\left(\frac{1}{f_s} - \frac{1}{f_r}\right)}{\frac{1}{2 f_s}} \qquad (3.24)$$

The duty cycle in which there is no conduction through the secondary rectifiers can be further simplified as

TABLE 3.II
Design Example.

	Three-discrete Transformers	Integrated Transformer (Design based on Region 2)
Magnetic core topology	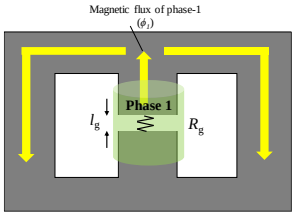 *Each phase consists of highly-coupled primary and secondary windings.	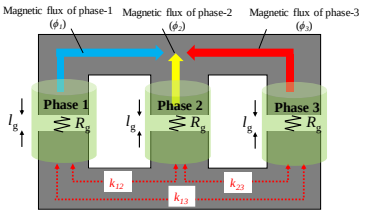 *Each phase consists of highly-coupled primary and secondary windings.
A. Material selection	Ferrite, Mn-Zn PC40	Ferrite, Mn-Zn PC40
B. Area product	A_p = 1.55 x 2.4 = 3.72 cm^4 > 2 cm^4	A_p = 6.4 x 2.8 = 17.9 cm^4 > 1.38 cm^4
C. Core selection	3 x (PC40 EER42/42/20-Z)	1 x (PC40 EC70x69x16)
D. Transformer turns ratio	$N = \frac{N_p}{N_s} = \frac{V_i/2}{V_o + V_f} = \frac{390/2}{12 + 0.82} = 15.2 \approx 16$	$N = \frac{N_p}{N_s} = \frac{V_i/2}{V_o + V_f} = \frac{390/2}{12 + 0.82} = 15.2 \approx 16$
E. Effective permeability [H/m]	$\mu_{eff} = \frac{L_m MPL}{\mu_o N_p^2 A} = \frac{(132x10^{-6})(0.099)}{(4\pi x10^{-7})(32)^2(2.4x10^{-4})} = 42$	$\mu_{eff} = \frac{L_m MPL}{\mu_o N_p^2 A} = \frac{(132x10^{-6})(0.144)}{(4\pi x10^{-7})(32)^2(2.8x10^{-4})} = 53$
F. Magnetic reluctance and the air gap Length	$R_{eq} = R_c + R_g \approx R_g$ $R_{eq} = \frac{MPL}{\mu_r \mu_o A_c} + \frac{l_g}{\mu_o A_c} = \frac{MPL}{\mu_o A_c}\left[\frac{1}{\mu_r} + \frac{l_g}{MPL}\right]$ $\mu_{eff} = \frac{1}{\frac{1}{\mu_r} + \frac{l_g}{MPL}} \approx \frac{MPL}{l_g}$ $l_g = \frac{MPL}{\mu_{eff}} = \frac{0.099}{42} = 2.35mm$ $R_{eq} = \frac{0.099}{4\pi x10^{-7}(2.4x10^{-4})}\left[\frac{1}{2500} + \frac{2.35x10^{-3}}{0.099}\right] = 7757477H^{-1}$	$R_{eq} = R_c + R_g + \frac{R_g}{2} = R_c + \frac{3}{2}R_g \approx \frac{3}{2}R_g$ $R_{eq} = \frac{MPL}{\mu_r \mu_o A_c} + \frac{3}{2}\frac{l_g}{\mu_o A_c} = \frac{MPL}{\mu_o A_c}\left[\frac{1}{\mu_r} + \frac{3}{2}\frac{l_g}{MPL}\right]$ $\mu_{eff} = \frac{1}{\frac{1}{\mu_r} + \frac{3}{2}\frac{l_g}{MPL}} \approx \frac{2}{3}\frac{MPL}{l_g}$ $l_g = \frac{2}{3}\frac{MPL}{\mu_{eff}} = \frac{2}{3}\frac{0.144}{53} = 1.8mm$ $R_{eq} = \frac{0.144}{4\pi x10^{-7}(2.8x10^{-4})}\left[\frac{1}{2500} + \frac{3}{2}\frac{1.8x10^{-3}}{0.144}\right] = 7837244H^{-1}$
G. Designed value of Magnetizing inductance	$L_m = \frac{N^2}{R} = \frac{(32)^2}{7757477} = 132\mu H$	$L_m = \frac{N^2}{R} = \frac{(32)^2}{7837244} = 131\mu H$
H. Flux density (B_m) *[based on the effective cross section area of the core]*	$B_m = \frac{1}{2}\left[\frac{12x0.465}{2x225x10^3 x2.4x10^{-4}}\right] = 0.026T$	$B_m = \frac{1}{2}\left[\frac{12x0.445}{2x165x10^3 x2.8x10^{-4}}\right] = 0.029T$ The outer leg cross section area =1.5cm^2, therefore the maximum flux in the outer leg is $B_{m\_outer} = \frac{1}{2}\left[\frac{12x0.445}{2x165x10^3 x1.5x10^{-4}}\right] = 0.054T$
I. Reluctance Factor (α)	Not applicable.	$\alpha = \frac{R_i}{R_o} = \frac{R_g}{R_g} = 1$

$$d_{nc} = d_s\left(1-\frac{f_s}{f_r}\right) \tag{3.25}$$

The effective duty cycle can be expressed by substituting (3.25) in (3.22) as

$$d_{eff} = d_s - d_s\left(1-\frac{f_s}{f_r}\right) \tag{3.26}$$

Equation (3.26) can be further simplified as

$$d_{eff} = \frac{f_s}{2f_r} = \frac{f_n}{2} \tag{3.27}$$

It is noticeable that when the when the primary switches are driven with a frequency equals to the resonance ($f_n = 1$), the duty cycle $d_{nc} = 0$. In this case, the effective duty cycle equals the switching duty cycle ($d_{eff} = d_s = 0.5$).

3.3 Design Example

The integrated transformer is intended to be utilized in a 500W three-phase LLC resonant converter. This LLC converter is 390V/12V step down converter. The specifications of this converter are tabulated in table V. The desired gain is shown in Fig.3.8 and calculated as follows

$$M_g = \frac{N_p}{N_s}\frac{(V_o+V_f)}{(V_i/2)} = 16\frac{(12+1.08)}{(390/2)} = 1.07 \tag{3.28}$$

Where V_i, V_o, and V_f are the input voltage, output voltage, and secondary diode voltage drop; respectively. The gain curve of the three-phase LLC converter had been calculated and drawn in this discussion based on the derivation of FHA circuit presented in [18]. In LLC resonant converter the gapped transformer operates with high frequency current variation, resulting large B-H loop and high core losses. Therefore, the maximum flux density must be limited by the core losses rather than the saturation. Ferrite material is suitable for such application, and Mn-Zn PC40 with a situation flux density of 0.38T has been selected for that purpose. The magnetic core has selected based on the area product. Area product is defined as the product of core window area W_a and cross section area A_c. The area product can be interpreted as an indication of how the selected core can handle the magnetic energy with a permissible temperature rise, and it can be calculated in a unit of [cm^4] as follows [33]

$$A_p = \left[\frac{\sqrt{k_u}L_m I_{m\_\max} I_{r\_rms}}{B_{\max} k_u K_t \sqrt{\Delta T}}\right]^{\frac{8}{7}} x10^8 \tag{3.29}$$

TABLE 3.III
MEASURED VALUES OF THE THREE-DISCRETE TRANSFORMERS

Parameters	Transformer No.1	Transformer No.2	Transformer No.3
Magnetic core	3 cores (PC40 EER42/42/20-Z)		
Open circuit test	157 µH	146.8 µH	149.2 µH
Resonance inductance L_r	20 µH	24.2 µH	21.5 µH
Magnetizing inductance L_m	137 µH	122.6 µH	127.7 µH
Number of Turns	32:2:2	32:2:2	32:2:2

TABLE 3.IV
MEASURED VALUES OF THE INTEGRATED TRANSFORMER

Parameters	Phase No.1	Phase No.2	Phase No.3
Magnetic core	1 core (PC40 EC70x69x16)		
Open circuit test	160.3 µH	158.4 µH	156.7 µH
Resonance inductance L_r	34.5 µH	34 µH	35.3 µH
Magnetizing inductance L_m	125.8 µH	124.4 µH	121.4 µH
Number of Turns	32:2:2	32:2:2	32:2:2

(a)

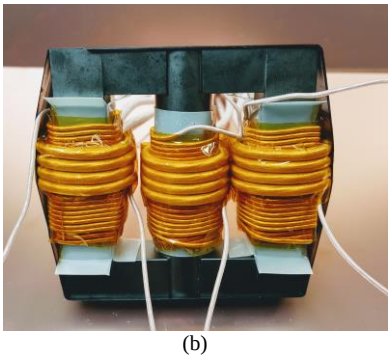

(b)

Fig.3.9 The three discrete transformers and the integrated transformer.

The window utilization factor, K_u, is defined as the ratio of the total conduction area W_c, for all conductors to the total window area W_a. ($K_u = W_c / W_a$).

The window area W_a of PC40 EC70x69x16 is = 6.4 cm^2 and the total area of the primary windings is 0.628x32= 20mm^2=0.2cm^2 and the secondary winding is 3.8x4=15.2 mm^2 =0.15cm^2. However,

TABLE 3.V
DESIGN SPECIFICATIONS FOR THE LLC RESONANT CONVERTER WITH INTEGRATED TRANSFORMER

Symbol	Quantity	Value
P_o	Output power	500 W
V_i	Input voltage	390 V
V_o	Output voltage	12 V
f_s	Switching frequency range	165kHz - 230kHz
C_{r1}, C_{r2}, C_{r3}	Resonant capacitance	22 *n*F
N	Turns ratio	16

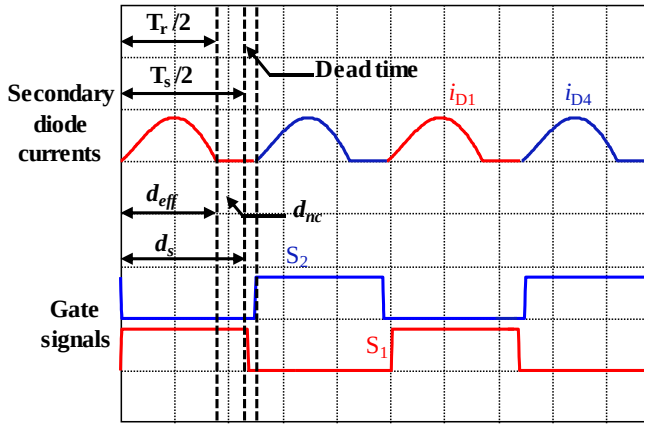

Fig.3.7 Secondary rectified current waveforms for one phase.

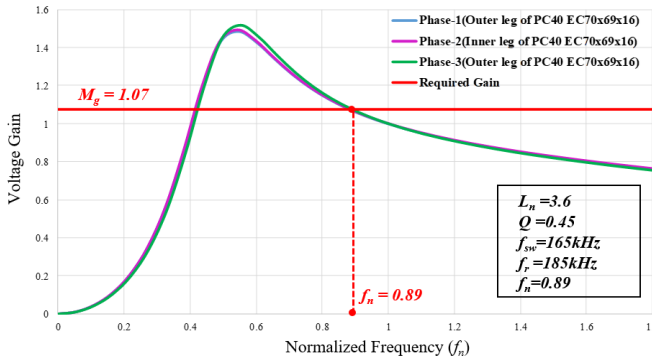

Fig.3.8 Voltage gain curve of three-phase LLC with integrated transformer.

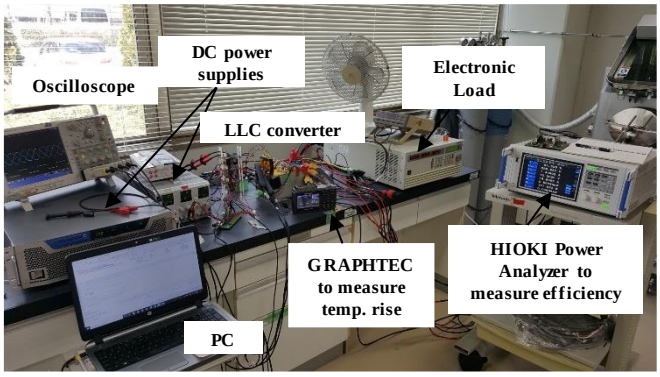

Fig.3.10 Experimental environment.

within the integrated transformer one window is shared between two phases, therefore the winding utilization factor K_u= (2x0.2+2x0.15)/6.4 = 0.1. In case of the three discrete transformers, K_u= (0.2+0.15)/1.55 = 0.22. A lower value of window utilization factor improves the thermal performance of the integrated transformer, as shown in the thermal evaluation results in section 3.4.4.

Maximum flux density in the outer leg is calculated in Table. 3.II as 0.054T for the integrated transformer. K_t is a constant and equals $48.2x10^3$. Therefore, the area product equals

$$A_p = \left[\frac{(\sqrt{0.1})(132x10^{-6})(1.82)(2.5)}{(0.054)(0.1)(48.2x10^3)\sqrt{30}} \right]^{\frac{8}{7}} x10^8 = 1.38cm^4 \qquad (3.30)$$

In case of the three discrete transformers

$$A_p = \left[\frac{(\sqrt{0.22})(132x10^{-6})(1.82)(2.5)}{(0.026)(0.22)(48.2x10^3)\sqrt{30}} \right]^{\frac{8}{7}} x10^8 = 2cm^4 \qquad (3.31)$$

The area product calculation helps us to evaluate the magnetic energy handling capability of the two transformer prototypes. In other words, the core which has higher area product value indicates that it can handle the same magnetic energy with less temperature rise, than a core with lower area product value [33]-[34]. In this context, the window area and the cross-section area of PC40 EC70x69x16 are W_a = 6.4 cm^2 and A_c = 2.8 cm^2, respectively, leading to an area product of A_p = 17.9 cm^4. Whereas, the window area and the cross-section area of PC40 EER42/42/20-Z are W_a = 1.55 cm^2 and A_c = 2.4 cm^2, respectively, yield to an area product of A_p = 3.72cm^4 for the three discrete cores. Therefore, both cores are suitable. However, it worth mentioning that, as the area product of the integrated transformer is much bigger, it has a better thermal performance compared with the three-discrete transformer, as shown later in section 3.4.4.

The primary number of turns are calculated to be 32 turns, and the secondary number of turns are calculated to be 2 turns. The effective permeability is calculated to equal 53H/m. Litz wires have been utilized, and their cross-section area is 0.628mm^2, 3.8mm^2 for the primary and secondary windings, respectively.

In order to achieve a soft switching operation for the LLC converter, the effective permeability of the magnetic core shall be intentionally minimized. Therefore, the magnetic core transfers the power to the secondary side, and store energy in the air gap to discharge the steady state output capacitance of the primary switches during the dead time [35].

Reducing the value of effective permeability can be realized by inserting air gap in the Ferrite core. The parameters of the two prototypes are calculated and depicted in Table 3.II. The magnetic cores of the three-discrete transformers and the integrated transformer are shown in Fig.3.9. The experimental setup is shown in Fig.3.10.

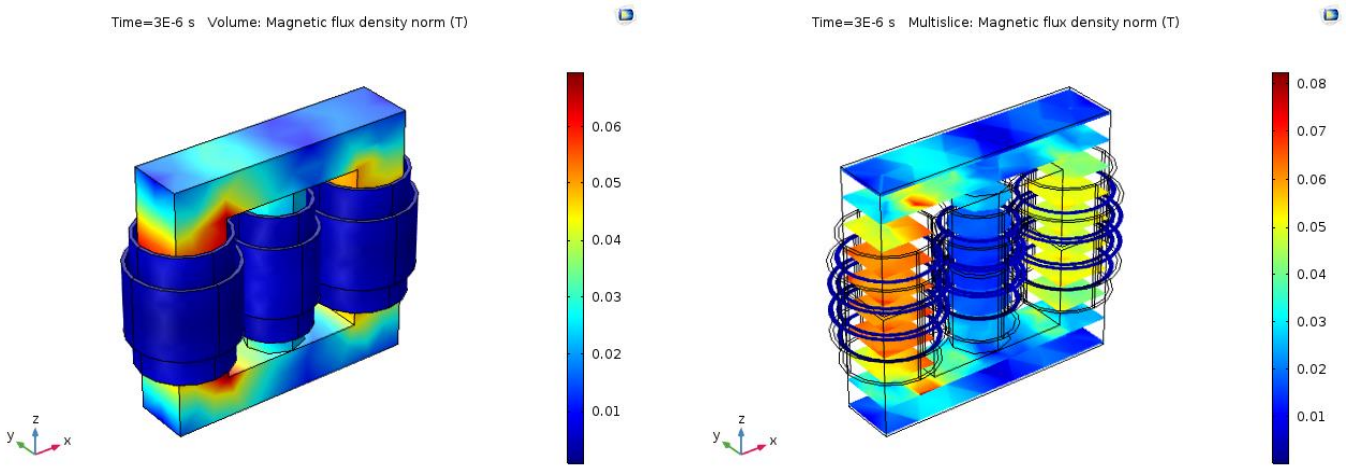

Fig.3.11 FEA simulations of the proposed integrated transformer.

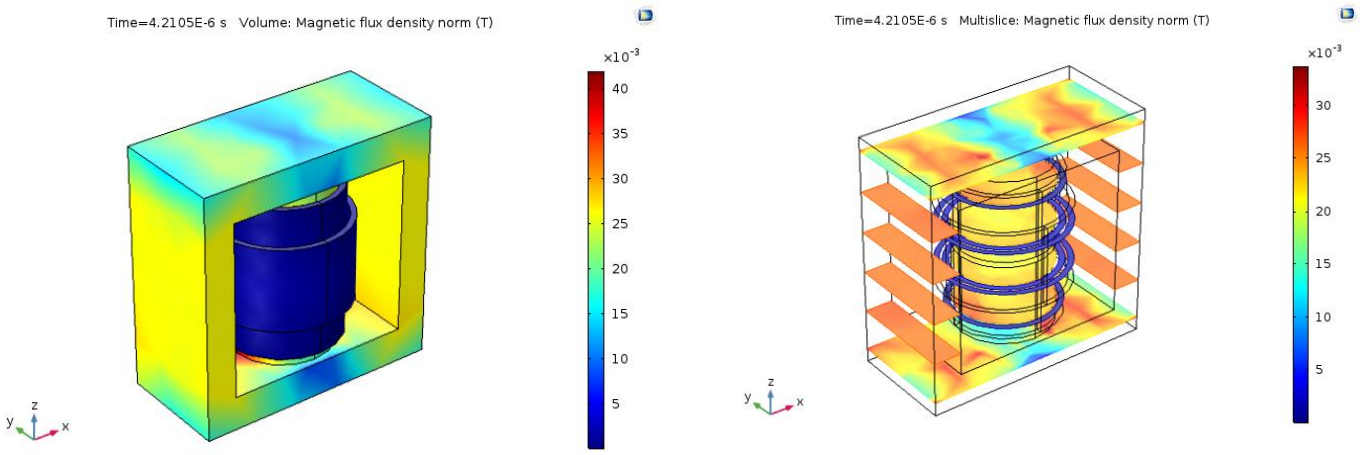

Fig.3.12 FEA simulations of single transformer out of the three discerte transformers.

3.4 Simulation Tests, Experimental Evaluation and Power Losses Distribution

3.4.1 FEA Simulation

This subsection presents the Finite Element Analysis (FEA) for the proposed EC70 integrated transformer, alongside with the EER42 core utilized for the three discrete transformers.

The simulation parameters are listed in Table 3.III and Table 3. IV. The electromagnetic simulation was carried out using COSMOL Multiphysics software. The simulation results for the integrated transformer is shown in Fig.3.11, this figure was captured at fraction of second where phase-3 has it is maximum value of flux density, while the flux density in the other two phases have lower value. The simulation for a single transformer out of the three units is depicted in Fig.3.12 (b).

Low magnetic flux density can be observed from the simulation results, since there is no DC biased magnetization, and the transformers operate with purely high frequency ac currents. The magnetic flux density values are consistent with the theoretical calculation of the design example shown in Table 3.II.

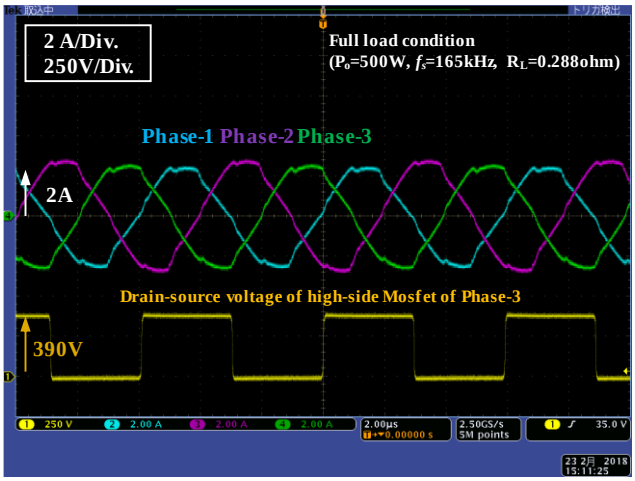

(a)

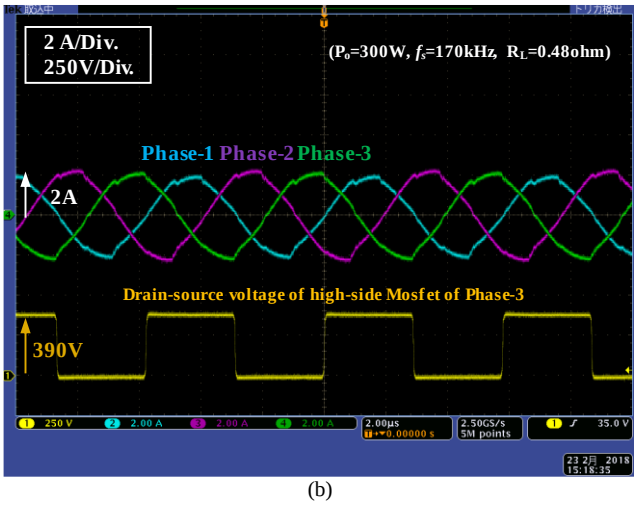

(b)

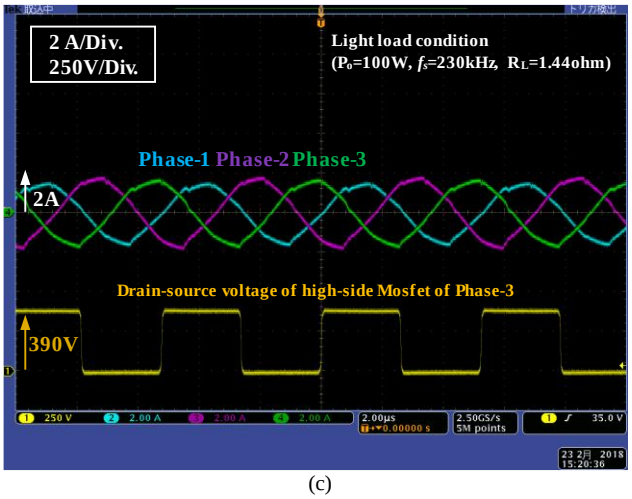

(c)

Fig.3.13 The resonant current waveforms for the integrated transformer. (a) full load condition 500W. (b) 300W condition. (c) 100W output power.

3.4.2 Experimental Environment and Results

In order to evaluate the proper operation of the three-phase LLC resonant converter with the three-legged integrated transformer, the converter was constructed and experimentally tested. The LLC prototype uses Schottky diodes (VS-100BGQ100), primary Mosfets (Toshiba, TK20E60W). Texas Instruments DSP is used to drive the primary switches. The three-legged integrated transformer can be implemented with different magnetic core

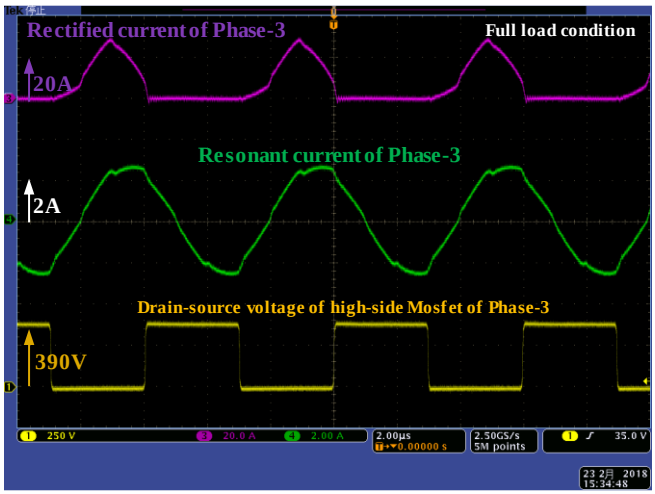

(a)

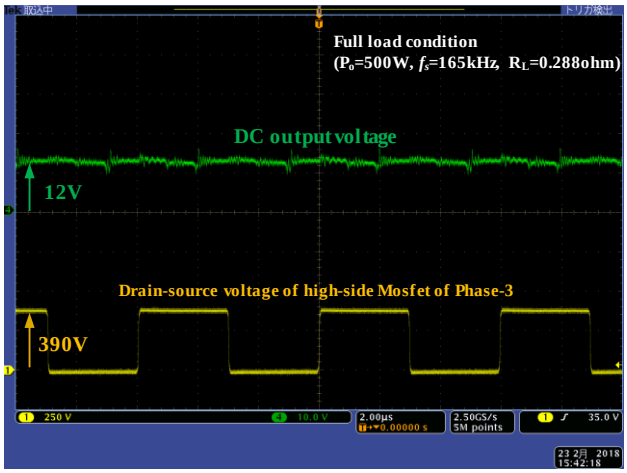

(b)

Fig.3.14 Experimental waveforms. (a) Phase-3 resonant and rectifier current with the drain-source voltage of the high-side. (b) dc output voltage.

structures, in this discussion we utilized ferrite core, PC40 EC70x69x16. The measured parameters of the three discrete transformers are listed in Table 3.III, where three magnetic cores of PC40EER42/42/20-Z are utilized. The measured parameters of the integrated transformer are listed in Table 3.IV.

The experimental results are shown in this section to show the proper operation of the power converter. Fig.3.13 (a) shows the resonant current with and drain-source voltage, where the integrated transformer is utilized and the converter operates at full load condition (i.e P_o=500W, V_o=12V, I_o=41.67, and f_s =165kHz). In Fig.3.13 (b) shows the waveforms during (P_o=300W, V_o=12V, I_o=25, and f_s =170kHz). The light load condition is presented in Fig.3.13 (c) where (P_o=100W, V_o=12V, I_o=8.3, and f_s =230kHz). Fig.3.14 (a) shows the rectified current, resonant current, drain-source voltage of on phase-3. The *DC* output voltage is shown in Fig.3.14 (b). The integrated transformer is connected into star connection helps to suppress the current unbalance which arises from the uneven resonant tank parameters.

It worth mentioning that the resonant current waveform becomes pure sinusoidal only when the frequency of resonant tank equals the switching frequency (i.e $f_n = 1$). However, usually the LLC converter operates in the below resonance region to realize soft switching operation. A feature of the operating below resonance is that the resonant current reaches the value of the magnetizing current before the end of the half-cycle. Therefore, the magnetizing current imposes some distortion to the pure sinusoidal waveform, as in this discussion $f_n = 0.89$ at full load condition.

3.4.3 Efficiency

In this section, the efficiency measurements are presented for both the integrated transformer and the three-discrete transformers. The efficiency evaluation had been conducted using HIOKI PW6001 Power Analyzer. The efficiency tests were conducted at several power output levels, in particular: 100W, 200W, 300W, 400W, and 500W. The input voltage was fixed at 390V and output voltage at 12V. The measurements are tabulated in Table 3.VI and Table 3.VII. The maximum efficiency of the LLC utilizing the integrated transformer is 91%, while the three-discrete transformers could achieve a maximum efficiency of 90.1%, as shown in Fig.3.15.

The core loss of the integrated transformer is disclosed in section 3.4.6 to be lower than the sum of the core loss in three discrete transformers. However, as the transformer maximum flux density is relatively low in this LLC converter, the core loss contribution into the total converter loss can be considered small, in both prototypes. The major power loss is originated in the secondary rectifiers due to the high value of output current. Furthermore, the three discrete transformers prototype has a higher copper loss in the transformer windings, because the windings has higher ac resistance, as the switching frequency of the three transformers prototype is higher than the integrated transformer's prototype. The power loss breakdown is presented in more details in section 3.4.6.

TABLE 3.VI
Efficiency measurements for the LLC resonant converter utilizing single PC40 EC70x69x16 integrated transformer

	Inductor average current 6A								
	Input Power	Input Voltage	Input current	Switching Frequency	Output Power	Output Voltage	Output current	Power Losses	Efficiency
P_o = 500W	550.8W	390V	1.41A	165kHz	500W	12.01V	41.67A	49.8W	90.95%
P_o = 400W	442.8W	390V	1.14A	167kHz	400W	12.07V	33.33A	40.1W	91%
P_o = 300W	334.8W	390V	0.86A	170kHz	300W	12.1V	25A	33.5W	90.8%
P_o = 200W	219.5W	390V	0.56A	187kHz	200W	11.95V	16.67A	20.9W	90.5%
P_o = 100W	111.4W	390V	0.285A	230kHz	100W	11.9V	8.3A	12.7W	88.6%

* This evaluation has been done using HIOKI PW6001 Power Analyzer and the electronic load was current controlled.

TABLE 3.VII
Efficiency measurements for the LLC resonant converter utilizing three PC40EER42/42/20-Z transformers

	Inductor average current 6A								
	Input Power	Input Voltage	Input current	Switching Frequency	Output Power	Output Voltage	Output current	Power Losses	Efficiency
P_o = 500W	568W	390V	1.46A	225kHz	500W	12.1V	41.67A	59.4W	89.7%
P_o = 400W	452W	390V	1.15A	236kHz	400W	12.1V	33.33A	44.7W	90.1%
P_o = 300W	340.9W	390V	0.87A	246kHz	300W	12.1V	25A	33.3W	90.2%
P_o = 200W	224.9W	390V	0.58A	275kHz	200W	12.1V	16.67A	23.2W	89.7%
P_o = 100W	114W	390V	0.29A	335kHz	100W	12V	8.3A	14W	87.67%

* This evaluation has been done using HIOKI PW6001 Power Analyzer and the electronic load was current controlled.

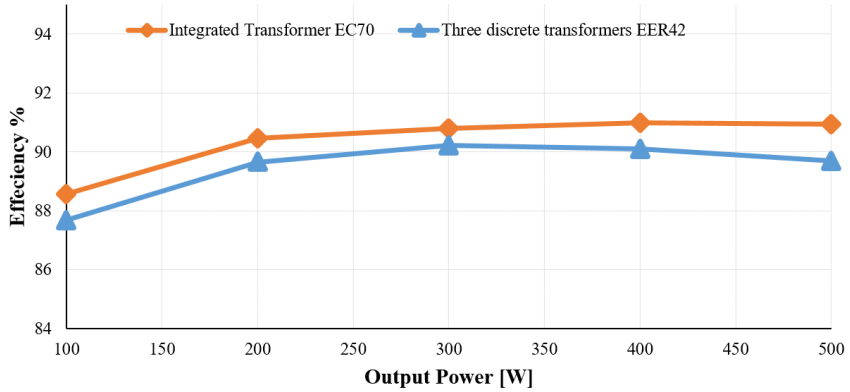

Fig.3.15 Efficiency measurements for the integrated transformers and the three-discrete transformers.

3.4.4 Thermal Performance

An important aspect to consider while evaluating the integrated transformer is to evaluate its thermal performance. The core temperature rise was tested experimentally using Graphtec, midi logger GL240. No external fans have been used while conducting this thermal measurement test.

The first three minutes are left without operating the converter to measure the ambient temperature of our power electronics laboratory. Then the temperature rise test lasts for 1 hour. The device was set to capture 1 sample each 2 seconds. Therefore, the total number of samples is 1800 samples. The temperature rise of the integrated transformer is depicted in Fig.3.16, and for the three-transformers the temperature rise is shown in Fig.3.17. Furthermore, we used FLIR thermal imaging camera to capture the thermal image of the both transformer configurations. The thermal image of the integrated transformer is depicted in Fig.3.18, and for the three-discrete transformers are shown in Fig.3.19. In case of the integrated transformer, the maximum winding temperature is around 40^{o}C and the core temperature saturates at around 37^{o}C.

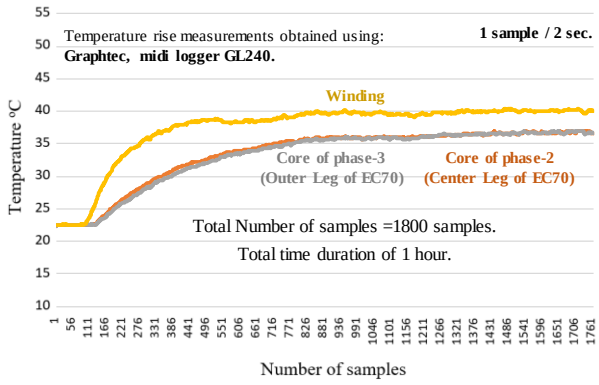

Fig.3.16 Temperature rise of integrated transformer.

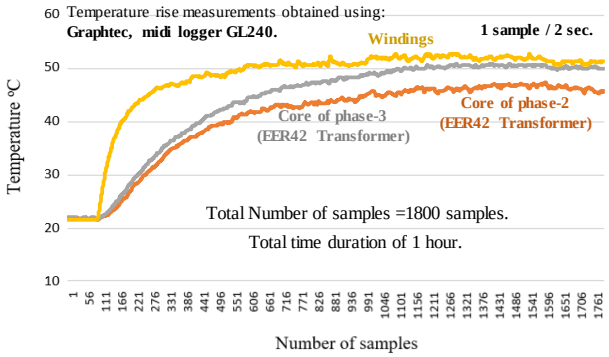

Fig.3.17 Temperature rise of integrated transformer.

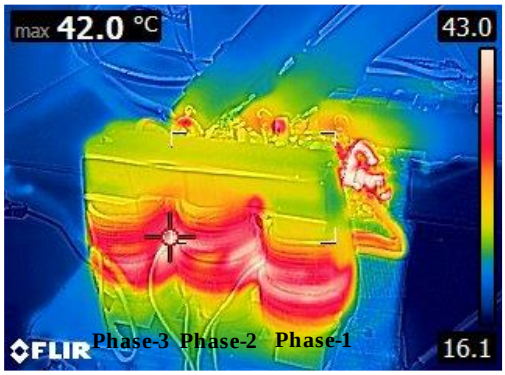

Fig.3.18 Thermal image of the integrated transformer.

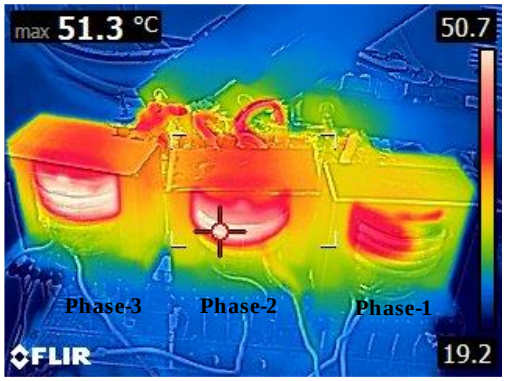

Fig.3.19 Thermal image of the three discrete transformers.

It worth mentioning that as the three-phases share the same magnetic core, therefore a uniform temperature distribution along the core had been realized. As shown in Fig.3.16, the temperature of both the center leg and outer leg is almost identical. On the other hand, in case of the three-discrete transformers, each phase temperature deviates a little from the other ones.

It can be deduced from that the integrated transformer has a better thermal performance than the discrete transformers, it is because a transformer temperature rise depends upon the core external thermal resistance R_{ET} (°C/Watt). The external thermal resistance can be estimated as a function of the core window area, using a simple formula based on rule of thumb [36], during an average situation of natural convection cooling, as follows

$$R_{ET} = \frac{36}{W_a[cm^2]} \ ^{o}\text{C/Watt} \qquad (3.32)$$

The integrated transformer has a higher value of window area (W_a = 6.4 cm^2), than the window area of the discrete transformers (W_a = 1.55 cm^2). Therefore, and based on (3.32), it can be deduced that the integrated transformer has a lower external thermal resistance compared to the discrete transformers.

3.4.5 Volume, weight and Cost Comparison between integrated and discrete transformers

In this section, the merits of employing the integrated transformer from practical point of view are reported. The discussion includes a comparison between the three integrated transformer and the three-discrete transformers on the basis of volume, weight and cost as follow: Referring to the product catalog of TDK [37], the magnetic core's volume and weight of the integrated transformer are 40.42 cm^3 and 250g. Referring to [38], the total volume and weight of the discrete transformers are 3x23.7 = 71.1 cm^3 and 3x116=348g. In other words, for the same LLC resonant converter, the integrated transformer enables an approximate 43% transformer volume reduction as compared with the three discrete transformer, and a weight reduction of 28%. Moreover, the dead spaces between the discrete transformers are no longer required in case of utilizing the integrated transformer. From the website of Allied Electronics [39], the estimated cost of magnetic core for the integrated transformer is 7.06 USD/unit. However, the total cost for the three discrete magnetic cores is 3x2.8 = 8.4 USD/unit. The windings cost is out of comparison. Therefore, employing the magnetic integrated transformer would achieve a cost reduction of 16%.

3.4.6 Power loss distribution

In this section, the loss breakdown of the three-phase LLC resonant converter is presented with the two transformer topologies. The power loss in the three-discrete transformers topology can be calculated as follow

(i) Conduction loss of primary switches:

$$P_{con} = I_{r-rms} R_{ds-on} \tag{33}$$

The MOSFETs utilized in our prototype are Toshiba, TK20E60W, with a drain-source resistance of 0.13Ω. The effective current value through the switches is 1.66A. The total conduction loss of the MOSFETs = 6 x 0.13 x $(1.66)^2$= 2.15W.

(ii) Conduction loss of secondary rectifiers:

$$P_{diode} = V_F . I_{D-rms} \tag{34}$$

The secondary rectifiers are Schottky diodes VS-100BGQ100 with a V_f=0.6 at 6.9A rms value of the half-wave secondary current, leading to a total conduction loss of = 6 x 0.6 x 6.95 = 25W.

(iii) The copper loss of the transformer

$$P_{copp-T} = I^2_{pri-rms} R_{pri-ac} + I^2_{\sec-rms} R_{\sec-ac} \tag{35}$$

The *ac* resistance of the transformers primary winding was measured as 2.93Ω and for the secondary winding is 0.37Ω, leading to a total copper loss of 27.5W.

(iv) The core loss is estimated using the improved generalized Steinmetz equation *iGSE* [40], because in the LLC converter the excitation voltage on the transformer is a rectangular waveform, and there is no DC bias magnetization.

$$P_{core} = \frac{1}{T_s}\int_0^{T_s} k_i \left|\frac{dB}{dt}\right|^{\alpha} (\Delta B)^{\beta-\alpha} dt \tag{36}$$

$$k_i = \frac{k}{2^{\beta+1}\pi^{\alpha-1}\left(0.2761 + \frac{1.7061}{\alpha+1.354}\right)} \tag{37}$$

For PC40, Steinmetz parameters are extracted as [k=55.85, α=1.143, β=2.396]. The core loss is calculated as 11398 W/m^3. The PC40 EER42/42/20-Z core volume is 23700 mm^3 ($2.37x10^{-5}$ m^3). Therefore, the total core losses contributed by the three transformers is 0.81W.

(v) The difference between the total loss and the sum of these aforementioned losses is 3.9 W and it is denoted by "others". These losses mainly comprise the switching loss of the primary MOSFETs and other parasitics of the circuit.

The power loss in the integrated transformer topology can be calculated as follow

(i) Conduction loss of primary switches:

The MOSFETs utilized in our prototype are Toshiba, TK20E60W, with a drain-source resistance of 0.13Ω. The effective current value through the switches is 1.66A. The total conduction loss of the MOSFETs = 6 x 0.13 x $(1.66)^2$= 2.15W.

Conduction loss of secondary rectifiers: The secondary rectifiers are Schottky diodes VS-100BGQ100 with a V_f=0.6 at 6.9A rms value of the half-wave secondary current, leading to a total conduction loss of = 6 x 0.6 x 6.95 = 25W.

(ii) The copper loss of the transformer:

The *ac* resistance of the transformers primary winding was measured as 2.15Ω and for the secondary winding is 0.31Ω, leading to a total copper loss of 20.8W.

(iii) The core loss is calculated based on iGSE [40] as 10387 W/m^3. The PC40 EC70x69x16 core volume is 40420mm^3. Therefore, the total core losses contributed by the three transformers is 0.42W.

(iv) The difference between the total loss and the sum of these aforementioned losses is 1.2 W and it is denoted by "others". These losses mainly comprise the switching loss of the primary MOSFETs and other parasitics of the circuit.

The power loss breakdown is depicted in Fig.3.20 (a). It is clear that the conduction loss on the rectifiers contributes with the major power loss components, alongside with the transformer's winding copper losses. The integrated transformer topology exhibits a lower core loss than the three discrete transformers, as shown in Fig.3.20 (b). Nonetheless, the core loss contribution in this circuit topology is small, as the maximum value of flux density has a low value. From the power loss perspective, the integrated transformer topology would be more promising in high-frequency LLC converters, as it will highly reduce the core loss compared to the three discrete transformers.

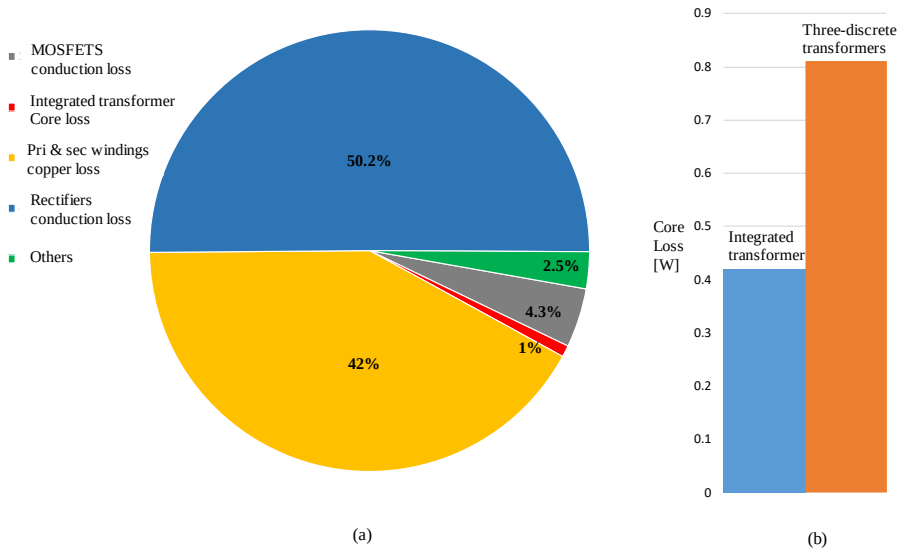

Fig.3.20 Power losses distribution. (a) Pie chart of the loss distribution in the integrated transformer topology. (b) Core loss comparison between the integrated transformer and the three-discrete transformers.

3.5 Summary

A three-phase LLC resonant converter with a three-phase integrated transformer is proposed and experimentally evaluated. The study of this three-phase integrated transformer hasn't been reported before in the literature. The advantage of the proposed magnetic core is that it is commercially available. Therefore, it is easier for the industry engineer to implement. The integrated transformer attains a 43% volume reduction, 28% weight reduction and an approximate of 16% cost reduction, compared with the three-discrete transformer topology (which is already implemented in the market as in the DC-DC converter of TESLA Model 3). Furthermore, the proposed integrated transformer has been proven to be efficient and has a uniform thermal distribution along the magnetic core. The proposed integrated transformer topology would be highly beneficial in high-frequency applications, in which keeping the core loss at a minimal value is hard to realize. The FEA simulation and Experimental tests showed a proper operation of the integrated transformer. It is believed that the merits of the integrated transformer reported in this study would promote the industrial applications of the three-phase LLC resonant converter topologies.

3.6 Appendix

The leakage inductance can be controlled by inserting a flexible magnetic material between the primary and the secondary. If a low values of leakage inductances is targeted, the air shall be the medium between the primary and secondary windings. The air reluctance is much higher than a magnetic material with a high permeability. Therefore, the leakage flux encounters a higher resistance with the air, as a medium between the primary and the secondary. Adjusting the space between the primary and

secondary would result in controlling the leakage value within a specific range. However, inserting a flexible magnetic material between the primary and secondary windings increases the leakage flux, and hence the leakage inductance. In other words, the leakage encounters a path with low reluctance. Targeting a higher or lower value of leakage inductance can be controlled by adjusting the thickness or the permeability of the flexible sheet. The higher the thickness, the more leakage can be realized. As an example to alter the leakage inductance of the integrated transformer, a flexible magnetic sheet had been inserted between the primary and the secondary windings. The magnetic sheet is TDK Flexield (part number IFL12-100NB300x200), with a magnetic permeability of 180 and thickness of 0.1mm, as shown in Fig.3.21. The leakage inductance has increased to reach a value of 56.4µH, instead of 35.3µH.

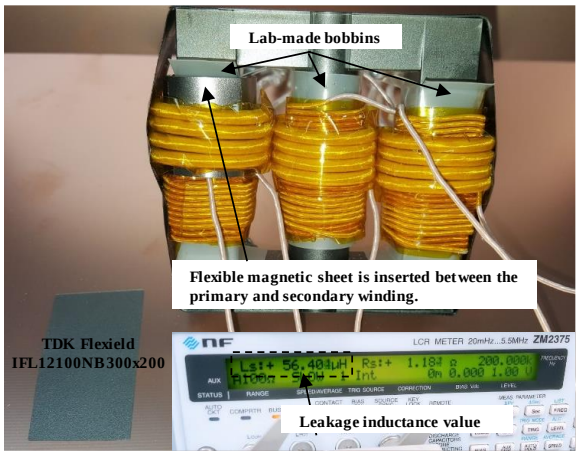

Fig.3.21 Inserting a magnetic sheet between the windings to purposefully to alter the leakage inductance value.

References

[1] Z. Liu, X. Huang, M. Mu, Y. Yang, F. C. Lee and Q. Li, "Design and evaluation of GaN-based dual-phase interleaved MHz critical mode PFC converter," in Proc. IEEE Energy Conversion Congress and Exposition (ECCE), Pittsburgh, PA, pp. 611-616, Sep. 2014.

[2] W. Zhang, Y. Long, Z. Zhang, F.Wang, L. Tolbert, B. Blalock, S. Henning, C. Wilson, and R. Dean, "Evaluation and Comparison of Silicon and Gallium Nitride Power Transistors in LLC resonant converter," in Proc. Energy Conversion Congress and Exposition (ECCE), 2012 IEEE, pp.1362-1366, 15-20 Sep. 2012.

[3] M. Kanechika, T. Uesugi and T. Kachi "Advanced SiC and GaN Power Electronics for Automotive Systems" in Electron Devices Meeting (IEDM), San Francisco, CA, pp.1351-1354, Dec. 2010.

[4] M. Hirakawa, M. Nagano, Y. Watanabe, K. Andoh, S. Nakatomi and S. Hashino, "High Power Density DC/DC Converter using the Close-Coupled Inductors", in Proc. IEEE Energy Conver. Cong. and Expo. (ECCE), pp. 1760-1767, Sep. 2009.

[5] M. Pavlovsky´, G. Guidi, and Atsuo Kawamura, "Assessment of Coupled and Independent Phase Designs of Interleaved Multiphase Buck/Boost DC-DC Converter for EV Power Train", IEEE Trans. on Power Electron., Vol. 29, No. 6, pp. 2693-2704, Jun. 2014.

[6] K. J. Hartnett, J. G. Hayes, M. G. Egan and M. S. Rylko, "CCTT-Core Split-Winding Integrated Magnetic for High-power DC-DC Converters", IEEE Trans. on Power Electron., Vol. 28, pp. 4970-4984, Nov. 2013.

[7] Q. Li, Y. Dong, F. C. Lee, and D. J. Gilham, "High-Density Low-Profile Coupled Inductor Design for Integrated Point-of-Load Converters", IEEE Trans. on Power Electron., Vol. 28, No. 1, pp. 547-554. Jan. 2012.

[8] J. Imaoka, S. Kimura, Y. Itoh, W. Martinez, M. Yamamoto, M. Suzuki, and K. Kawano, "Feasible Evaluations of Coupled Multilayered Chip Inductor for POL Converters", IEEJ J. of Ind. App., Vol. 4, No. 3, pp. 126-135. May. 2015.

[9] K. J. Hartnett, J. G. Hayes, M. G. Egan, M.S. Rylko, B. J. Barry and J. W. Masłoń, "Comparison of 8-kW CCTT IM and Discrete Inductor Interleaved Boost Converter for Renewable Energy Applications", IEEE Trans. on Ind. App., Vol. 51, No. 3, pp.2455-2469, May. 2015.

[10] T. Qian and B. Lehman, "Coupled Input-Series and Output-Parallel Dual Interleaved Flyback Converter for High Input Voltage Application", IEEE Trans. on Power Electron., Vol. 23, No. 1, pp. 88-95. Feb. 2008.

[11] F. Forest, E. Labouré, T. A. Meynard and J. Huselstein, "Multicell Interleaved Flyback Using Intercell Transformers", IEEE Trans. on Power Electron., Vol. 22, No. 5, pp. 1662-1671. Sep. 2007.

[12] L. Wong, Y. Lee, D. K. Cheng, and M. H. L. Chow, "Two-Phase Forward Converter using an Integrated Magnetic Component", IEEE Trans. on Aerospace and Electron. Sys., Vol. 40, No.4, pp.1294-1310 Sep. 2004.

[13] Y. Su, D. Hou, F. C. Lee and Q. Li, "Low Profile Coupled Inductor Substrate with Fast Transient Response", in Proc. of IEEE Applied Power Electron. Conf. and Expo., (APEC), pp. 1161-1168, Mar. 2015.

[14] M. Noah, J. Imaoka, Y. Ishikura, K. Umetani, and M. Yamamoto, "Review of Current Balance Mechanism in Multiphase LLC Resonant Converters", in Proc. IEEE International Symposium on Industrial Electronics (ISIE 2018), Cairns, Australia, June 2018.

[15] H. Kim, J. Baek, M. Ryu, J. Kim and J. Jung, "The high-efficiency isolated AC–DC converter using the three-phase interleaved LLC resonant converter employing the Y-connected rectifier", IEEE Trans. on Power Electron., Vol. 29, No. 8, August 2014.

[16] K. Murata, F. Kurokawa, "An interleaved PFM LLC resonant converter with phase-shift compensation," IEEE Trans. on Power Electron., Vol. 31, No. 3, pp. 2264-2272, March 2016.

[17] E. Orietti, P. Mattavelli, G. Spiazzi, C. Adragna, and G. Gattavari, “Current sharing in three phase LLC interleaved resonant converter,” in Proc. IEEE Energy Convers. Congr. Expo. (ECCE), pp. 1145–1152, Sep. 2009.

[18] Y. Nakakohara, H. Otake, T. Evans, T. Yoshida, M. Tsuruya and K. Nakahara, “Three-phase LLC series resonant DC/DC converter using SiC MOSFETs to realize high-voltage and high-frequency operation,” IEEE Transactions on Industrial Electronics, Vol. 63, No. 4, pp. 2103-2110, April, 2016.

[19] H. Wand, Y. Chen, Y. Liu, J. Afsharian and Z. Yang, “A passive current sharing method with common inductor multi-phase LLC resonant converter”, IEEE Trans. Power Electron, Vol. PP, No.99, pp.1-1, 2016.

[20] H. Wand, Y. Chen, Y. Qiu, P. Fang, Y. Zhang, L. Wang and Y. Liu,“A common capacitor multi-phase LLC converter with passive current sharing ability”, IEEE Trans. Power electronics, Vol. PP, No.99, pp.1-1 Jan. 2017.

[21] H. Wand, Y. Chen, Y. Liu, J. Afsharian and Z. Yang, "A common inductor multi-phase LLC converter", in Proc. IEEE Energy Convers. Congr. Expo. (ECCE), pp. 548-555, Sep. 2015.

[22] M. Smit, J. Ferreria, J. Wyk and M. Ehsani, "An Ultrasonic Series Resonant Converter with Integrated L-C-T," IEEE Trans. Power Electron., vol.10, no.1, pp. 25-31, Jan 1995.

[23] W. Liu, J. Wyk, "Design of Integrated LLCT Module for LLC Resonant Converter," in Proc. IEEE Appl. Power Electron Conf., pp. 362-368, March 2005.

[24] Y. Zhang, D. Xu, K. Mino and K. Sasagawa,"1MHz-lkW LLC Resonant Converter with Integrated Magnetics," in Proc. IEEE Appl. Power Electron Conf., pp. 1630-1635, 2007.

[25] B.Yang, R. Chen, and F. Lee, "Integrated magnetics for LLC resonant converter", in Proc. IEEE Applied Power Electronics Conf. Exposition (APEC) 2002, Dallas, TX, USA, pp. 346–351, March 2002.

[26] Y. Zhang, D. Xu, K. Mino, and K. Sasagawa, ‘1 MHz–1 kW LLC resonant converter with integrated magnetics’, in Proc. IEEE Applied Power Electronics Conf. Exposition (APEC) 2007, Anaheim, CA, USA, pp. 955–961, Feb. 2007.

[27] W. Liu, and J. D. Wyk, "Design of integrated LLCT module for LLC resonant converter", In Proc. IEEE Applied Power Electronics Conf. Exposition (APEC) 2005, Austin, TX, USA, pp. 362–368, March 2005.

[28] M. Noah, K. Umetani, J. Imaoka, and M. Yamamoto, "Winding Orientation Method to Minimise the Secondary Leakage of a Gapped Transformer Utilised in LLC Resonant Converter" IET Electronics Letters, Volume:54, Issue:3, Page:157-159, Feb. 2018.

[29] W. Martinez, M. Noah, S. Endo, K. Nanamori, S. Kimura, M. Yamamoto, J. Imaoka and K. Umetani, “Three-phase LLC Converter with Integrated Magnetics,” in Proc. IEEE Energy Conver. Cong. and Expo. (ECCE),pp. 1-8, Sep. 2016.

[30] M. Noah, K. Umetani, S. Endo, H. Ishibashi, J. Imaoka, and M. Yamamoto, “A Lagrangian Dynamics Model of Integrated Transformer Incorporated in a Multi-phase LLC Resonant Converter,” in Proc. IEEE Energy Conver. Cong. and Expo. (ECCE),pp. 1-8, Sep. 2017.

[31] M. Noah, K. Umetani, J. Imaoka, M. Yamamoto.: ‘Lagrangian dynamics model and practical implementation of an integrated transformer in multi-phase LLC resonant converter’, IET Journal on Power Electronics Volume:11, issue:2, Page:339-347, February 2018.

[32] M. Noah, et al.:” A Current Sharing Method Utilizing Single Balancing Transformer for a Multiphase LLC Resonant Converter with Integrated Magnetics," IEEE Journal of Emerging and Selected Topics on Power Electronics, Volume: 6, Issue:2, Page:977-992, June 2018.

[33] J. Zhang, W. Hurley, and W. Wölfle, “Gapped Transformer Design Methodology and Implementation for LLC Resonant Converters,” IEEE Transaction on Industry Applications, Vol. 52, No. 1, pp. 342-350, Jan./Feb. 2016.

[34] W. G. Hurley and W. H. Wolfle, Transformers and inductors for power electronics. Theory, Design and Applications. Chichester, U.K.: Wiley, 2013.

[35] M. Noah, S. Endo, S. Kimura, M. Yamamoto, J. Imaoka, and K. Umetani, and E. Hiraki“An Investigation into a Slight-Variation of the Transformer Effective Permeability in LLC Resonant Converter” in Proc. IEEE 19th Conference on Power Electronics and Applications, EPE 2017, Sep. 2017.

[36] Texsas instrument, “Section 4 - Power Transformer Design”. Available online: https://www.ti.com/lit/ml/slup126/slup126.pdf

[37] Large size ferrite cores for high power, TDK. Available online: https://product.tdk.com/info/en/catalog/datasheets/ferrite_mz_large_e_en.pdf.

[38] Ferrite core for switching power supplies, TDK. Available online: product.tdk.com/info/en/catalog/datasheets/ferrite_mz_sw_e_en.pdf.

[39] Allied Electronics Co. Ltd, USA, “Passive components”. Available online: http://www.alliedelec.com/passive-components/

[40] K. Venkatachalam, C. R. Sullivan, T. Abdallah, and H. Tacca, “Accurate prediction of ferrite core loss with nonsinusoidal waveforms using only Steinmetz parameters,” in Proc. IEEE Workshop on computers in Power Electronics, pp. 36-41, June 2002.

Chapter 4: Current Balance Mechanism in Three-phase LLC Resonant Converter

4.1 Introduction

4.1.1 Research Motivation: Current Balance Mechanism

One of the most popular resonant topologies is the LLC resonant converter, where soft switching and high efficiency can be attained over entire load range [1]-[6]. However, adapting single phase LLC resonant converter in high current applications comes with drawbacks. Since the current ripple stress on the output capacitor could be severely high to handle. Therefore, a quite large output smoothing capacitor may be needed to compensate the high output current ripples. In this regard, Multi-phase LLC resonant converters have several advantages over the single-phase topologies. In a multi-phase circuit, the current is distributed among the phases, resulting in lower conduction loss and less thermal stresses on the power devices. Moreover, rectifying a three identical sinusoidal waves, 120^0 phase-shifted, allows for a lower current ripple on the output filter than the single-phase topologies [7]-[9]. The three-phase LLC resonant converter is depicted in Fig.4.1. In this circuit topology the values of the phase parameters are never exactly identical, thus each phase encounters a gain characteristic different than other phases, aggravating the output current ripples and hence, a quite larger output capacitor may be needed to compensate the current imbalance. In this regard, a current balancing method is proposed in this chapter. The proposed method can improve the current sharing between the paralleled phases relying on a single balancing transformer, and its theory is based on Ampere's law, by forcing the sum of the three resonant currents to zero. Theoretically, if an ideal balancing transformer has been utilized, it would impose the same effect of connecting the integrated transformer in a solid star connection. However, as the core permeability of the balancing transformer is finite, the unbalanced current can't be completely suppressed. Nonetheless, utilizing a single balancing transformer has an advantage over the star

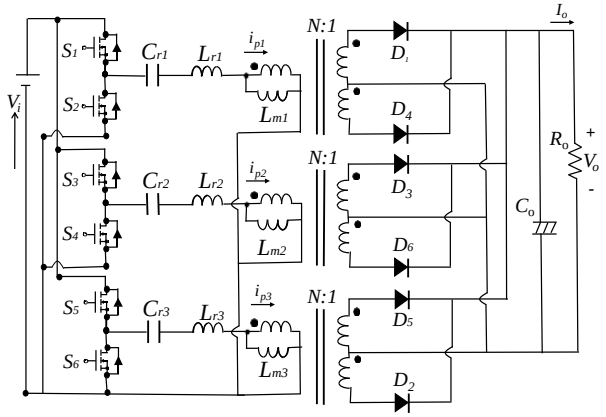

Fig.4.1 Three-phase LLC resonant converter with three-discrete transformers, conventional parallel connection.

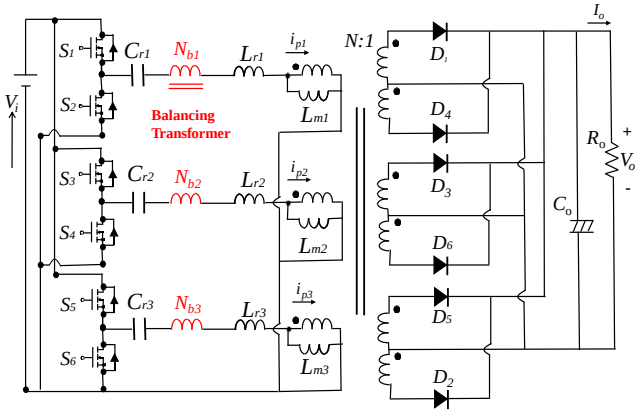

Fig.4.2 Proposed three-phase LLC resonant converter with 4-leg integrated transformer and balancing transformer.

connection, as it keeps the interleaving structure simple which allows for traditional phase-shedding techniques, and it can be a solution for the other multi-phase topologies where realizing a star connection is not feasible. Along with the theoretical discussion, simulation and experimental results are also presented to evaluate the proposed method considering various sources of the unbalance such as a mismatch in: 1) Resonant and magnetizing inductances 2) Resonant capacitors 3) Transistor on-resistances of the Mosfets 4) Propagation Delay of the gate drivers.

4.1.2 Current Unbalance in Three-phase LLC Resonant converter- Literature Review:

The multi-phase LLC resonant converters have been previously proposed in [10]–[11]. However, these studies did not address the unbalanced current sharing problem, which arises from the components mismatch. Nonetheless, the current unbalance has been widely discussed in the literature. The proposed current balance methods can be split into three main strategies as follow:

- ***Control-based strategy.***

  The authors of [12] have proposed a control scheme to compensate the gain difference between the phases by controlling the PFC's output voltage and adjusting the input voltage for each converter according to peak value of the rectifier current. In [13] the unbalanced current in the interleaved LLC converter has been tackled by phase-shift modulation (PSM).

  In [14], The proposed current sharing method is realized by controlling the turn-on timing of the secondary synchronous switches. These methods achieved very good current sharing performance. However, in general, applying control schemes tend to make the system more complex.

  On the other hand, several active control methods have been proposed in the literature. The basic principal of the active control methods is to modulate the resonant frequency instead of the switching frequency. Based on the fact that the output voltage is determined by the ratio of switching frequency to resonant frequency, and hence each gain of the paralleled module can be adjusted to equalize the current sharing among the phases. For instance, in [15] switch-controlled inductor (SCI) and switch-controlled capacitor (SCC) methods have been presented to regulate the power converter. The SCC is reported to be much better than the SCI in high-frequency applications. In SCC a capacitor is connected in parallel with two switches, and each phase uses an SCC to regulate the output voltage to achieve balanced current sharing. For example, when the controller detects that one phase is providing more output current than other phases, it slightly increases the control angle α of the corresponding phase, which increases the resonant capacitance and lowers the resonant frequency, and thus reduces the output current until it reaches the balanced point. This concept has been applied in various applications to obtain constant switching frequency operation [16]–[21].

  However, the disadvantage of employing a constant switching frequency SCC–LLC converter is being inferior compared to conventional LLC converters, in terms of peak gain range and normalized frequency variation range [22]-

TABLE 4.I
Designer Guide: Merits and Demerits of Balancing Transformer, Active Control and Star Connection Current Sharing Methods.

	Current Balance Methods		
	Active Control-based Current Sharing Method	Circuit topology Current Sharing Method	Single Balancing Transformer
Additional Components	■ Two switches, capacitor, in addition to a control circuit.	■ No	■ Single Transformer.
Type of Power Losses	■ Switching losses.	■ No	■ Copper and Core losses.
Implementation of Phase Shedding	■ Yes	■ No	■ Yes
Interleaving Structure	■ Simple.	■ Complicated	■ Simple.
Applicability for Various Multi-phase Topology	■ Yes	■ Has limitations.	■ Yes.
Current Sharing Performance	■ Perfect	■ Perfect	■ Very good
Switching Frequency	■ Constant.	■ Variable.	■ Variable
Designer Authority to control the Unbalance	■ Yes	■ No	■ Yes
Complexity	■ Complex.	■ Simple.	■ Simple.

[23]. In order to overcome this drawback, an improved switch controlled capacitor (SCC) method has been proposed in [24]. In this study, Z. Hu has proposed a new control strategy for the SCC–LLC converter, which enables a variable switching frequency operation; thus, it provides uncompromised performance while achieving interleaved operation. Yet, the load sharing among the paralleled phases can be achieved by changing the equivalent resonant capacitance using the SCC technique.

The merits of the active control methods include: i) They allow a simple interleaving structure. ii) Excellent load-sharing performance. iii) They allow for traditional phase shedding implementations. Nonetheless, the demerits of this current balance approach is the need of adding more components, which increase the cost and it makes the control scheme more complicated, in comparison with the circuit topology and magnetic-based current balance approaches.

- ***Circuit topology strategy.***

In a circuit topology-based current sharing method, the traditional interleaving structure of the converter paralleled phases is adjusted to allow for a balanced current sharing. For instance, in [25], [26], [27] the current balance can be improved by connecting the input capacitors in series. In a two-phase LLC resonant converter, the two input DC capacitor voltages are the same, and equal to half of the input bus voltage. However, during unbalance, the mid-point voltage can be adjusted to equalize the currents among the phases. In [28], connecting the transformer primary in star has been proposed with the aid of phase-shift control technique. This method achieves very good current sharing, however it is only suitable for the three-phase topology where having a star connection is feasible. Furthermore, it

precludes implementing traditional phase shading, which is usually implemented to realize high efficiency at different load levels [29].

The circuit topology-based strategy has low cost and good load current sharing performance, and doesn't need additional components. However, it is not very effective on a system level, if the number of the paralleled phases increase.

- ***Magnetic-based strategy.***

  In [30]-[32] common passive components current sharing methods have been proposed to realize an equalized current between the phases. In [31], the resonant inductors of the transformers are connected in parallel, in which they receive the current of each phase, and then they redistribute it evenly. These methods can minimize the output current ripples, and hence the output capacitor size can be effectively reduced. However, this current balancing method can't be implemented in the applications where the leakage inductance of the transformer is utilized as a resonant inductance, because it is not physically feasible for resonant inductors to be connected in parallel. In [33] three transformers have been utilized in the three-phase LLC converter to equalize the currents between the phases, the physical connection of those three transformers are as follow: the primary side of each transformer is connected with the relevant phase resonant capacitor in series, and the secondary side is connected with primary side of the other phase in parallel. However, adding three magnetic cores would cost the circuit additional power losses.

Designer Trade-off guideline: Circuit designers always in a need to trade-off between different current balancing methods, based on their specific system requirements. As a guideline for the designers, Table 4.I summarizes the merits and demerits of the proposed method, alongside with the active control and circuit topology-based current sharing methods.

The problem to be solved in this chapter is the current unbalance in the three-phase LLC resonant converter. The proposed single current balancing transformer has never been proposed before in the relevant literature. Most of the literature studies relies on adding complicated control circuits to counter the current unbalance. This chapter proposes a simple method can be used by industry engineers and researcher to counter the current unbalance in the three-phase LLC resonant converter.

4.1.3 Chapter Contents

The proposed current sharing method in this chapter utilizes a single balancing transformer, which is connected in series between the resonant capacitors and the integrated transformer, as shown in Fig.4.2. The three phases of the LLC converter are placed on the same core's leg to share the same magnetic flux path, and to minimize the leakage. As a result, and based on Ampere's law; the net magnetic field along the closed loop in the transformer core is proportional to the total electric currents passing through this loop, forcing the sum of the three resonant currents to equal zero, and therefore, acts as a star connection. The proposed method

is simple and suitable for other multi-phase topologies where realizing a star connection is not feasible.

The proposed current balance method is employed with a spatial integrated transformer. The magnetic analysis for the integrated transformer is conducted, where the coupling coefficients between the phases are intentionally minimized to realize the magnetic behavior of the three-discrete transformers, with the purpose of eliminating the dead space. The current balance evaluation of the proposed method is conducted and compared with the conventional parallel and the star connections.

This chapter is organized as follows: in section 4.2 the magnetic analysis of the integrated transformer is conducted and the coupling factors between the phases are derived. Section 4.3 discusses the automatic current sharing effect of the proposed balancing transformer. In section 4.4, the analysis of different circuit topologies is conducted, and the mechanism of the current balance transformer and the star connection is revealed. In section 4.5, the simulation and experimental tests are conducted for a 500W, 200kHz three-phase LLC resonant converter prototype considering the following three circuit topologies: a) The integrated transformer's conventional parallel connection. b) Utilizing the balancing transformer. c) Connecting the integrated transformer in a star connection. Finally, the appendix is presented in section 4.6.

4.2 Three-phase LLC with Spatial Integrated Transformer

Magnetic integration is a technique whereby various inductive and transformer elements are combined on a single core. In this discussion, the windings of the three phases are advantageously combined into a single spatial magnetic core. The three-phase converter is depicted in Fig.4.2, where V_i and V_o are the input and output voltages; I_o is the DC output current. The spatial core geometry is shown in Fig.4.3. The equivalent magnetic circuit for the spatial integrated transformer is shown in Fig.4.4, where N_{p1}, N_{p2} and N_{p3} are the primary windings; N_{s1}, N_{s2} and N_{s3} are the secondary windings; R_1, R_2, R_3 and R_c are the magnetic reluctances of the three outer legs and the center leg, respectively.

Utilizing the spatial core would enable the converter manufacturer to reduce the usage of the magnetic material. A weight comparison is conducted between the spatial core and its three non-coupled transformers to show the reduction in usage of the magnetic material. As shown in Fig.4.5, the total mass of the spatial core is 690g and the total mass of the three-non coupled transformers is 765g. Therefore, employing the spatial core reduces the usage of the magnetic material. In other words, an approximate 10% of mass downsizing can be realized.

The following assumptions have been made while conducting the magnetic analysis: a) the number of turns on the primary of the three phases are equal; similarly, for the secondary windings. b) the magnetic reluctance of the three outer legs are equal ($R_1 = R_2 = R_3 = R$); which can be realized by adjusting the air gap lengths to the same value. c) the external leakage fluxes are neglected to simplify analyzing the magnetic circuit. By applying Kirchhoff's current law and Kirchhoff's voltage law on the magnetic circuit, the following equations could be obtained

Fig.4.3 Core geometry of the spatial integrated transformer.

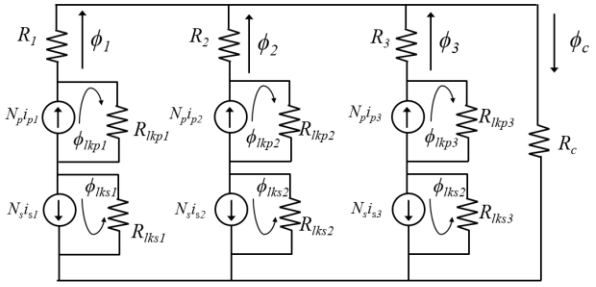

Fig.4.4 Magnetic circuit for spatial integrated transformer.

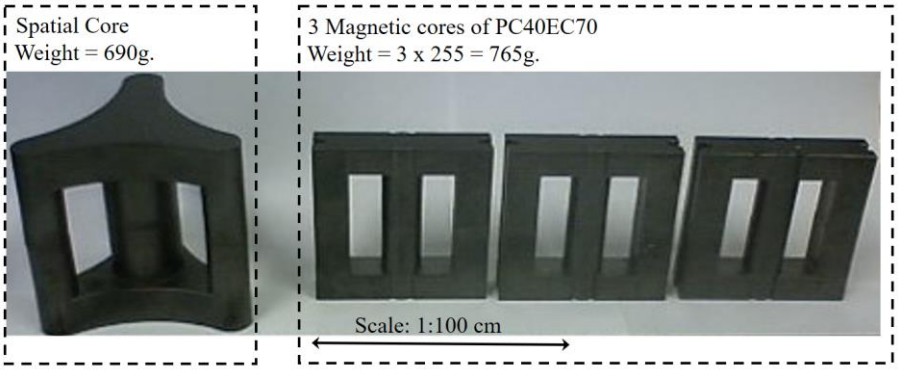

Fig.4.5 Spatial magnetic core side by side with the three-discrete cores.

$$R_1\phi_1 - R_2\phi_2 = N_{p1}i_{p1} - N_{s1}i_{s1} - N_{p2}i_{p2} + N_{s2}i_{s2} \quad (4.1)$$

$$R_2\phi_2 - R_3\phi_3 = N_{p2}i_{p2} - N_{s2}i_{s2} - N_{p3}i_{p3} + N_{s3}i_{s3} \quad (4.2)$$

$$R_1\phi_1 + R_c\phi_c = N_{p1}i_{p1} - N_{s1}i_{s1} \quad (4.3)$$

$$\phi_1 + \phi_2 + \phi_3 = \phi_c \quad (4.4)$$

Solving the preceding equations with respect to the fluxes, and considering the symmetry of the outer legs reluctances, we obtain:

$$\phi_1 = \left(\frac{N_p i_{p1} - N_s i_{s1}}{R}\right) - \frac{\alpha}{(1+3\alpha)}\left(\frac{N_p i_{p1} - N_s i_{s1} + N_p i_{p2} - N_s i_{s2} + N_p i_{p3} - N_s i_{s3}}{R}\right) \quad (4.5)$$

$$\phi_2 = \left(\frac{N_p i_{p2} - N_s i_{s2}}{R}\right) - \frac{\alpha}{(1+3\alpha)}\left(\frac{N_p i_{p1} - N_s i_{s1} + N_p i_{p2} - N_s i_{s2} + N_p i_{p3} - N_s i_{s3}}{R}\right) \quad (4.6)$$

$$\phi_3 = \left(\frac{N_p i_{p3} - N_s i_{s3}}{R}\right) - \frac{\alpha}{(1+3\alpha)}\left(\frac{N_p i_{p1} - N_s i_{s1} + N_p i_{p2} - N_s i_{s2} + N_p i_{p3} - N_s i_{s3}}{R}\right) \quad (4.7)$$

Where α is the ratio of the reluctance of the center leg to the outer leg. ($\alpha = R_c/R$). We propose a relevant coupling factor between the three-phases k, where it is denoted by

$$k = \frac{\alpha}{(1+3\alpha)} \tag{4.8}$$

Therefore (4.5), (4.6) and (4.7) could be reconstructed as

$$\phi_1 = \left(\frac{N_p i_{p1} - N_s i_{s1}}{R} \right) - k\left(\frac{N_p i_{p1} - N_s i_{s1} + N_p i_{p2} - N_s i_{s2} + N_p i_{p3} - N_s i_{s3}}{R} \right) \tag{4.9}$$

$$\phi_2 = \left(\frac{N_p i_{p2} - N_s i_{s2}}{R} \right) - k\left(\frac{N_p i_{p1} - N_s i_{s1} + N_p i_{p2} - N_s i_{s2} + N_p i_{p3} - N_s i_{s3}}{R} \right) \tag{4.10}$$

$$\phi_3 = \left(\frac{N_p i_{p3} - N_s i_{s3}}{R} \right) - k\left(\frac{N_p i_{p1} - N_s i_{s1} + N_p i_{p2} - N_s i_{s2} + N_p i_{p3} - N_s i_{s3}}{R} \right) \tag{4.11}$$

As shown in Fig.4.6, this coupling factor is determined by the reluctance ratio R_c / R. in case of inserting air gaps in the outer legs, the value of R_c will become far less than R. Consequently, the value of the reluctance ratio α becomes very small, and hence a low coupling factor between the phases can be realized. Under this condition, the magnetic behavior of the integrated transformer acts as a three discrete transformers.

Theoretically, if the coupling factor equals zero, the flux equations will represent the behavior of three-discrete transformers with three independent flux paths as follow.

$$\phi_1 = \left(\frac{N_p i_{p1} - N_s i_{s1}}{R} \right) \tag{4.12}$$

$$\phi_2 = \left(\frac{N_p i_{p2} - N_s i_{s2}}{R} \right) \tag{4.13}$$

$$\phi_3 = \left(\frac{N_p i_{p3} - N_s i_{s3}}{R} \right) \tag{4.14}$$

Based on this analysis, a single magnetic core can replace the three discrete transformers, reducing the usage of the magnetic material and eliminating the dead space required between the three transformers.

4.3 Current Balance Evaluation Using Single Balancing Transformer

In a multi-phase LLC resonant converter, the values of the resonant tank parameters are never exactly identical among the phases; therefore, each phase encounters a gain characteristic different than other phases. In practice, the unbalance power sharing between the phases may arise due to one or more of the followings: unequal values of the resonant inductances, magnetizing inductances, transistor forward voltage drops, and gate driver delay on the primary switches. Consequently, the phase currents deviate. We propose a current deviation factor δ (CDF in short in the following paragraphs), which denotes the deviation of the

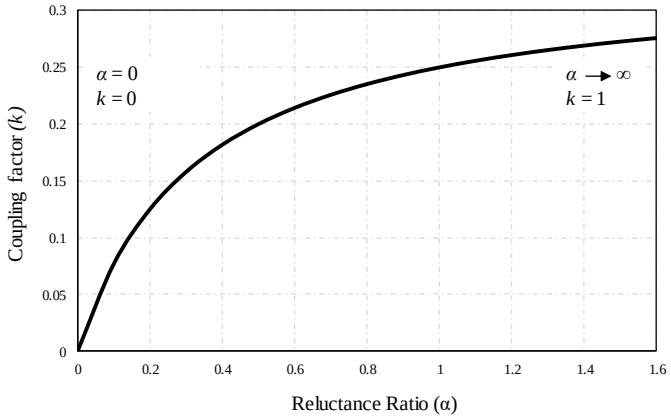

Fig.4.6 Relationship between coupling factor k and reluctance ratio α within the integrated transformer.

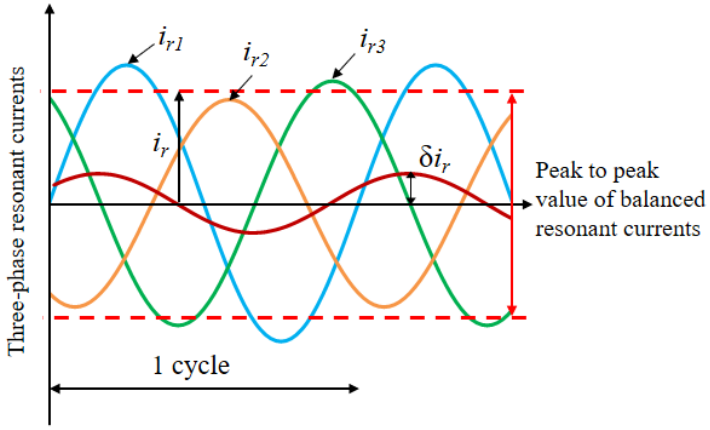

Fig.4.7 Unbalanced current δi_r which arises from the unbalanced phase currents i_{r1}, i_{r2}, i_{r3}

sum of the three phase currents from its prospective value under a complete balancing conditions. Under complete balancing conditions, the value of CDF goes to zero $\delta = 0$, as shown in Fig.4.7.

In this section, a single balancing transformer is utilized to equalize the current sharing between the phases of a three-phase LLC resonant converter. The balancing transformer can be implemented with different magnetic core structures, in this discussion we utilized ferrite core, PC40 EER-25.5-Z. The basic principle of the proposed current balance method relies on forcing the sum of the phase current to equal zero. The magnetic circuit of the proposed balancing transformer is shown in Fig.4.8. The magneto-motive forces follow Kirchhoff's voltage law and the fluxes follow Kirchhoff's current law; therefore, the following expression can be obtained from the magnetic circuit.

$$N_b\left(i_{r1}+i_{r2}+i_{r3}\right)=\phi_b R_b \qquad (4.15)$$

Where i_{r1}, i_{r2} and i_{r3} are the resonant currents of the three-phases; R_b is the reluctance of the magnetic core. The leakage can be neglected, as the three windings are placed on the same leg.

If the balancing transformer is an ideal transformer with an infinite core permeability and zero magnetic reluctance, (4.15) can be reduced to the following

TABLE 4.II
DESIGN SPECIFICATIONS FOR THE LLC RESONANT CONVERTER

Symbol	Quantity	Value
P_o	Output power	500 W
f_{sw}	Switching frequency	200 kHz
V_i	Input voltage	390 V
V_o	Output voltage	12 V
L_{m1}, L_{m2}, L_{m3}	Magnetization inductances	132 µH
L_{r1}, L_{r2}, L_{r3}	Resonant inductances	23 µH
C_{r1}, C_{r2}, C_{r3}	Resonant capacitance	22 *n*F
L_n	Inductance ratio	5.7
Q_e	Quality factor	0.338
N:1	Turns ratio	16:1

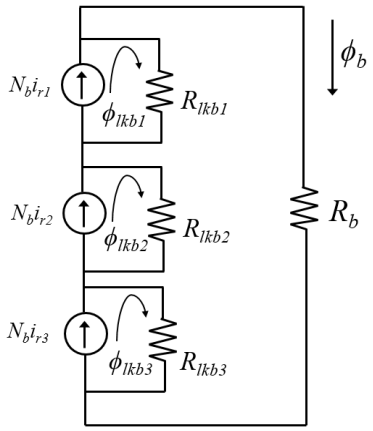

Fig.4.8 The equaivelent magnetic circuit of balancing transformer.

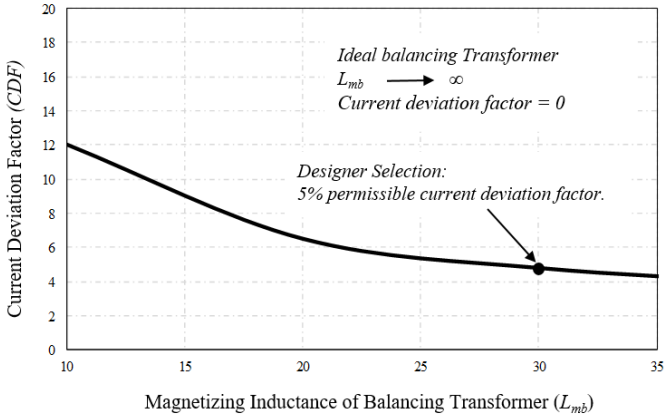

Fig.4.9 The relationship between permissible current deviation factor (δ) and balancing trnasformer magnetizing inductance (L_{mb}).

$$i_{r1} + i_{r2} + i_{r3} = 0 \tag{4.16}$$

Eq. (4.16) indicates that an ideal balancing transformer forces the sum of the three-phase currents to equal zero, and it imposes the same effect of connecting the integrated transformer's primary side in a star connection. However, in a practical balancing transformer the magnetizing inductance is finite. Therefore, it has a less unbalance suppressing effect than the star connection.

In order to provide a design guideline for the balancing transformer. A relationship between the CDF δ and the magnetizing inductance L_{mb} of the balancing transformer is derived based on the following

$$i_{r1} + i_{r2} + i_{r3} = \delta i_r = \frac{\phi_b N_b}{L_{mb}} \tag{4.17}$$

This relationship is depicted in Fig.4.9. It is clear that the CDF factor is inversely proportional to magnetizing inductance (L_{mb}). This relationship has been obtained by conducting several simulation tests using PLECS software (Plexim Inc.).

4.4 Equivalent Circuits of Different Topologies

In this section, the equivalent circuit of the magnetic component in different circuit topologies are presented. The mechanism of the current balancing transformer and the star connection is presented. Furthermore, the analogy between the different topologies is pointed out.

4.4.1 Paralleled non-coupled three transformers

The equivalent circuit of the three paralleled non-coupled transformers is presented in Fig.4.10. (a) In this topology, there is no interphase coupling, the coupling only exists between the primary and secondary of each phase. Furthermore, the non-coupled transformers are connected in parallel. Based on this circuit topology, the applied voltage on the primary winding can be obtained as

$$v_{\mathrm{A}} = L_{lkp1}\frac{di_{r1}}{dt} + L_{m1}\frac{di_{m1}}{dt} \tag{4.18}$$

$$v_{\mathrm{B}} = L_{lkp2}\frac{di_{r2}}{dt} + L_{m2}\frac{di_{m2}}{dt} \tag{4.19}$$

$$v_{\mathrm{C}} = L_{lkp3}\frac{di_{r3}}{dt} + L_{m3}\frac{di_{m3}}{dt} \tag{4.20}$$

This circuit topology has one condition to be satisfied. Since the sum of the three resonant currents has a return path to the ground. Therefore, in case of unbalance, the sum of the three resonant current equals the unbalanced current, based on the following equation

$$i_{\mathrm{r1}} + i_{\mathrm{r2}} + i_{\mathrm{r3}} = \delta i_{\mathrm{r}} \tag{4.21}$$

This method suffers from a poor current balance performance. Because, there is neither a magnetic coupling (balancing transformer) nor electric coupling (star connection) exists between the phases. For instance, if there's a mismatch in the resonant components of phase one, the unbalanced current of phase one would only encounter the mismatch of this phase and return back to the ground. Similarly, for phase two and phase three.

4.4.2 Parallel connection integrated transformer

In this topology, there is interphase coupling (three transformer actions between the three-phases T12, T13, and T23), beside the coupling between the primary-secondary of each phase. The primary windings are connected in parallel. Based on this circuit topology shown in Fig.4.10. (b), the applied voltage on the primary winding can be obtained as

$$v_{\mathrm{A}} = L_{lk1}\frac{di_{r1}}{dt} + L_{m1}\frac{di_{m1}}{dt} + L_{m12}\frac{di_{m12}}{dt} + L_{m13}\frac{di_{m13}}{dt} \tag{4.22}$$

$$v_B = L_{lk2}\frac{di_{r2}}{dt} + L_{m2}\frac{di_{m2}}{dt} - L_{m12}\frac{di_{m12}}{dt} + L_{m23}\frac{di_{m23}}{dt} \quad (4.23)$$

$$v_C = L_{lk3}\frac{di_{r3}}{dt} + L_{m3}\frac{di_{m3}}{dt} - L_{m13}\frac{di_{m13}}{dt} - L_{m23}\frac{di_{m23}}{dt} \quad (4.24)$$

However, the air-gaps are inserted in the outer leg, therefore the inter-phase coupling factor goes to zero, as previously explained in section 4.2. Consequently, the values of magnetizing inductances L_{m12}, L_{m13} and L_{m23} will be approximately zero (i.e short circuit, since $L=N^2/R$). Therefore, equations (4.22) - (4.24) becomes analogous to (4.18) - (4.20). Likewise, this circuit topology acts as the three-non coupled transformer, with only obtaining the benefit of reducing the magnetic material and eliminating the dead space. Nonetheless, the previous conditions in (4.21) is still satisfied in this topology, which leads to a poor current sharing because each phase behaves separately due to the absence of the coupling.

4.4.3 Star connected non-coupled three transformers

The equivalent circuit of the star connected non-coupled transformers is depicted in Fig.4.10. (c). The only difference in this topology compared to the conventional parallel connection is that this topology forces the sum of the three resonant currents to equal zero. The mechanism of the star connection can be explained as follow:

This circuit topology behaves the same as the conventional parallel connection under balancing conditions, since the three sinusoidal resonant current equal in magnitude and 120^0 phase-shifted. However, during unbalance, the star connection circuit behaves differently. For instance, as shown in Fig.4.11 (a), in the parallel connection the unbalanced current of each phase will only encounter the impedance of its relevant phase Z_i (which is deviated from other phases), and return back into the ground, because it is a zero impedance path. On contrary, within a Star connection, as shown in Fig.4.11 (b), the unbalanced current will never find a zero impedance return path, indeed it will encounter an equivalent impedance of the three-phases Z_1, Z_2, and Z_3. That means that the unbalanced resonant inductances have been averaged for the three phases. Therefore, a better current balance performance can be realized.

Nonetheless, as reported in Section 4.1.2., employing a star connection has some drawbacks, as the interleaving structure becomes unconventional and precludes the traditional phase-shedding techniques. Therefore, as an alternative solution we propose a magnetic-based current sharing method, which is analogous to this topology.

4.4.4 Integrated transformer with a current balance transformer

In this topology, a current balancing transformer is connected in series with the integrated transformer, as shown in Fig.4.10 (d).

This method gives an authority to the circuit designer to control the unbalanced current, as it becomes a function of the balancing transformer parameters. The mechanism of the current balancing transformer can be explained from different perspectives. From

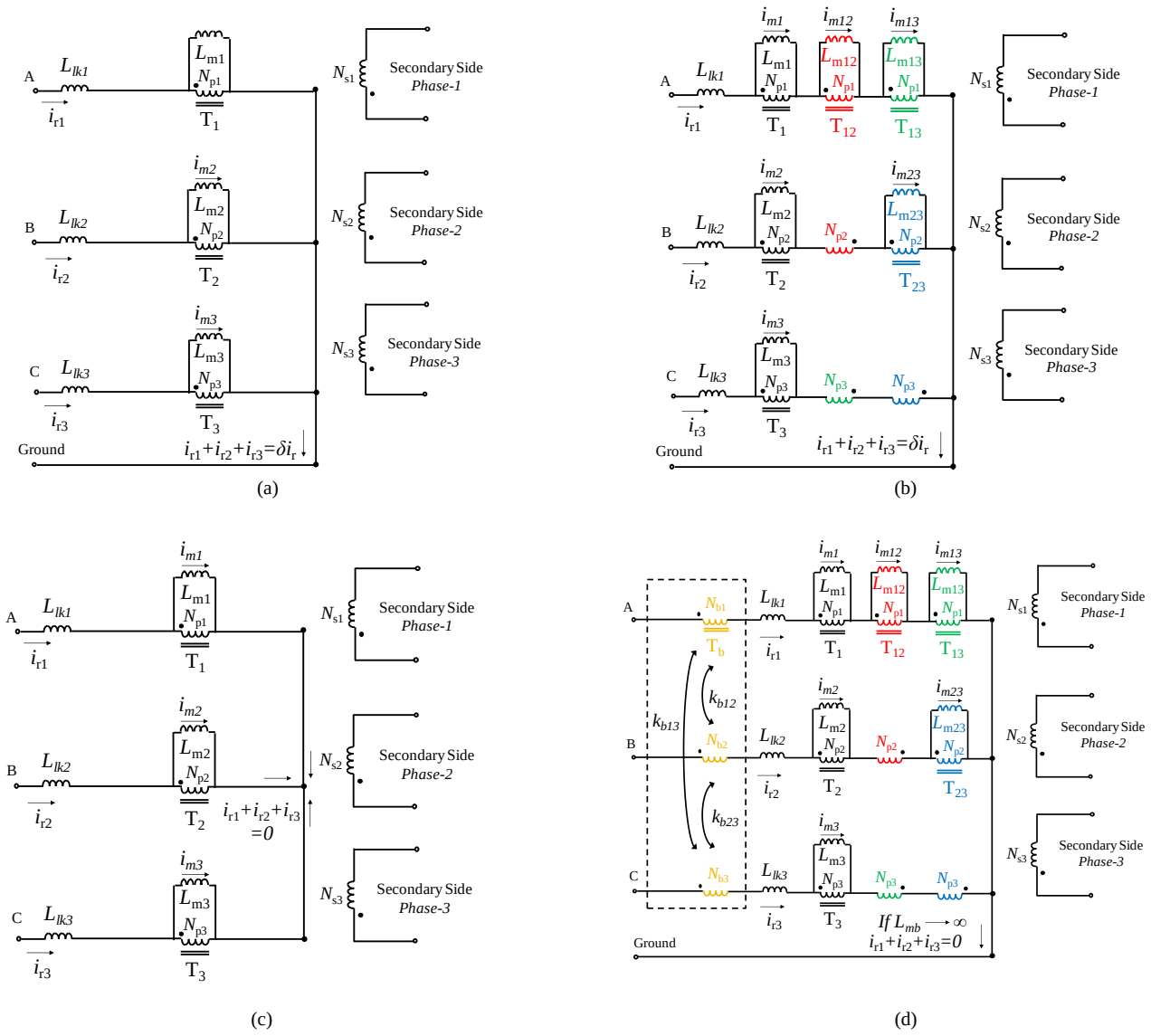

Fig.4.10 Equivalent circuits of different circuit topologies of the three-phase LLC resonant converter. (a) Non-coupled transformers and their primary windings are connected in parallel (conventional connection). (b) One integrated transformer and its primary windings are connected in parallel (conventionalconnection). (c) Non-coupled transformers and their primary windings are connected in Star. (d) The proposed circuit topology, one integrated transformer and its primary windings are connected in parallel (conventional connection) connected with a single balancing transformer.

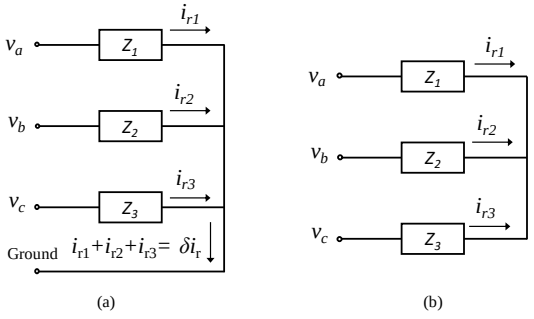

Fig.4.11 Basic circuit connection. (a) Conventional parallel connection (b) Star connection.

the circuit theory perspective, the three windings are positively coupled. Therefore, by applying Ampere's law around the contour "loop1" shown in Fig.4.12, it is clear that it imposes the same effect of connecting the transformer into a solid star connection. In

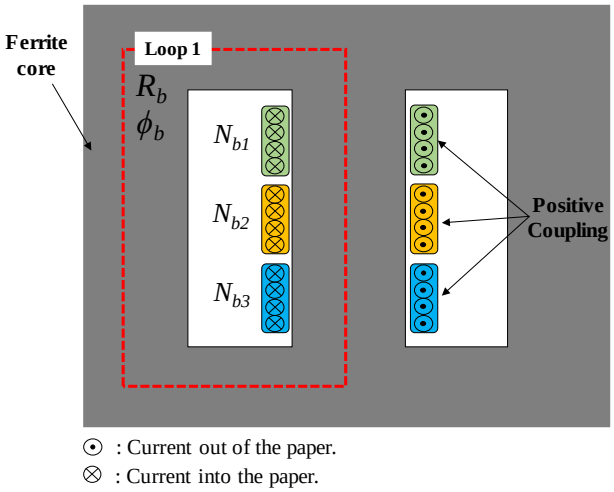

Fig.4.12 The proposed magnetic core structure for the balancing transformer.

other words, it forces the sum of the three currents to equal zero, with the benefit of realizing a simple conventional interleaving structure. From the magnetic point of view, and based on (4.15), it can be deduced that the balancing transformer has no effect under the balancing condition. Since the number of turns are equal, and the sum of the three sinusoidal currents goes to zero ($i_{r1} + i_{r2} + i_{r3} = 0$). Therefore, under balance condition there is no magneto motive force (*mmf*) in the balancing transformer. However, during unbalance conditions it behaves differently. For instance, if unbalance occurs in phase-one, and the current started to increase, a magneto motive force will be initiated by this unbalanced current. According to Faraday's law of induction, this mmf induce a voltage on the other two phases, and consequently induce currents in those two phases. The direction of the current will be such in a way that opposes the original mmf trying to cancel it, based on Lenz's law, leading to a suppression of the unbalanced current. Owing to the high coupling factor between the three-phases.

4.5 Simulation and Experimental Evaluation

4.5.1 Evaluation Considering Uneven Leakage and Magnetizing Inductances:

In a transformer utilized in the LLC converter, the leakage inductance is controlled by varying the distance between the primary and secondary winding on the same leg.

Therefore, in practice it is very difficult to realize identical values of resonant inductances between the phases, since the transformer leakages are utilized as resonance inductances.

On the other hand, the designed value of magnetizing inductance is achieved through realizing a proper value of the core effective permeability. The core permeability can be altered by inserting air gaps in each leg. Likewise, obtaining an identical values of magnetizing inductance among the three-phases is very difficult, since the air gap length is in a scale of millimeters. For those two reasons, the unbalanced current sharing is inevitable.

The current sharing performance of the balancing transformer is evaluated for both of the integrated and non-coupled transformers,

through simulation and experimental tests under unbalanced conditions. The results of the non-coupled transformers have been presented here as a benchmark to show a poor current sharing. The parameters of the three-phase LLC resonant converter are listed in Table 4.II.

Along with the simulation tests, the proposed topology has been experimentally evaluated. The experimental evaluation is conducted utilizing three circuit topologies: a) conventional parallel connection for the integrated transformer/non-coupled transformers. b) utilizing the balancing transformer c) connecting the integrated transformer/non-coupled transformers in a star connection. Fig.4.13 shows the experimental prototype using the conventional parallel connection for the spatial integrated transformer. The prototype use Schottky diodes (VS-100BGQ100), primary Mosfets (Toshiba, TK20E60W). Litz wires for the transformer's windings, and their cross-section area are 0.628 mm^2, 3.297 mm^2 for the primary and secondary windings, respectively. Texas Instruments DSP is used to drive the primary switches. The air gaps are purposely placed on the three outer legs of the integrated transformer to minimize the coupling factors, resulting in a reluctance ratio of $\alpha = 1.86x10^{-3}$; and a coupling factor k = 0.002. However, in practice, the actual values of the resonance and magnetizing inductances of the three phases are not exactly the same, leading to unbalanced current sharing between the phases. The measured parameters of the integrated transformer are listed in Table III, and the parameters of the non-coupled transformers are depicted in Table 4.IV.

4.5.2 Conventional parallel connection for the transformer.

In this case, the integrated transformer is connected in a conventional parallel connection. Due to the integrated transformer's uneven parameters, the resonant current per phase deviates, and therefore, the peak value of the unbalance current is 1.4 A, which is the sum of the three-phase currents (the red waveform), as shown in Fig.4.14. On the other hand, Fig.4.15 shows the resonant currents of the non-coupled transformers suffer from a poor current sharing performance, as the peak value of the unbalanced current is 2.6A. This has been presented as a benchmark, to effectively evaluate the proposed current balancing transformer.

4.5.3 Utilizing the balancing transformer

In this case study, we aim to reduce the peak of the unbalanced current into 5% balanced current (i.e δ=5%). Based on Fig.4.9, a CDF of 5% can be obtained by realizing a magnetizing inductance of 30µH. The balancing transformer is depicted in Fig.4.16, and its measured parameters are listed in Table 4.V.

Simulation tests were conducted using PLECS software (Plexim Inc.). In this section, the simulations tests have been done considering only the uneven resonant and magnetizing inductances listed in Table 4.III and Table 4.IV. The simulation result is depicted in Fig.4.17 (a), where the maximum value of the unbalanced current is around 0.2A, which is the sum of the three-phase currents, (the red waveform). The experimental result of the integrated transformer is shown in Fig.4.17 (b). The peak value of the unbalanced current is around 0.4 A (the red waveform).

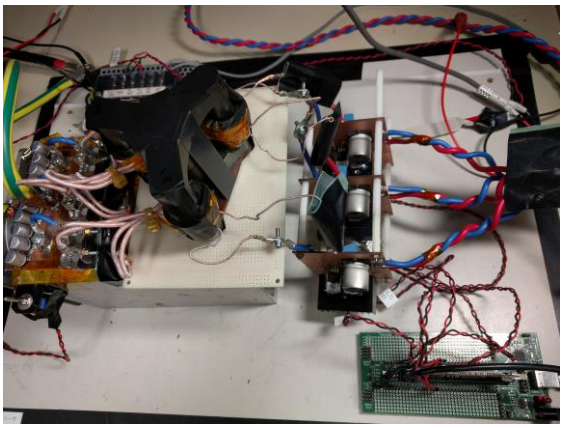

Fig.4.13 Experimental set-up of the three-phase LLC resonant converter with a 4-leg integrated transformer.

TABLE 4.III
MEASURED VALUES OF THE INTEGRATED TRANSFORMER

Parameters	Phase No.1	Phase No.2	Phase No.3
Resonance inductance L_r	24.5 µH	23 µH	21.9 µH
Magnetizing inductance L_m	129.5 µH	125 µH	130.1 µH
Number of Turns	32:2:2	32:2:2	32:2:2

TABLE 4.IV
MEASURED VALUES OF THE NON-COUPLED TRANSFORMER

Parameters	Phase No.1	Phase No.2	Phase No.3
Resonance inductance L_r	18.4 µH	24.8µH	19.3 µH
Magnetizing inductance L_m	139.6 µH	122 µH	116.5 µH
Number of Turns	32:2:2	32:2:2	32:2:2

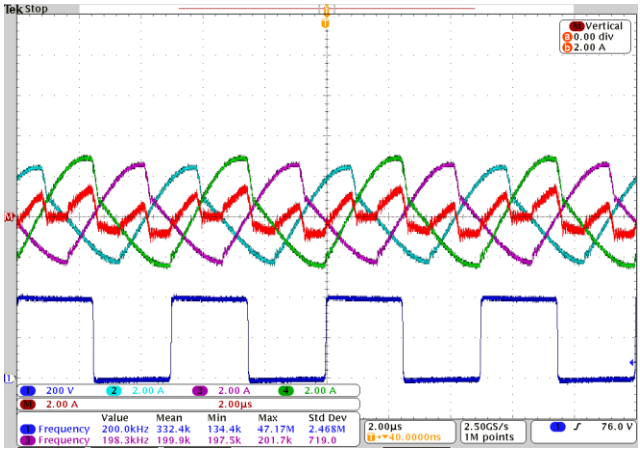

Fig.4.14 Experimental results while connecting the integrated transformer in a conventional parallel connection considering uneven magnetizing and leakage inductances.

Fig.4.17 (c) shows the experimental waveforms of the three non-coupled transformer topology connected in series with the current balance transformer. It worth mentioning that the leakage inductances of the balancing transformer are lumped into the resonant inductance L_{r1}, L_{r2}, and L_{r3}. However, since the value of the leakage inductances is very small (in scale of Nano Henry), their

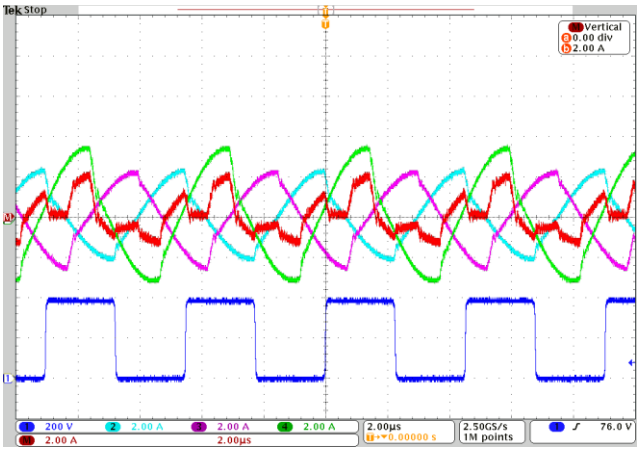

Fig.4.15 Experimental results while connecting the three non-coupled transformers in a conventional parallel connection considering uneven magnetizing and leakage inductances.

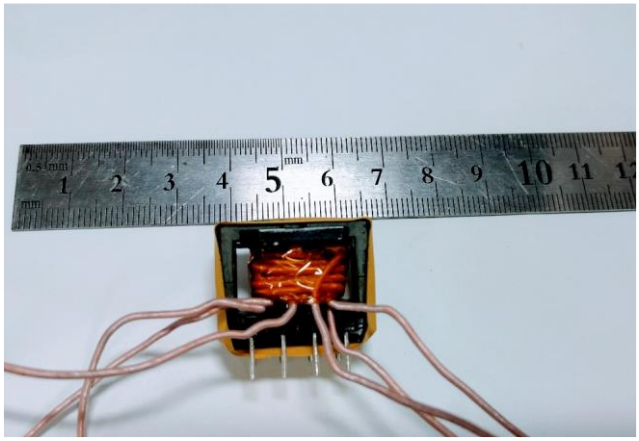

Fig.4.16 The balancing transformer

TABLE 4.V
MEASURED VALUES OF THE BALANCING TRANSFORMER

Parameters	Phase No.1	Phase No.2	Phase No.3
Number of turns (N_b)	4	4	4
Magnetizing inductance	30.2 µH	29.9 µH	30 µH
Leakage inductance	430 nH	370 nH	510 nH
Coupling factors	99%	99%	99%

influence is minimal and can be neglected. On the other hand, since the coupling coefficients equal 99% as shown in Table 4.V, the magnetizing current is approximately zero, which implies that the magnetizing inductance of the balancing transformer is open circuit (i.e doesn't participate in the resonance).

4.5.4 Connecting the transformer in star

Connecting the integrated transformer's primary side in star gives the same effect of an ideal balancing transformer. The simulation waveform ia shown in Fig.4.18 (a), where the maximum value of the unbalanced current approximately equals 0 A.

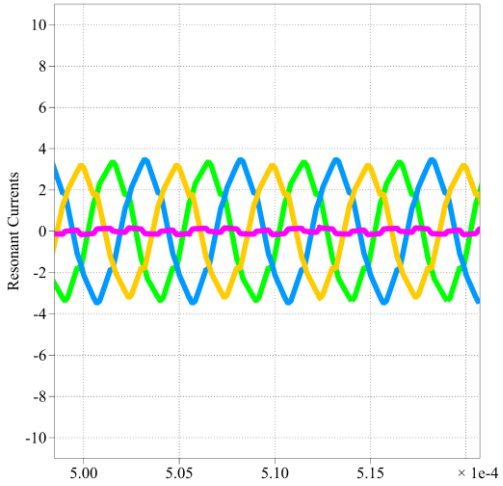

(a)

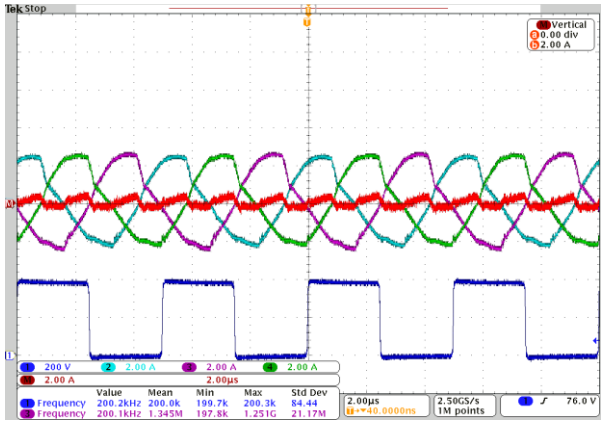

(b)

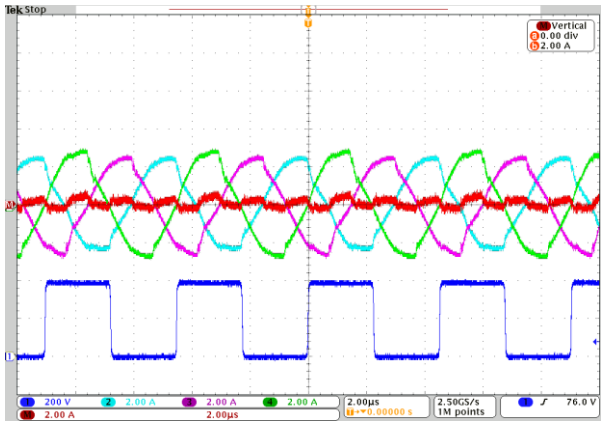

(c)

Fig.4.17 Waveforms utilizing a 30µH balancing transformer and considering uneven magnetizing and leakage inductances.(a) Simulation waveforms of resonant currents. (b) Experimental waveforms of resonant currents for integrated transformer. (c) Experimental waveforms of resonant currents for Three non-coupled transformers.

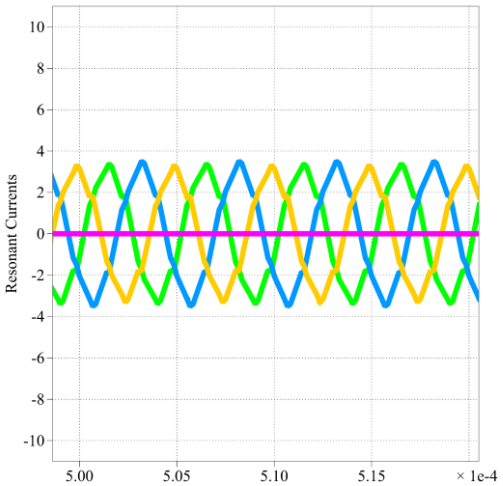

(a)

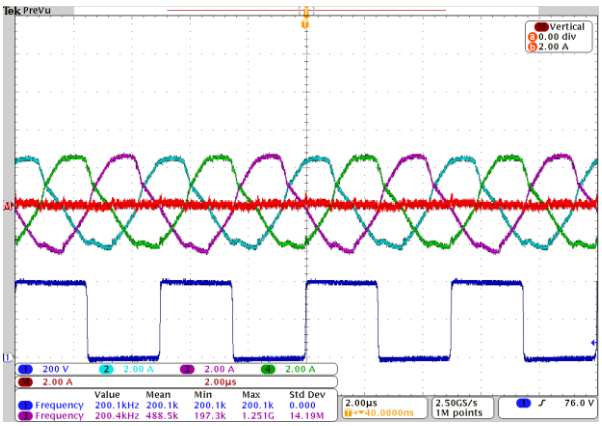

(b)

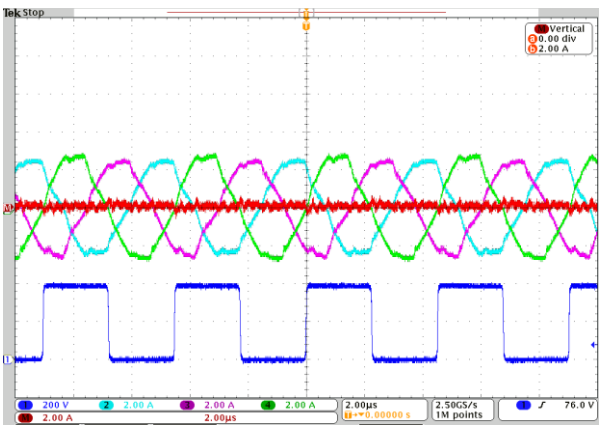

(c)

Fig.4.18 Waveforms utlizing a star connection and considering uneven magnetizing and leakage inductances.(a) Simulation waveforms of resonant currents. (b) Experimental waveforms of resonant currents for integrated transformer. (c)) Experimental waveforms of resonant currents for three non-coupled transformers.

On the other hand, whilst utilizing the integrated transformer, the experimental output of the peak unbalanced current is around

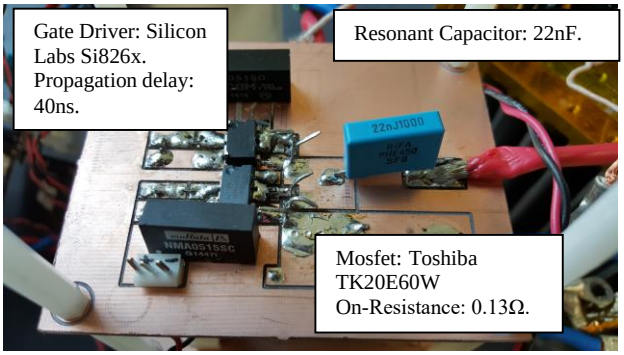

(a)

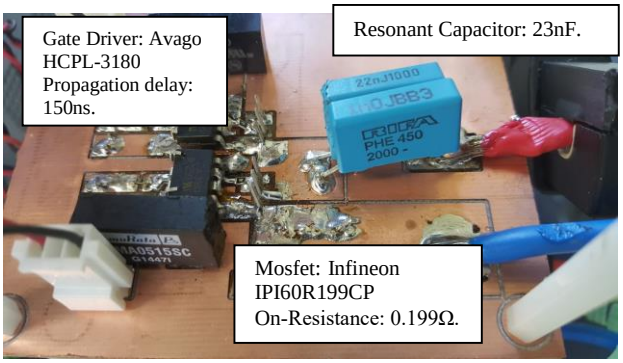

(b)

Fig.4.19 The primary bridge (a) Utilizing the balanced components for phase one and phase three. (b) Inserting additional resonant capacitor, utilizing different type of gate driver and Mosfet to add different sources of unbalance to phase two.

0.1 A, as shown in Fig.4.18 (b). Likewise, Fig.4.18 (c) shows the experimental waveforms of the three non-coupled transformer topology connected in star connection.

4.5.5 Further Evaluation Considering Other Sources of Unbalance:

In order to further validate the effectiveness of the proposed method under sever unbalancing conditions, several simulation and experimental tests have been conducted considering other sources of unbalance. The sources of the unbalance which are considered and added to the mismatch of the transformers inductances are: 1) Resonant capacitor. 2) Transistor on-resistance. 3) Propagation Delay of the gate drivers.

In this evaluation, the resonant capacitance value of phase two is intentionally altered into 23 nF instead of 22 nF. For this purpose, a 1 nF capacitor has been added in parallel with the 22 nF resonant capacitor of phase two. Moreover, in order to realize the unbalance of the on-resistance of the power transistor, the on-resistance values of S3 and S4 of phase two are intentionally altered into 0.199 Ω instead of 0.13 Ω. This has been realized by using a different power transistor, Infineon IPI60R199CP whose drain-source resistance is 0.199 Ω, instead of Toshiba TK20E60W, whose drain-source resistance is 0.13 Ω. Furthermore, in order to evaluate the balancing performance with a control mismatch, the gate driver Avago HCPL-3180 is intentionally utilized in phase 2, whose average propagation delay is 150ns. On contrary, in phase one and phase three, Silicon Labs Si826x gate drivers have been utilized, whose propagation delays are 40ns. The primary bridge circuits are depicted in Fig.4.19.

The simulation waveforms are shown in Fig.4.20. The unbalance behavior under the conventional parallel connection is shown in Fig.4.20 (a). The peak of the unbalanced current had been suppressed utilizing the balancing transformer, as shown in Fig.4.20 (b). The effect of the star connection is shown in last figure, Fig.4.20 (c).

The experimental waveforms utilizing the three non-coupled transformers and integrated transformer are shown in Fig.4.21 and Fig.4.22, respectively. The waveforms during the conventional parallel connection are shown in Fig.4.21 (a) and Fig.4.22 (a), where it is clear that the LLC converter suffers from an extremely poor current sharing among the phases in case of the non-coupled transformers because of the measured inductances are far from being close to the designed inductance values. In Fig.4.21 (b) and Fig.4.22 (b), the resonant current waveforms are shown while utilizing the current balancing transformer, it is clear that the balancing transformer had succeeded to suppress the peak value of the unbalanced current. In Fig.4.21 (c) and Fig.4.22 (c), the waveforms are presented to show the effect of connecting the three transformers in a star connection, which has the same effect of utilizing an ideal balancing transformer.

4.5.6 Design Procedures:

One of the advantages of utilizing the proposed balancing transformer to improve the current balance is its simplicity. The design procedures are listed into the given below steps: Step 1: Utilizing the converter specifications to drive a relationship between the magnetizing inductance of the balancing transformer and the CDF, as mentioned in section 4.3. Step 2: Based on the designer selection of the permissible unbalance in the circuit, a proper value of the magnetizing inductance for the balancing transformer shall be selected. (The circuit designer has to tradeoff between improving the circuit balancing performance, and the circuit efficiency. Since, to realize a higher value of magnetizing inductance more number of turns will be needed, and thus the copper losses will be increased).

Step 3: The balancing transformer shall be designed based on the magnetizing inductance value chosen in the previous step.

Step 4: Constructing the prototype of the multi-phase LLC converter.

4.6 Summary

In this chapter, a balancing transformer has been proposed to tackle the unbalanced current, which arises from the uneven phase parameters in the three-phase LLC resonant converter. The basic principle of the balancing transformer is based on Ampere's law, by forcing the sum of the three resonant currents to zero. Beside the leakage and magnetizing inductances, further evaluation has been performed under harsh unbalancing conditions, considering uneven values of 1) Resonant capacitors. 2) Transistor on-resistance. 3) Propagation delay of the gate drivers. The proposed balancing transformer has been proven to be effective and it had been concluded from this study that connecting the integrated transformer in a star provides the best current balance performance because it acts as an ideal balancing transformer. Nonetheless, utilizing a balance transformer might be a solution for other multi-

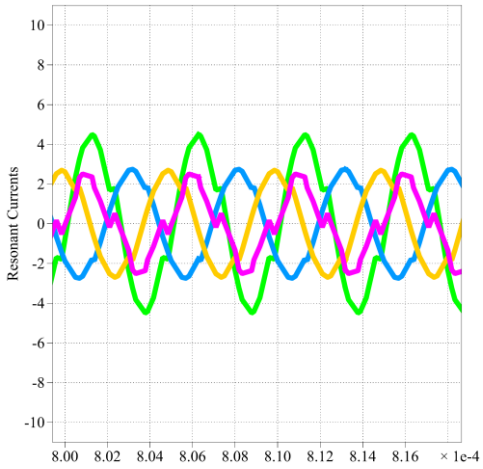

(a)

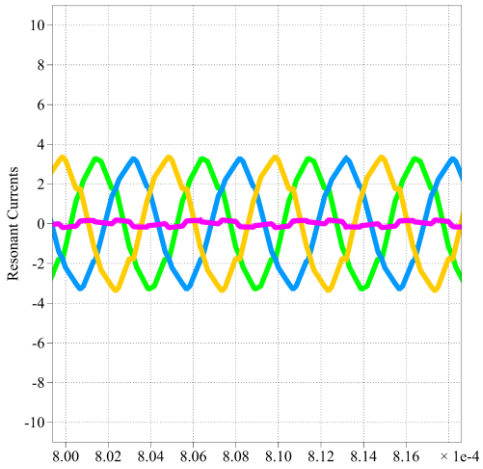

(b)

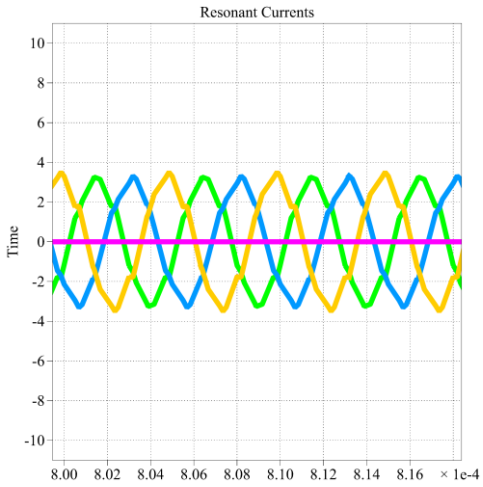

(c)

Fig.4.20 Simulation waveforms considering uneven magnetizing and leakage inductances, uneven resonant capacitance, uneven on-resistance of the primary switches, and propagation delay of the gate driver. (a) Conventional parallel connection. (b) Utilizing a 30µH balancing transformer. (c) in case of transformer is Star connected.

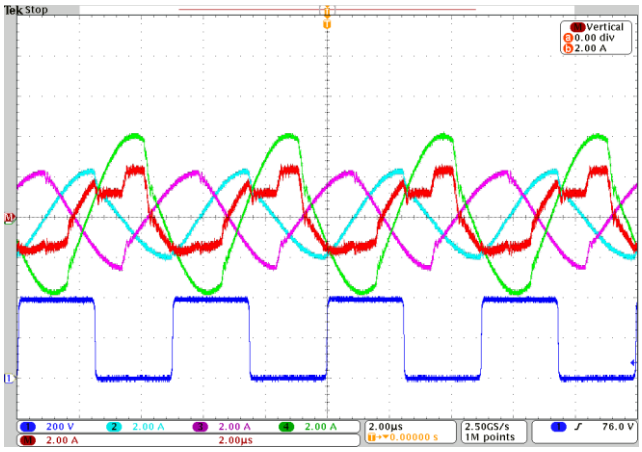

(a)

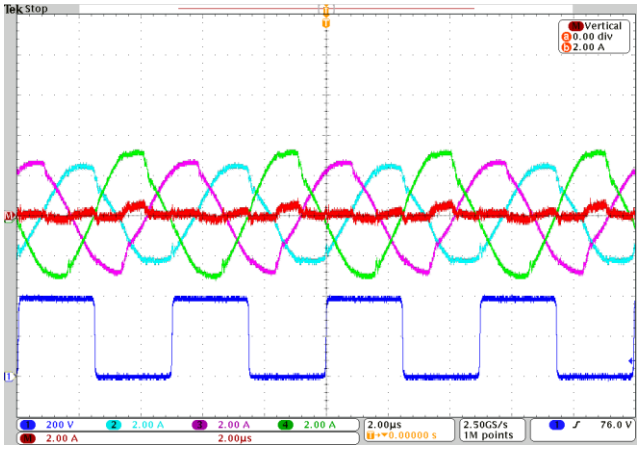

(b)

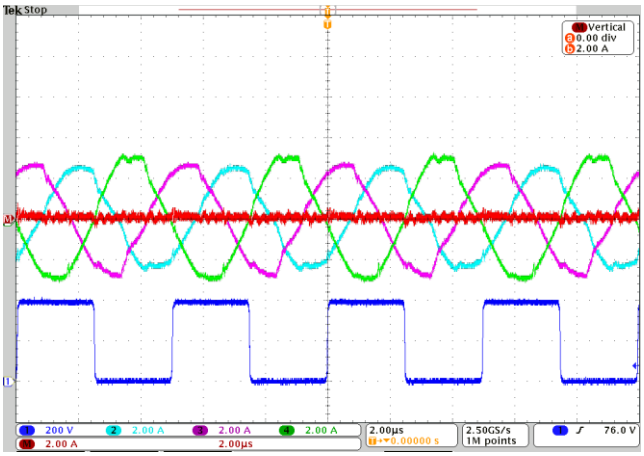

(c)

Fig.4.21 Experimental waveforms of the three non-coupled transformers considering uneven magnetizing and leakage inductances, uneven resonant capacitance, uneven on-resistance of the primary switches, and propagation delay of the gate driver. (a) Conventional parallel connection. (b) Utilizing a 30µH balancing transformer. (c) in case of transformer is Star connected.

phase topologies where realizing a star connection is not feasible. Moreover, utilizing a current balance transformer keeps the

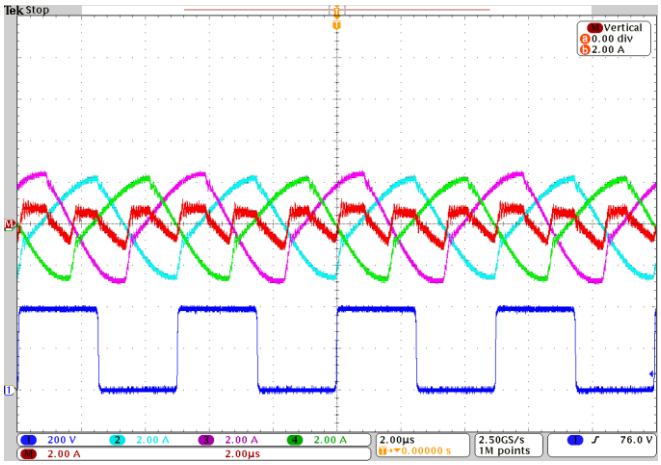

(a)

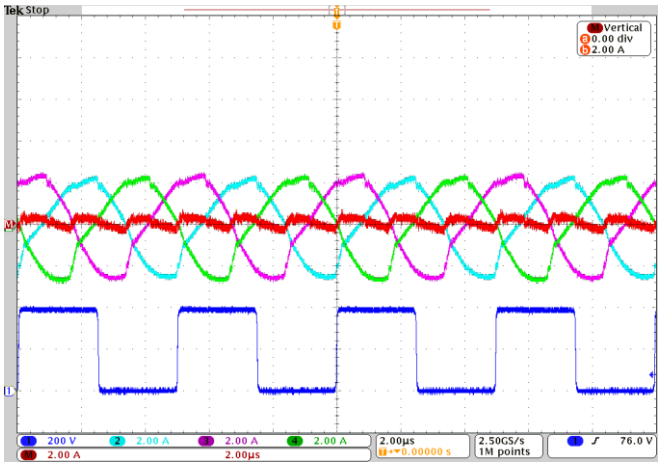

(b)

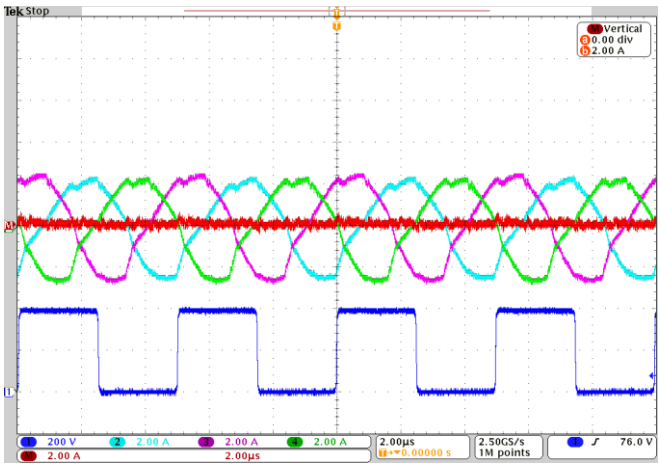

(c)

Fig.4.22 Experimental waveforms of the three non-coupled transformers considering uneven magnetizing and leakage inductances, uneven resonant capacitance, uneven on-resistance of the primary switches, and propagation delay of the gate driver. (a) Conventional parallel connection. (b) Utilizing a 30µH balancing transformer. (c) in case of transformer is Star connected.

interleaving topology of the LLC converter simple, and it allows the traditional phase-shedding to be easily implemented. The

proposed current balancing transformer is easy to be implemented by the industry engineers compared with other control methods. Implementing the proposed current balancing transformer can protect three-phase LLC resonant converters from the current unbalance issues, and hence keep them efficient.

4.7 Appendix

In this chapter, the spatial core is proposed for the integrated transformer. This magnetic structure is symmetric, and it offers an equalized magnetic reluctance for the three-phases. In other words, the three-phases are distributed among symmetrical outer limbs (having same magnetic path length, cross sectional area), and the center leg is functioning as a common return path for the magnetic flux of the three-phases, as shown in Fig.4.23. Nonetheless, employing planar magnetic cores would improve the transformer packaging.

In a 4-leg planar core, as shown in Fig.4.24. each magnetic flux is encountering a magnetic path length different than the other phase, that may complicate the transformer design because the structure is no longer symmetric.

In fact, there is a possibility of a further reduction of the center limb because the sum of the three ac fluxes is reduced, due to the superimposition of the three ac fluxes in the center leg (act as a return path for each phase), owing to the 120^0 phase shift switching of the primary bridge. In other words, the peak flux of the outer legs is higher than the peak flux of the center leg.

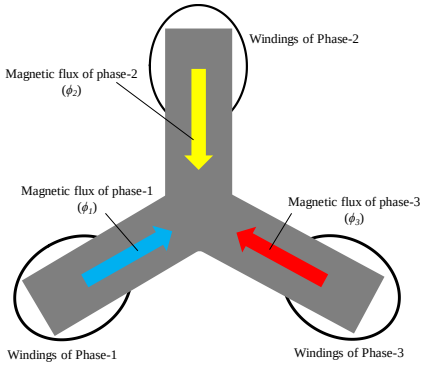

Fig.4.23 Top view of the spatial four-legs magnetic core.

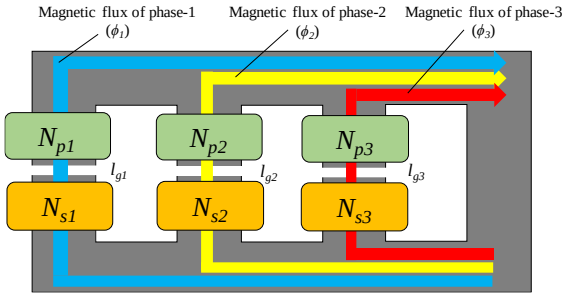

Fig.4.24. Four-Leg Planar structure

References

[1] I. Batarseh, "Resonant Converter Topologies with Three and Four Energy Storage Elements", IEEE Trans. Power Electron, Vol. 9, No. 1, pp. 64-73, Jan. 1994.

[2] T. Jiang, Q. Lin , J. Zhang and Y. Wang "A novel ZVS and ZCS three-port LLC resonant converter for renewable energy systems" in Proc. IEEE Energy Conversion Congress and Expo. (ECCE), pp. 2296-2302, Sep. 2014.

[3] J. Hong and J. Kwon, "Theoretical analysis and optimal design of LLC resonant converter," in Proc. IEEE European Conf. on Power Electr. and Apps., pp. 1-10, Sep. 2007.

[4] S. Zong, H. Luo, W. li, Y. Deng and X. He, "Asymmetrical Duty Cycle-Controlled LLC Resonant Converter with Equivalent Switching Frequency Doubler," IEEE Trans. Power Electron, Vol. 31, No. 7, pp. 4693-4973, 2016.

[5] S. Arumugam, E. Karthikeyan and P. Saikumar, "A novel analysis of high frequency LLC converter for fuel cell systems," International Conference on Information Communication and Embedded Systems (ICICES), pp. 913-918, 2013.

[6] Z. Fang, S. Duan, C. Chen, X. Chen and J. Zhang, "Optimal design method for LLC resonant converter with wide range output voltage," IEEE Applied Power Electronics Conference and Exposition (APEC), pp. 2106-2111, March, 2013.

[7] E. Orietti, P. Mattavelli, G. Spiazzi, C. Adragna and G. Gattavari, "Analysis of multi-phase LLC resonant converters," in Proc. Brazilian Power Electronics Conference, COBEP 2009.

[8] T. Jin and K. Smedley, "Multiphase LLC Series Resonant Converter for Microprocessor Voltage Regulation," in Proc. IEEE Industry Applications Conference, 2006.

[9] K. Yi and G. Moon, "Novel two-phase interleaved LLC series-resoant converter using a phase of the resonant capacitor," IEEE Transactions on Industrial Electronics, Vol. 56, No. 5, pp. 1815-1819, April 2009.

[10] T. Jin and K. Smedley, "Multiphase LLC Series Resonant Converter for Microprocessor Voltage Regulation," IEEE Industry Applications Conference, (41st IAS Annual Meeting.) Oct. 2006.

[11] T. Jin, K. Smedley "Multiphase resonant converter for DC-DC applications" US patent 8259477 B2, Sep. 2012.

[12] H. Kim, J. Baek, M. Ryu, J. Kim and J. Jung, "The high-efficiency isolated AC-DC converter using the three-phase interleaved LLC resonant converter employing the Y-connected rectifier", IEEE Trans. Power Electron, Vol. 29, No. 8, Aug. 2014.

[13] K. Murata, F. Kurokawa, "An interleaved PFM LLC resonant converter with phase-shift compensation," IEEE Trans. Power Electron, Vol. 31, No. 3, pp. 2264-2272, March 2016.

[14] M. Sato, R. Takiguchi, J. Imaoka and M. Shoyama, "A Novel Secondary PWM-Controlled interleaved LLC Resonant Converter for Load Current Sharing", in Proc. IEEE 8th International Power Electronics and Motion Control Conference (IPEMC-ECCE Asia), pp. 1-5, May 2016.

[15] W.-J. Gu and K. Harada, "A new method to regulate resonant converters," IEEE Trans. Power Electron., vol. 3, no. 4, pp. 430-439, Oct. 1988.".

[16] W. J. Gu and K. Harada, "A circuit model for the class E resonant DC-DC converter regulated at a fixed switching frequency," IEEE Trans. Power Electron., vol. 7, no. 1, pp. 99-110, Jan. 1992.

[17] J. Cheng, A. Witulski, and J. Vollin, "Dynamic analysis of the Class-D converter at fixed frequency using amplitude and phase modulation," in Proc. Power Electron. Spec. Conf., vol. 1, pp. 387-393, May, 1998.

[18] J. Cheng, A. Witulski, and J. Vollin, "A generalized DC model and low-frequency dynamic analysis for the Class-D converter at fixed frequency," IEEE Trans. Power Electron., vol. 15, no. 6, pp. 1212-1220, Nov. 2000.

[19] L. Huber and M. Jovanoviae, "Evaluation of AC VRM topologies for high-frequency power distribution systems," in Proc. Appl. Power Electron. Conf. Expo., vol. 1, pp. 160-166, March, 2001.

[20] Y.-T. Chen,W.-M. Lin, and Y.-H. Liu, "Analysis and design of a dimmable electronic ballast controlled by a switch-controlled capacitor," IEEE Trans. Ind. Electron., vol. 52, no. 6, pp. 1564-1572, Dec. 2005.

[21] H.-J. Chiu and S.-J. Cheng, "Single-stage voltage source charge-pump electronic ballast with switched-capacitor dimmer for multiple fluorescent lamps," IEEE Trans. Ind. Electron., vol. 54, no. 5, pp. 2915-2918, 2007.

[22] Z. Hu, Y. Qiu, L. Wang, and Y.-F. Liu, "An Interleaved LLC Resonant Converter Operating at Constant Switching Frequency," IEEE Power Electronics Transactions on, vol. 29, pp. 2931-2943, 2014.

[23] Z. Hu, Y. Qiu, L. Wang, and Y.-F. Liu, "An interleaved LLC resonant converter operating at constant switching frequency," in Energy Conversion Congress and Exposition (ECCE), 2012 IEEE, 2012, pp. 3541-3548.

[24] Z. Hu, Y. Qiu, Y.-F. Liu, and P. C. Sen, "A Control Strategy and Design Method for Interleaved LLC Converters Operating at Variable Switching Frequency," IEEE Trans. Power Electron, vol. 29, pp. 4426-4437, 2014.

[25] B.-C. Kim, K.-B. Park, C.-E. Kim, and G.-W. Moon, "Load sharing characteristic of two-phase interleaved LLC resonant converter with parallel and series input structure," in Proc. IEEE Energy Conversion Congress and Exposition, (ECCE), pp. 750-753, Sep. 2009.

[26] F. Jin, F. Liu, X. Ruan, and X. Meng, "Multi-phase multi-level LLC resonant converter with low voltage stress on the primary-side switches," in Proc. IEEE Energy Conversion Congress and Exposition (ECCE), pp. 4704-4710, 2014.

[27] B. C. Kim, K. B. Park, C. E. Kim, and G. W. Moon, "Load sharing characteristic of two-phase interleaved LLC resonant converter with parallel and series input structure," in Proc. IEEE Energy Conversion Congress and Exposition, 2009. (ECCE), pp. 750-753, Sep. 2009.

[28] E. Orietti, P. Mattavelli, G. Spiazzi, C. Adragna, and G. Gattavari, "Current sharing in three phase LLC interleaved resonant converter," in Proc. IEEE Energy Convers. Congr. Expo. (ECCE), pp. 1145-1152, Sep. 2009.

[29] E. Orietti, P. Mattavelli, G. Spiazzi, C. Adragna, and G. Gattavari, "Analysis of multi-phase LLC resonate converter," in Brazilian Power Electronics Conference, Dec. 2009.

[30] H. Wand, Y. Chen, Y. Qiu, P. Fang, Y. Zhang, L. Wang and Y. Liu,"A common capacitor multi-phase LLC converter with passive current sharing ability", IEEE Trans. on power electronics, Vol. PP, No.99, pp.1-1 Jan. 2017.

[31] H. Wand, Y. Chen, Y. Liu, J. Afsharian and Z. Yang,"A common inductor multi-phase LLC converter", in Proc. IEEE Energy Convers. Congr. Expo. (ECCE), pp. 548-555, Sep. 2015.

[32] H. Wand, Y. Chen, Y. Liu, J. Afsharian and Z. Yang, "A passive current sharing method with common inductor multi-phase LLC resonant converter", IEEE Trans. Power Electron, Vol. PP, No.99, pp.1-1, Nov. 2016.

[33] Y. Nakakohara, H. Otake, T. Evans, T. Yoshida, M. Tsuruya and K. Nakahara, "Three-phase LLC series resonant DC/DC converter using SiC MOSFETs to realize high-voltage and high-frequency operation," IEEE Trans. on Ind. Electron., Vol. 63, No. 4, pp. 2103-2110, April 2016.

Chapter 5: Effects of Secondary Leakage Inductance on the LLC Resonant Converter

5.1 Introduction

5.1.1 Research Motivation: Secondary Leakage Inductance

Resonant power converters, specifically, the LLC resonant converters are considered as promising power converter topologies; because of their potential to achieve high switching frequencies, lower switching losses, and their ability to absorb the transformer leakage and magnetizing inductances, and utilizing them in the resonant tank. The use of an integrated transformer allows for a drastic footprint and weight reduction of the passive component in the circuit [1]-[7]. The single-phase LLC converter is depicted in Fig.5.1. A proper design for the gapped transformer in the LLC converter is essential as it affects the whole operation of the LLC converter. For instance, air gaps are intentionally inserted in a transformer utilized in the LLC resonant converter to reduce the effective permeability of the magnetic core, and hence to minimize the magnetizing inductance (L_m). Minimizing the magnetizing inductance is essential for the soft switching operation of the LLC converter, despite the fact that it results in higher values of magnetizing current (i_m), which may deteriorate the converter efficiency [8]-[9]. On the other hand, the resonant inductance plays an important role in determining the voltage gain [10].

It is quite often to utilize the transformer leakage inductance in the resonant tank of the LLC resonant converter to allow for a drastic reduction in the converter cost, weight, and footprint. The effects of the secondary leakage inductance on the operation of the LLC resonant converter are not well-discussed in the relevant literature, and it is the purpose of this chapter to give an insight into these effects. The contribution of this chapter lies in the following: (1) highlighting that it is not always an accurate assumption to consider that the values of the primary and secondary leakage inductance are identical, specifically in asymmetric magnetic core structures. (2) it is disclosed in this chapter that the well-known coupling factor (k_{12}) cannot properly express the unequalized leakage inductance distribution in the proposed transformer. Therefore, for this purpose, the primary coupling factor (k_1) and secondary coupling factor (k_2) are brought into practice to appropriately express the unequalized leakage distribution on the primary and secondary windings, which can be controlled by: (i) allocation of the relevant winding with respect to the air gap. (ii) utilizing noise absorber. (iii) changing the distance between the winding. Several transformer prototypes had been built and experimentally tested to validate these hypotheses (3) it has been observed from the experimental tests conducted in this chapter that the transformer voltage gain and efficiency can be improved when the transformer leakage inductance is concentrated on the secondary side to avoid the voltage drop inflicted by the relatively large value of the magnetizing current (i_m), especially at light

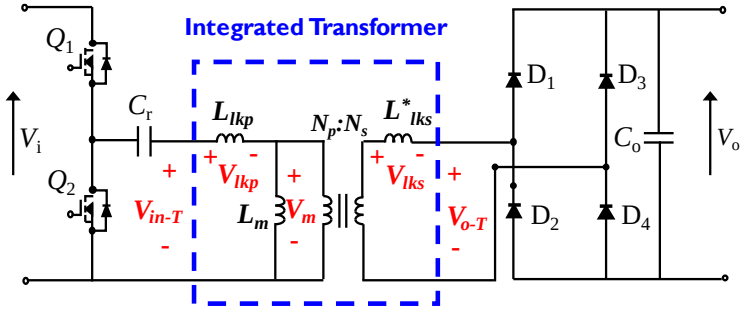

Fig. 5.1 Single-phase LLC resonant converter with integrated transformer.

load condition (4) it is reported in this chapter that in a transformer structure with concentrated value of leakage on secondary side would decrease the resonant tank input impedance, vertically widen the voltage-gain curve of the converter, and eventually increase the frequency control bandwidth with respect to the load variation. Transformer prototypes had been constructed and tested in 390V/12V-220W LLC resonant converter to evaluate the proposed analysis.

5.1.2 Secondary Leakage Inductance - Literature Review:

While it is true to say that the LLC resonant converter is well-documented in the literature, the additional issues that arise from the transformer secondary leakage need more attention. For instance, the design methodology for the transformer has been presented in [8]-[9]. The design method reported in these studies is based on the area product approach. The presented area product approach has treated the LLC transformer as an energy storage component (i.e inductor), since the air gap plays an important role to store the magnetic energy, and allows for a soft switching operation for the converter. Those two discussions did not take the secondary leakage into account. Other studies [11]-[14] proposed Matrix transformer which is suitable for the applications with high step-down ratio and high output currents. The purpose of the work done in [15]-[16] is to reveal that the gain curve of the LLC converter is very sensitive to the parasitic components, namely, the steady state output capacitance of the switching devices, capacitance of the transformer windings, junction capacitance of the rectifier diode. Nonetheless, no solutions have been reported to tackle the effects of the aforementioned parasitics, except for the diode junction capacitance, where a dummy load has been added to reduce the diode junction capacitance effect.

The transformer intra-winding and inter-winding capacitances, have been addressed in [17]-[18], and the authors proposed an optimized winding layouts and core structures to mitigate the parasitic capacitances, which usually lead to an unpredictable behavior of output voltage and loss of the regulation. The proposed design has been proven efficient. In [19], the rectifier diode junction capacitance and the winding capacitance had been considered. The authors of [19] added an additional capacitor to the transformer secondary side to extend the operating frequency range of the LLC, and improve its regulation. A detailed magnetic design method for a three-phase integrated transformer had been presented in [20], where the magnetizing and leakage inductances

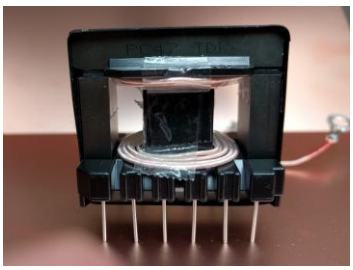

Fig.5.2 structure presented in [26] with identical 5:5 winding turns.

of the three phases were integrated into a single commercially available magnetic core. Nonetheless, the effects of the secondary leakage inductance are not discussed in this study.

It can be concluded that while a lot of work has been done on the LLC topology, most of them have followed the first harmonic approximation (FHA) to obtain a simplified ac equivalent circuit by completely ignoring the secondary leakage [21]-[25]. Nonetheless, the voltage gain of the LLC converter is very sensitive to the resonant tank parameters. Therefore, within an integrated transformer, where the transformer leakage is utilized as a resonant component, ignoring the secondary leakage would result in an imprecise design.

The secondary leakage was first considered by Choi in [6] while deriving the FHA approximated equivalent circuit. However, this study considered that the secondary leakage equals the primary leakage inductance, and no in-depth analysis had been reported neither to control the value of the secondary leakage inductance nor to evaluate the effects of secondary leakage on the performance of the LLC resonant converter.

In [26], an asymmetric transformed structure has been presented with identical turns ration of 5:5, as shown in Fig.5.2. Nonetheless, in [26] there is no theoretical analysis had been presented to discuss the effects of the secondary leakage inductance on the LLC converter operation, such as efficiency, transformer voltage gain, and frequency control bandwidth. Furthermore, neither simulation nor experimental results have been presented in [26] to evaluate the effects of the secondary leakage inductance on the operation of the LLC converter. In this discussion, it is revealed that the secondary leakage inductance can be manipulated and intentionally controlled by placing the secondary winding in a close contact with the magnetic core and adding noise absorber layers. Moreover, it has been disclosed that (k_{12}) cannot properly express the unequalized leakage distribution in the proposed transformer. Therefore, the primary coupling factor (k_1) and secondary coupling factor (k_2) are brought into practice to appropriately express the unequalized leakage inductance distribution on the primary and secondary windings, which has never been reported previously in the relevant literature. It is proven that the proposed transformer voltage gain has been increased, at light load condition, as the voltage drop on the primary leakage due to the magnetizing current has been eliminated. Moreover, the frequency control bandwidth with respect to the load variation is investigated and it turned out that the proposed transformer has a wider frequency control bandwidth due to the secondary leakage inductance.

5.1.3 Chapter Contents

This chapter is organized as follows. In section 5.2, the unbalanced magnetic leakage distribution is intentionally achieved to minimize the primary leakage inductance to realize a transformer structure with concentrated value of leakage inductance on secondary side. The purpose of realizing this transformer structure is to evaluate the effects of the secondary leakage inductance (transformer voltage gain, efficiency, and frequency control bandwidth) on the LLC resonant converter, as later explained in sections 5.4 and section 5.5.

In section 5.3, several experimental tests showed that in some cases (k_{12}) might be constant, however, (k_1) and (k_2) change while inserting noise absorber layer, which completely affects the operation of the LLC resonant converter.

In section 5.4, the circuit analysis of the transformer T-model is provided, with the purpose of highlighting that at light load condition the magnetizing inductance (L_m) can relatively inflict a large voltage drop on the primary leakage inductance. Therefore, a transformer structure with concentrated leakage on secondary side would realize higher voltage gain, effective turns ratio and efficiency compared with a structure with primary leakage inductance.

In section 5.5, the effects of the secondary leakage inductance on the frequency control bandwidth with respect to load variation are examined.

In section 5.6, experimental and simulation tests are conducted for a 220W, 390V-12V single-phase LLC resonant converter. The voltage gains of the two transformers prototypes had been experimentally measured and presented for comparison. The transformer effective turns ratio had been calculated. Moreover, the efficiency has been measured to compare the performance of the LLC converter under the two transformer designs. Furthermore, the frequency bandwidth has been experimentally examined to evaluate the analysis presented in section 5.5.

The summary is presented in section 5.7 and the appendix is presented in section 5.8.

5.2 Transformer Structure with Concentrated Leakage on Secondary-side

The applied voltage on the transformer windings sets up a pure ac flux based on Faraday's law. Nonetheless, there is some flux which links only one winding but not the other, mostly by leaking into the air. Here after, the leakage magnetic field intensity (H_{lk}) is magnetic field distributed in the space between the primary and the secondary windings and the magnetic field intensity in the air gap length is denoted as H_g.

According to Dowell's model [26], [29], when considering the leakage due a particular winding layer, the only other layers needed to be considered are those lie between this particular layer and an adjacent position of zero magnetomotive force mmf. In this regard, the magnetic core can be considered as a zero mmf position, assuming infinite permeability. In this discussion, we had intentionally placed the primary winding in the vicinity of the air gap and the secondary winding in a close contact to the magnetic

core “zero mmf position”, as a result, the magnetic leakage energy between the primary and secondary windings originates due to the secondary winding. The theoretical discussion is as follows

In the proposed transformer structure shown in Fig.5.3. The proposed transformer structure is asymmetric (i.e the air gap is not centralized, named here as EI), this shape is unlike the symmetric core shape (i.e the air gap is centralized, named here as EE). The two core shapes are depicted side-by-side and shown in Fig.5.4. In the EI shape, the primary windings are located in the vicinity of the air gap, and the secondary windings are located in a close contact with the magnetic core (zero mmf position). By integrating Ampere’s law around loop 1, the following expression can be obtained

$$H_{lk} \cdot a = N_s \cdot i_s \tag{5.1}$$

Therefore, the leakage magnetic field intensity (H_{lk}) in the space between the primary and secondary windings can be expressed

$$H_{lk} = \left(\frac{N_s i_s}{a} \right) \tag{5.2}$$

On the other hand, integrating loop 2 will lead to

$$2H_g \cdot l_g = \left(N_s i_s - N_p i_p \right) \tag{5.3}$$

Where l_g is the air gap length.

From (5.3), the field intensity in the gap (H_g) can be expressed as

$$H_g = \left(\frac{N_s i_s - N_p i_p}{2 l_g} \right) \tag{5.4}$$

The magnetic energy can be considered as the sum of the energy stored in the air gap and the leakage energy. Therefore, the magnetic energy expression for structure a can be obtained as below

$$E = \frac{1}{2} \mu_o H_g^2 (4V_g) + \frac{1}{2} \mu_o H_{lk-a}^2 (2V_{lk}) \tag{5.5}$$

Where V_g, V_{lk}, a are the air-gap volume (the volume of the center leg is considered as $2V_g$), volume of the space between the primary and the secondary windings, and width of the core window, respectively.

Substituting (5.2), (5.4) in (5.5) results in

$$E = \frac{\mu_o V_g}{2 l_g^2} (N_p i_p - N_s i_s)^2 + \frac{\mu_o V_{lk}}{a^2} (N_s i_s)^2 \tag{5.6}$$

Equation (5.6) can be organized to the below formula

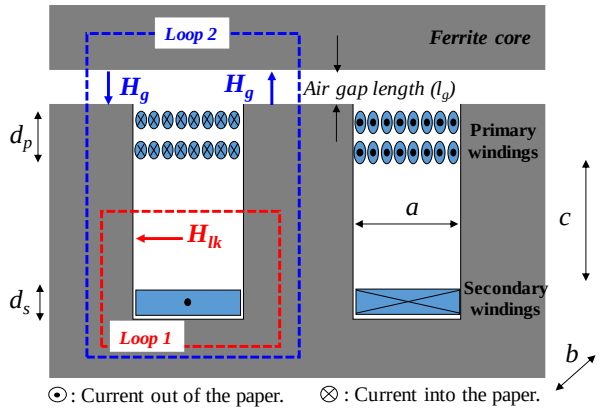

Fig.5.3 The proposed transformer structure with 16:1 turns ratio to allow the magnetic leakage between the windings to be originated from the secondary winding (the secondary winding is placed near a zero mmf position) and the primary winding is located at the vicinity of the air gap.

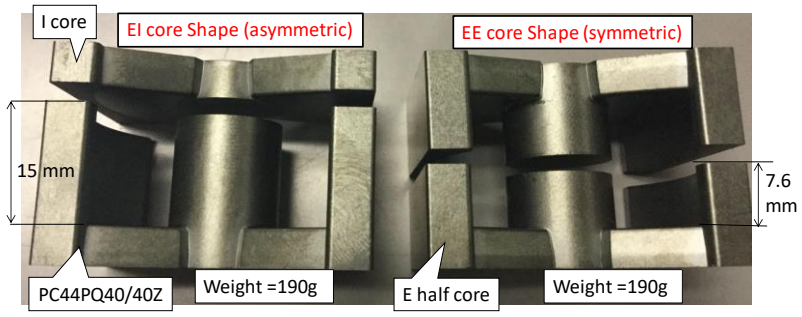

Fig.5.4 EI and EE shapes of the magnetic cores.

$$E = \frac{\mu_o V_g N_p^2}{2l_g^2}(i_p - \frac{N_s}{N_p} i_s)^2 + \frac{\mu_o V_{lk}}{a^2}(N_s i_s)^2 \qquad (5.7)$$

Equation (5.7) can be expressed as

$$E = \frac{\mu_o V_g N_p^2}{2l_g^2}(i_m)^2 + \frac{\mu_o S N_s^2}{a}(i_s)^2 \qquad (5.8)$$

Where S is the winding surface area.

On the other hand, the generic energy expression obtained from electric circuit model in Fig.5.5 (a) can be formulated as

$$E = \frac{1}{2}L_m(i_m)^2 + \frac{1}{2}L_{lkp}(i_p)^2 + \frac{1}{2}L_{lks}(i_s)^2 \qquad (5.9)$$

Comparing the obtained expression of (5.8) with the energy expression obtained from electric circuit model in (5.9) indicates that mostly the leakage inductance is originated from the secondary current, and that all the leakage flux is originated from the secondary winding in the proposed structure. This has been done to approximately realize the equivalent circuit depicted in Fig.5.5 (b).

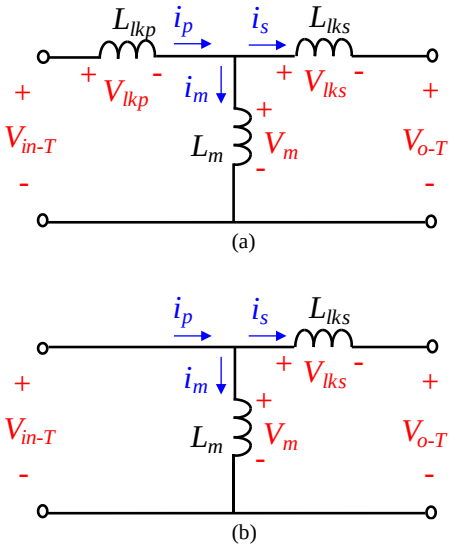

Fig.5.5 Equivalent circuit T-model of the transformers with the secondary leakage reflected to the primary side. (a) leakage inductance is distributed between Primary and secondary. (b) leakage inductance is concentrated on the secondary side.

5.3 Extracting the Transformer Parameters and Calculating the Coupling Factor

The purpose of this section is to measure the transformer parameters, extract the leakage inductance, and calculate the coupling factors. Controlling the leakage inductance values can be done using two methods: (a) the winding allocation with respect to the air-gap, as explained in section 5.2. (b) by adding multiple layers of noise absorber to the relevant winding. (c) changing the distance between the primary and secondary winding. Moreover, several transformer prototypes had been built and tested to investigate the effects of the noise absorber layers, and varying the distance between the windings.

The transformer has been built with a turns ratio of 16:1 (in order to be utilized in a 390V-12V LLC resonant converter as explained in the section 5.6). The magnetic core is depicted in Fig.5.6 (a). The primary and secondary windings are depicted in Fig5.6 (b). The primary winding consists of two layers; each consists of 8 turns. In this discussion, we used noise absorber TDK Flexield, part number: IFL12-100NB300x200, with a layer thickness of 0.1mm, as shown in Figs.5.6 (c) to reach the designed value of leakage inductance. The parameters had been extracted using the Differential-Cumulative method reported in [30].

The measured parameters for the transformer prototypes are listed in Table 5.I and the calculated coupling factors are shown in Table 5.II. Multiple layers of noise absorber TDK Flexield, part number: IFL12-100NB300x200, was attached to the secondary winding as shown in Figs.5.6 (c) to reach the designed value of leakage inductance in both prototypes.

The windings in the LLC converter are loosely coupled, because usually the magnetizing inductance is intentionally minimized and the leakage inductance is intentionally maximized to replace the resonant inductance. Therefore, the well-known coupling factor (k_{12}) is considered as an important parameter to describe how much the primary and secondary windings are coupled. The well-known coupling factor (k_{12}) can be expressed as [31]

TABLE 5.I Measured Parameters of the Transformers		
Parameter	Proposed structure	Conventional structure
Differentially coupled measurement	115.6 µH	132.4 µH
Cumulatively coupled measurement	147.8 µH	164 µH
Mutual inductance (M)	8.05 µH	8 µH
Self-inductance of primary (L_p)	132 µH	146.6 µH
Self-inductance of secondary (L_s)	0.752 µH	0.633 µH
Primary leakage inductance L_{lkp}	3.2 µH	20.2 µH
Secondary leakage inductance n^2*L_{lks}	63.7 µH	35.6 µH
Magnetizing inductance L_m	128.8 µH	128.8 µH
Turns ratio (n_p:n_s)	16:1	16:1

TABLE 5.II Calculated Coupling Factors of the Transformers		
Parameter	Proposed structure	Conventional structure
Coupling factor (k_{12})	0.81	0.82
Coupling factor on the primary (k_1)	0.97	0.86
Coupling factor on the secondary (k_2)	0.67	0.78

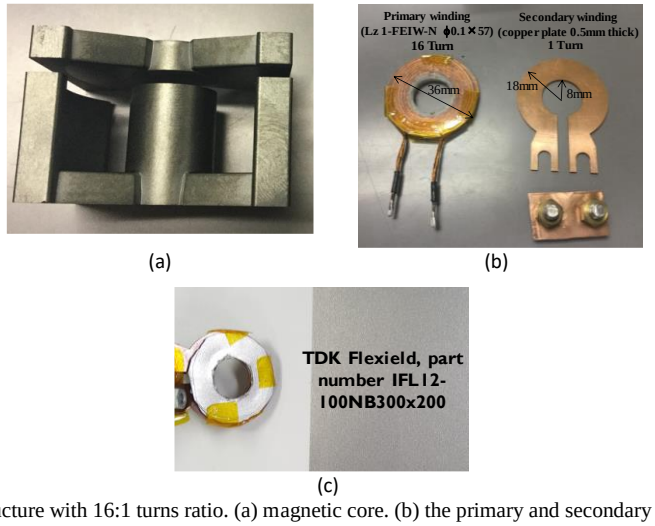

Fig.5.6 The proposed transformer structure with 16:1 turns ratio. (a) magnetic core. (b) the primary and secondary windings. (c) adding 4 layers of noise absorber [TDK Flexield, part number IFL12-100NB300x200] to secondary winding to realize the designed value of leakage inductance.

$$k_{12} = \frac{M}{\sqrt{L_p L_s}} \tag{5.10}$$

Nonetheless, this expression is sufficient in symmetric magnetic cores, where the leakage inductances of the primary and secondary are equal. The coupling factor (k_{12}) has to be split down into two factors in asymmetric core structures. Therefore, it is important to drive the primary coupling factor (k_1) and the secondary coupling factor (k_2), and use them separately. The coupling factor can be expressed as

$$k_{12}^2 = k_1 \times k_2 \tag{5.11}$$

Which can be reduced to

$$k_{12} = \sqrt{k_1 \times k_2} \tag{5.12}$$

In general, the coupling factor (k_{12}) can be obtained through multiplying the primary and secondary open voltage gains of the transformer as follow

$$k_{12}^2 = \frac{V_{o-T}}{V_{in-T}}\bigg|_{i_s=0} \times \frac{V_{in-T}}{V_{o-T}}\bigg|_{i_p=0} \tag{5.13}$$

$$k_{12}^2 = \frac{n \times M}{L_p} \times \frac{M/n}{L_s} = \frac{M^2}{L_p \times L_s} \tag{5.14}$$

Based on (5.11) and (5.14)

The primary coupling factor can be obtained as

$$k_1 = \frac{n \times M}{L_p} \tag{5.15}$$

And it is calculated as 0.97 as shown in Table 5.II.

Likewise, the secondary coupling factor can be obtained as

$$k_2 = \frac{M/n}{L_s} \tag{5.16}$$

And it is calculated as 0.67 as listed in Table 5.II, as well. The calculated coupling factors indicate that the leakage inductance is concentrated on the transformer secondary side. Furthermore, several experimental tests on the transformer with different number of noise absorber layers had been carried out to investigate the effect of attaching the noise absorber layers to the secondary winding. The transformer prototypes are shown in Fig.5.7. The tests had been carried out considering no layers, 4 layers, and 6 layers. The distance between the winding and the air gap length were kept constant. Their extracted parameters are shown in Table 5.III and Table 5.IV. The outcomes of this experiment reveals that although the coupling factor (k_{12}) is almost constant (Mutual inductance (M) is almost constant) in the three transformer prototypes. Nonetheless, the behavior of the leakage distribution in the primary is completely different than the secondary. For instance, as number of the noise absorber layers attached to the secondary increases, the secondary coupling factor (k_2) drops, and the primary coupling factor (k_1) increases. The outcomes had been summarized in Fig.5.8. On the other hand, the effect of changing the distance between the primary and secondary windings had been also investigated. The transformer prototypes with a different values of distance between the windings are shown in Fig.5.9. The tests had been carried out considering distances of 10mm, 5mm, and 2mm. Their extracted parameters are shown in Tables 5.V and 5.VI. The number of the noise absorber layers was constant**.** The outcomes of this experiment reveals that as the primary and secondary get closer to each other, a higher overall coupling factor (k_{12}) can be realized. Furthermore, the values of (k_1) and (k_2)

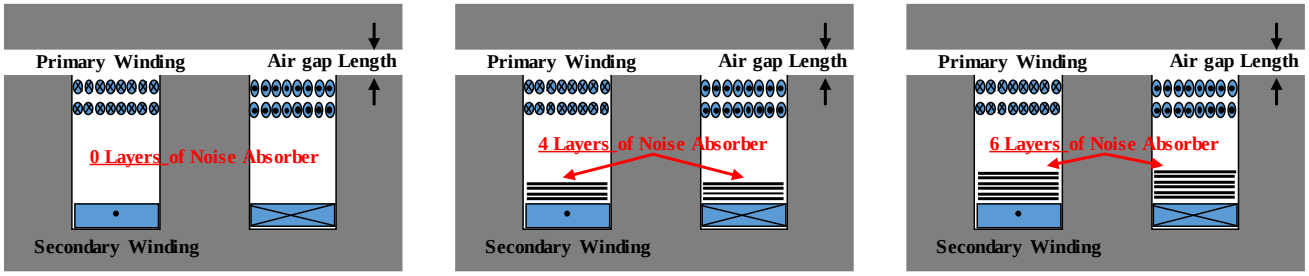

(a) (b) (c)

Fig.5.7 Transformer structures with different number of noise absorber layers [Thickness of one layer of *IFL12-100NB300X200* is 0.1mm].

TABLE 5.III (a)
Measured Parameters of Fig.5.7 (a)

Parameter	Value
Mutual inductance (M)	7.98 μH
Self-inductance of primary (L_p)	134.2 μH
Secondary Self-inductance (L_s)	0.728 μH
Primary leakage inductance L_{lkp}	7 μH
Secondary leakage inductance n^2*L_{lks}	59.2 μH
Magnetizing inductance L_m	127.2 μH
Turns ratio (n_p:n_s)	16:1

TABLE 5.III (b)
Measured Parameters of Fig.7 (b)

Parameter	Value
Mutual inductance (M)	8.05 μH
Self-inductance of primary (L_p)	132 μH
Secondary Self-inductance (L_s)	0.752 μH
Primary leakage inductance L_{lkp}	3.2 μH
Secondary leakage inductance n^2*L_{lks}	63.7 μH
Magnetizing inductance L_m	128.8 μH
Turns ratio (n_p:n_s)	16:1

TABLE 5.III (c)
Measured Parameters of Fig.7 (c)

Parameter	Value
Mutual inductance (M)	8 μH
Self-inductance of primary (L_p)	130.3 μH
Secondary Self-inductance (L_s)	0.762 μH
Primary leakage inductance L_{lkp}	2.3 μH
Secondary leakage inductance n^2*L_{lks}	67.1 μH
Magnetizing inductance L_m	128 μH
Turns ratio (n_p:n_s)	16:1

TABLE 5.IV (a)
Coupling Factors of Fig.7 (a)

Parameter	Value
Coupling factor (k_{12})	0.804
Coupling factor on the primary (k_1)	0.95
Coupling factor on the secondary (k_2)	0.68

TABLE 5.IV (b)
Coupling Factors of Fig.7 (b)

Parameter	Value
Coupling factor (k_{12})	0.808
Coupling factor on the primary (k_1)	0.97
Coupling factor on the secondary (k_2)	0.67

TABLE 5.IV (c)
Coupling Factors of Fig.7 (c)

Parameter	Value
Coupling factor (k_{12})	0.803
Coupling factor on the primary (k_1)	0.98
Coupling factor on the secondary (k_2)	0.65

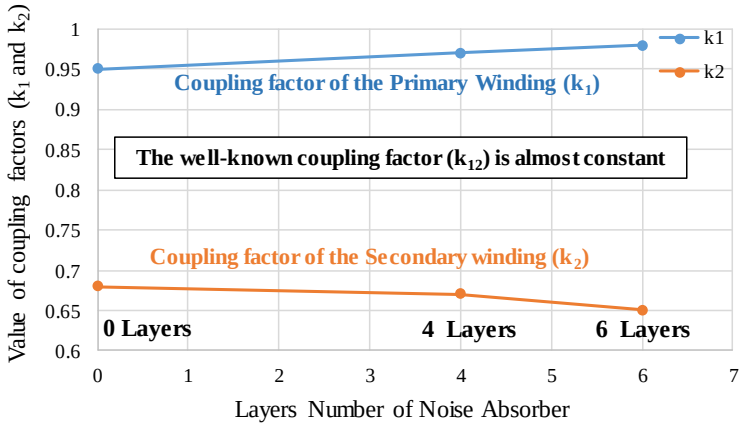

Fig.5.8 Value of the coupling factors (k_1 and k_2) with respect to the number of the noise absorber layers.

increases, which indicates that the leakage inductances at the primary and secondary sides drop. This result had been summarized in Fig.5.10.

5.4 T-Model and Voltage Gain of Gapped Transformer

The purpose of this section is to evaluate the transformer voltage gain of the symmetric (EE) and asymmetric (EI) transformer structures. Firstly, the voltage equations will be driven based on the equivalent circuits shown in Fig.5.5. Then, the voltage gain

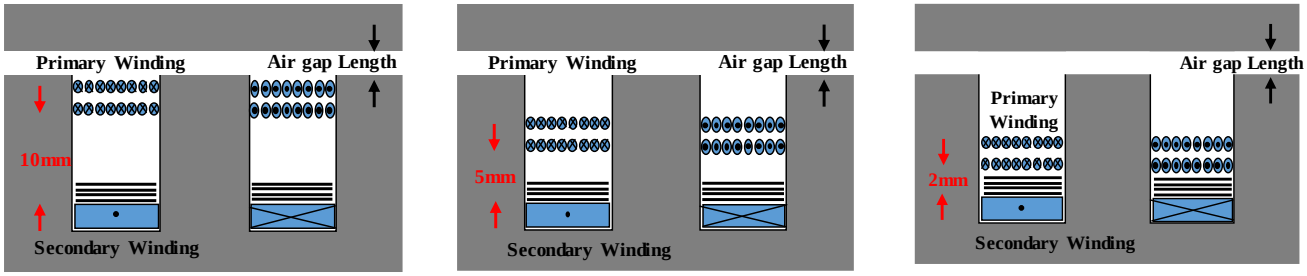

(a) (b) (c)

Fig.5.9 Transformer structures with variation in the distance between the primary and secondary windings

TABLE 5.V (a)
Measured Parameters of Fig.5.9 (a)

Parameter	Value
Mutual inductance (M)	8.05 µH
Self-inductance of primary (L_p)	132 µH
Secondary Self-inductance (L_s)	0.752 µH
Primary leakage inductance L_{lkp}	3.2 µH
Secondary leakage inductance n^2*L_{lks}	63.7 µH
Magnetizing inductance L_m	128.8 µH
Turns ratio (n_p:n_s)	16:1

TABLE 5.V (b)
Measured Parameters of Fig.5.9 (b)

Parameter	Value
Mutual inductance (M)	8.47 µH
Self-inductance of primary (L_p)	134.4 µH
Secondary Self-inductance (L_s)	0.774 µH
Primary leakage inductance L_{lkp}	0.2 µH
Secondary leakage inductance n^2*L_{lks}	62.5 µH
Magnetizing inductance L_m	135.6 µH
Turns ratio (n_p:n_s)	16:1

TABLE 5.V (c)
Measured Parameters of Fig.5.9 (c)

Parameter	Value
Mutual inductance (M)	8.7 µH
Self-inductance of primary (L_p)	137.7 µH
Secondary Self-inductance (L_s)	0.785 µH
Primary leakage inductance L_{lkp}	0.1 µH
Secondary leakage inductance n^2*L_{lks}	61.7 µH
Magnetizing inductance L_m	139.2 µH
Turns ratio (n_p:n_s)	16:1

TABLE 5.VI (a)
Coupling Factors of Fig.5.9 (a)

Parameter	Value
Coupling factor (k_{12})	0.81
Coupling factor on the primary (k_1)	0.97
Coupling factor on the secondary (k_2)	0.67

TABLE 5.VI (b)
Coupling Factors of Fig.5.9 (b)

Parameter	Value
Coupling factor (k_{12})	0.83
Coupling factor on the primary (k_1)	0.99
Coupling factor on the secondary (k_2)	0.69

TABLE 5.VI (c)
Coupling Factors of Fig.5.9 (c)

Parameter	Value
Coupling factor (k_{12})	0.84
Coupling factor on the primary (k_1)	0.998
Coupling factor on the secondary (k_2)	0.7

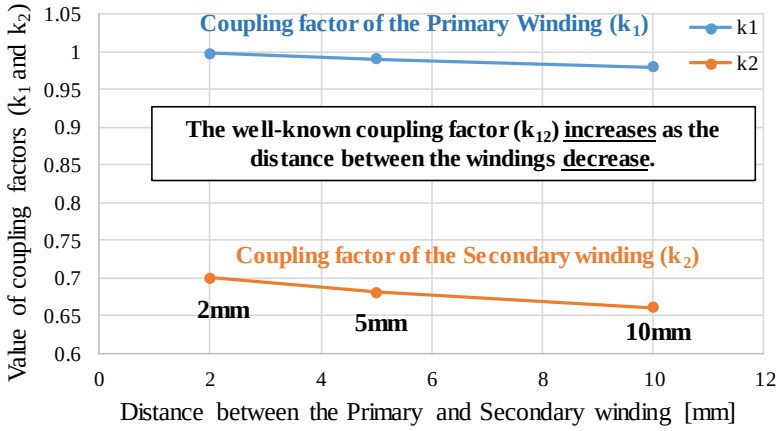

Fig.5.10 Value of the coupling factors (k_1 and k_2) with respect to a variation of the distance between the windings.

equations are obtained and compared to show the influence of the primary leakage inductance presence during the light load condition.

5.4.1 Equivalent circuit and voltage equations

In a symmetric EE transformer core, where the air-gap is inserted in the center leg, the values of the primary and secondary leakages would be close to each other. Leading to the equivalent circuit model shown in Fig.5.5 (a). The transformer input voltage can be expressed as

$$V_{in-T} = V_{o-T} + j\omega L_{lkp} i_p + j\omega L_{lks} i_s \quad (5.17)$$

Where V_{in-T}, V_{o-T}, i_p, i_s, i_m, L_{lkp}, L^*_{lks} and L_{lks} are the transformer input voltage, transformer output voltage, primary current, secondary current reflected into the primary side, magnetizing current, primary leakage inductance, secondary leakage inductance, and secondary leakage inductance reflected to the primary side; respectively. Eq. (5.17) can be reduced as

$$V_{in-T} = V_{o-T} + j\omega L_{lkp}(i_s + i_m) + j\omega L_{lks} i_s \quad (5.18)$$

Eq. (5.18) can be rearranged as follows

$$V_{in-T} = V_{o-T} + j\omega L_{lkp} i_m + j\omega(L_{lkp} + L_{lks}) i_s \quad (5.19)$$

In the LLC resonant converter, the transformer core is usually gapped to reduce value of magnetizing inductance, in order to realize a relatively high value of magnetizing current. Therefore, before the relative switching device is turned on, and during the dead time, the magnetizing current flows in the anti-parallel diode to allow for soft switching operation. This circulating magnetizing current is not contributing to the load side so it deteriorates the efficiency of the LLC converter, especially at light load condition.

In the transformer design, the applied voltage on the primary windings sets up a pure ac flux based on Faraday's law is as follows

$$V_{in-T} = N_p \frac{\phi_m}{T_{on}} \quad (5.20)$$

In case of asymmetric transformer, such as EI magnetic cores. The location of the primary and secondary windings with respect to the air-gap is no longer identical. Therefore, unbalanced magnetic leakage can be realized in such core geometry. As a result, the values of the primary and secondary leakage inductance become different, as explained in section 5.3.

Realizing the electrical circuit model of Fig.5.5 (b), where the leakage inductance is concentrated on the secondary side would eliminate the voltage drop on the primary leakage due to the magnetizing current. The transformer input voltage in Fig.5.5 (b) can be expressed as

$$V_{in-T} = V_{o-T} + j\omega L_{lks} i_s \quad (5.21)$$

5.4.2 Transformer Voltage Gain

The transformer output voltage of Fig.5.5 (a), where the leakage inductance is distributed equally between the primary and secondary sides can be obtained from (5.19) as follows

$$V_{o-T} = V_{in-T} - j\omega L_{lkp} i_m - j\omega(L_{lkp} + L_{lks}) i_s \quad (5.22)$$

By dividing (5.22) over the transformer input voltage, the transformer voltage gain (M_{T-a}) can be obtained as

$$M_{T-a} = \frac{V_{o-T}}{V_{in-T}} = 1 - \frac{j\omega L_{lkp} i_m}{V_{in-T}} - \frac{j\omega (L_{lkp} + L_{lks}) i_s}{V_{in-T}} \qquad (5.23)$$

On the other hand, the voltage gains for the equivalent circuit depicted in Fig.5.5 (b), where the leakage inductance is concentrated at the secondary side can be obtained from (5.21) as follows

$$V_{o-T} = V_{in-T} - j\omega L_{lks} i_s \qquad (5.24)$$

By dividing (5.24) over the transformer input voltage, the transformer voltage gain (M_{T-b}) can be obtained as

$$M_{T-b} = \frac{V_{o-T}}{V_{in-T}} = 1 - \frac{j\omega L_{lks} i_s}{V_{in-T}} \qquad (5.25)$$

From (5.23) and (5.25), it is clear that eliminating the voltage drop across the primary leakage inductance due to the magnetizing current would improve the transformer voltage gain.

The voltage gain improvement during the light load condition is because the transformer secondary voltage is clamped to the output voltage. During the light load, the secondary current is very small therefore, the transformer secondary voltage can be reflected to the primary according to the transformer turns ratio in the proposed transformer structure. Nonetheless, in the conventional structure, there will be a voltage drop on the primary leakage inductance due to the magnetizing current. The concept of the improvement in the transformer voltage gain in the proposed transformer during light load condition is explained in Fig.5.11. The experimental measurements will be obtained in section 5.6 to evaluate our hypothesis.

5.5 Frequency Control Bandwidth with respect to Load Variation

The purpose of this section is to address the effect of the secondary leakage inductance on the frequency control bandwidth with respect to load variation of the converter. It is revealed in this section that allocating the primary winding in the vicinity of the air-gap and placing the secondary winding in a close contact with the magnetic core widens the switching frequency bandwidth. The reason is in a structure with concentrated value of leakage on secondary side, the resonant tank input impedance drops (because the secondary leakage becomes connected in parallel with the magnetizing inductance, instead of series connection as the case of primary leakage inductance), and hence, the voltage gain curve of the LLC converter will be expanded, leading to a higher frequency control bandwidth.

The leakage inductance distribution affects the input impedance of the resonant tank, and consequently it affects the voltage-gain curve of the LLC resonant converter.

The input impedance curves of the resonant tanks had been obtained by using PLECS (Plexim) software. The circuit schematic diagram is shown in Fig.5.12. It is worth mentioning that both resonant tanks have similar value of magnetizing inductance, as the

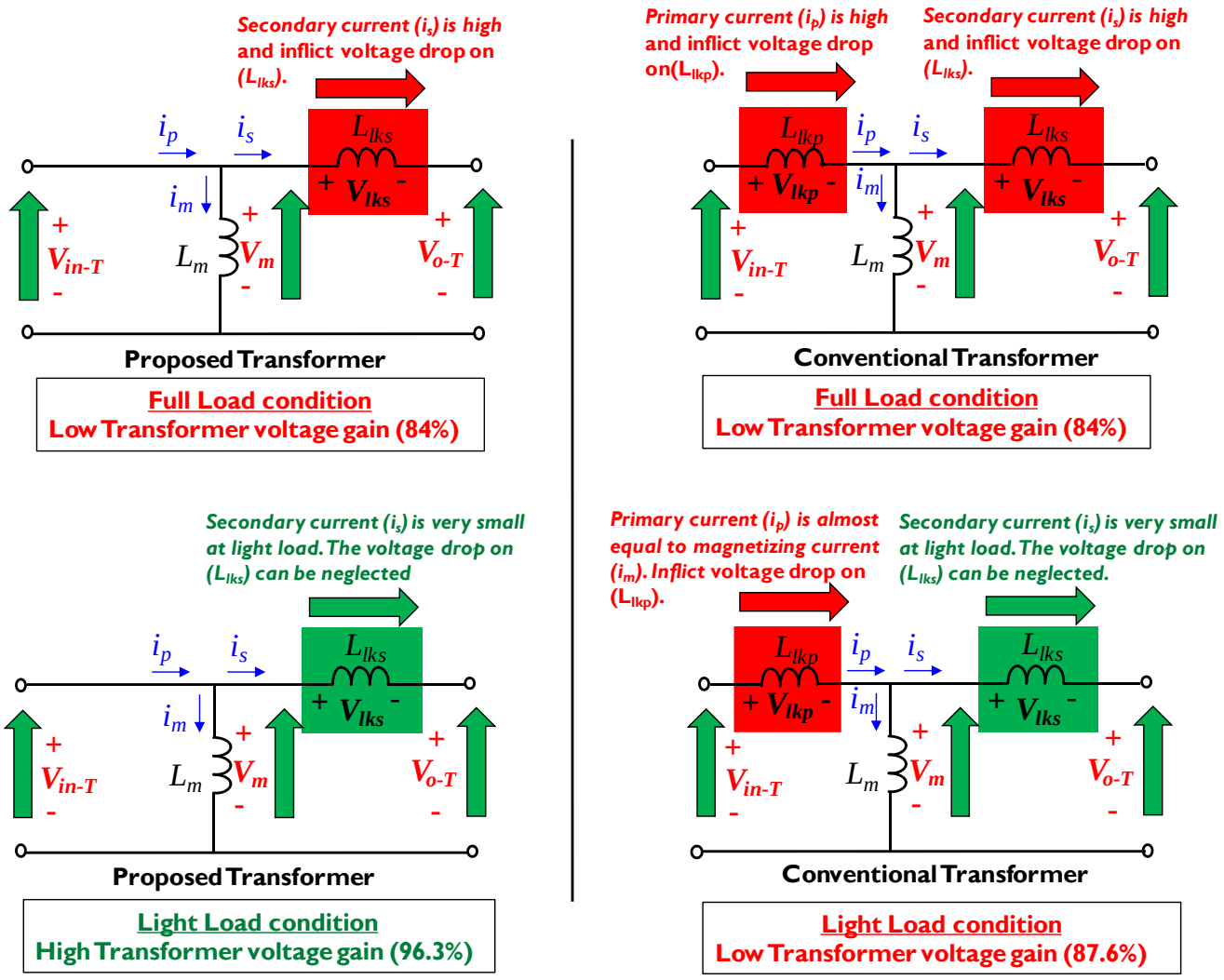

Fig.5.11 Concept of the transformer voltage gain improvement in the proposed transformer during the light load condition.

air gap length is kept constant. Furthermore, the parasitic resistances (R_{para}) have been used to avoid the simulation error. The parasitic resistances have very small values when they connected in series and very large values when they are connected in parallel to guarantee the model accuracy.

Concentrating the leakage inductance on the secondary side leads to a lower value of input impedance, because the leakage inductance becomes connected in parallel with the magnetizing inductance. This is shown in Fig.5.13 and marked by the red color. A lower value of input impedance results in a higher frequency control bandwidth with respect to load variation.

On the contrary, in a transformer structure with a distributed leakage inductance between the primary and secondary, the input impedance would be higher. Because the primary leakage inductance is connected in series, and it contributes to the resonant tank impedance. This curve is marked in Fig.5.13 by the blue color.

The voltage-gain curves had been obtained by using PLECS and they are shown in Fig.5.14, with the purpose of examining the frequency bandwidth of the LLC resonant converter, with respect to load variation, during full to light load conditions, (220W to

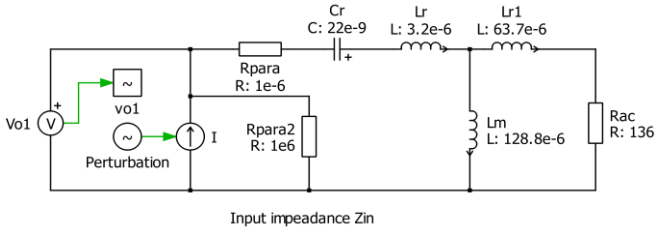

Fig.5.12 The schematic diagram of the resonant tank depicted on PLECS software (developed by Plexim) to measure the input impedance of the transformer structure with leakage inductance concentrated on secondary side.

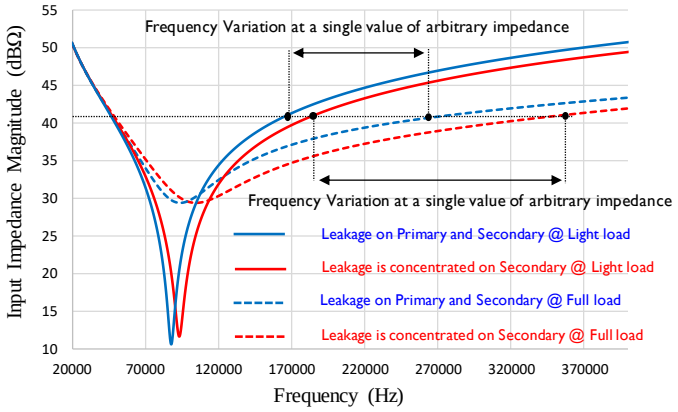

Fig.5.13 Input impedance characteristics for during full and light load conditions for two transformer prototypes.

20W). Fig.5.14 (a) shows the voltage-gain curves in a transformer with concentrated secondary leakage inductance. It can be noticed that at full load condition (220W) the switching frequency is around 217kHz. The switching bridge is driven at a frequency of 339kHz in case of light load condition (20W). It can be noticed that in this kind of transformer design the frequency control bandwidth range is relatively wide (Δf=122kHz). On the other hand, in a transformer structure with leakage inductance distributed on primary and secondary sides the switching frequency is around 203kHz at full load condition and it goes to 237kHz at light load condition. It can be noticed from Fig.5.14 (b) that the frequency control bandwidth is 34kHz which can be considered as relatively small, compared with the proposed transformer structure with concentrated secondary leakage inductance.

5.6 Experimental and Simulation Evaluation

This section is divided into five subsections. The first subsection presents the experimental environment for the LLC resonant converter to investigate the effects of the secondary leakage inductance. The second subsection presents a voltage gain comparison between the two transformer structures. Firstly, with the leakage inductance concentrated on the secondary side, and the other structure has the leakage inductance distributed between the primary and secondary sides, in which the air gap length is constant in the two transformer prototypes, and hence the magnetizing inductance has the same value. The third subsection presents the measured efficiency results and power losses distribution of the LLC converter which had been obtained to evaluate the proposed transformer. The fourth subsection explains why the proposed transformer has lower maximum flux density compared with the traditional transformer. The fifth subsection experimentally investigates the effects of the secondary leakage on the frequency control bandwidth. Furthermore, the simulation and experimental resonant current and drain-voltage waveforms are depicted.

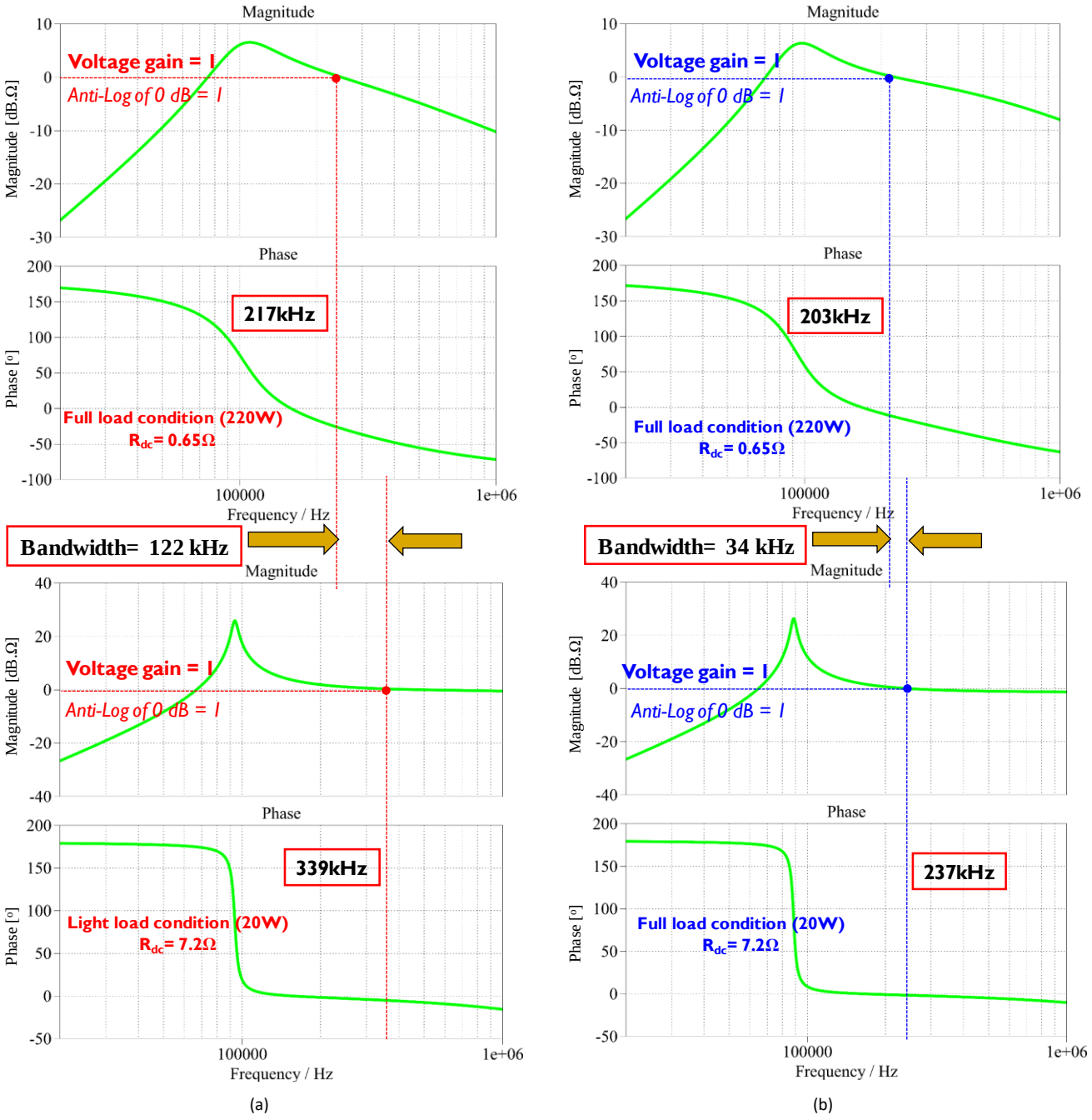

Fig.5.14 Voltage-gain characteristics during full and light load conditions for transformer prototypes. (a) leakage inductance is concentrated on transformer secondary side. (b) leakage inductance is distributed between primary and secondary sides.

5.6.1 Experimental set-up

In order to evaluate the proper operation of the proposed transformer in the LLC resonant converter, experimental tests had been conducted. Furthermore, the converter was constructed and experimentally tested. The single-phase LLC prototype is a step-down converter 390V-12V and it uses Schottky diodes (VS-100BGQ100), primary Mosfets (Toshiba, TK20E60W). The experimental set-up is shown in Fig.5.15. Texas Instruments DSP is used to drive the primary switches. The electronic load is Chroma Model 63201. The power analyzer is HIOKI PW6001. The main DC power supply provided the 390V as an input voltage to the converter,

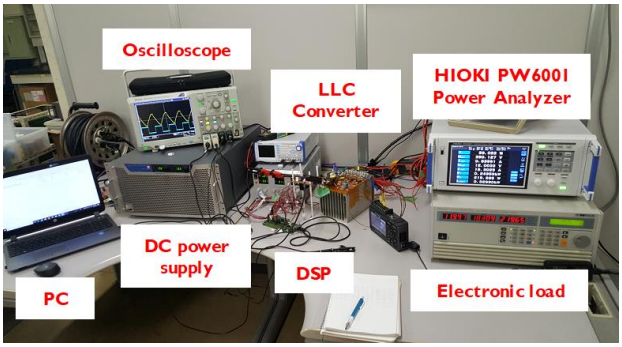

Fig.5.15 Experimental set-up

TABLE 5.VII
SPECIFICATIONS OF THE LLC RESONANT CONVERTER

Parameter	VALUE
Output power (P_o)	220W
Input voltage (V_i)	390V
Output voltage (V_o)	12V
Resonant capacitor (C_r)	22nF

and small power supply is used to provide the 5V for the gate drivers. The transformer parameters are listed in Table 5.I and Table 5.II. The parameters of the single-phase LLC resonant converter are tabulated in Table 5.VII.

5.6.2 Transformer voltage Gain and LLC converter

The purpose of this section is to provide a comparison between the proposed transformer (where the leakage inductance is concentrated on the secondary side), and the conventional transformer (where the leakage is equally distributed between the primary and secondary sides) to investigate the effects of the secondary leakage inductance.

As previously discussed in section 5.4, it is expected that the magnetizing current inflict a voltage drop on the primary leakage inductance, especially at light load condition, which lessens the transformer voltage gain and deteriorate the converter efficiency. Therefore, the in the transformer structure that has concentrated leakage inductance on the secondary side eliminates this voltage drop, and hence improves the transformer voltage gain and the efficiency of the whole converter. The definition of the voltage gain is the ratio between the transformer's secondary voltage and the transformer's primary voltage. A synonym for the voltage gain is the transformer effective turns ratio. In other words, in ideal transformer with infinite magnetizing inductance the voltage gain goes to 100% and the effective turns ratio goes to 16.

The measurements of the primary and secondary voltages are listed in Table 5.VIII and Table 5.IX. These measurements were obtained using HIOKI PW6001 Power Analyzer. It is clear that that the proposed transformer exhibits a higher voltage gain than the conventional transformer, at light load condition. Furthermore, the effective turns ratio of the proposed transformer is close to the theoretical turns ratio. The voltage gain comparison between the proposed transformer and the conventional transformer are shown in Fig.5.16 and the effective turns ratio comparison is shown in Fig.5.17.

5.6.3 Efficiency of LLC converter and power loss analysis

The efficiency measurements are presented for the two transformer prototypes. The efficiency evaluation had been conducted using HIOKI PW6001 Power Analyzer. The efficiency tests were conducted at several power output levels, in particular: 220W, 200W, 150W, 100W, 50W, 40W, 30W and 20W. The input voltage was fixed at 390V and output voltage at 12V. The

TABLE 5.VIII VOLTAGE GAIN AND EFFECTIVE TURNS RATIO OF THE PROPOSED TRANSFORMER				
Load condition[W]	Primary Voltage (V_{in-T}) [V]	Secondary Voltage (V_{o-T}) [V]	Voltage Gain %	Effective Turns ratio
220W	248.5	13	84%	19
200W	244.9	12.98	84.8%	18.9
150W	234	12.85	87.9%	18.2
100W	222.4	12.55	90.3%	17.7
50W	209.5	12.3	93.9%	17
40W	206.3	12.19	94.6%	16.9
30W	203	12.13	95.6%	16.7
20W	200.2	12.05	96.3%	16.6

TABLE 5.IX VOLTAGE GAIN AND EFFECTIVE TURNS RATIO OF TRANSFORMER WITH LEAKAGE INDUCTANCE DISTRIBUTED ON PRIMARY AND SECONDARY				
Load condition[W]	Primary Voltage (V_{in-T}) [V]	Secondary Voltage (V_{o-T}) [V]	Voltage Gain %	Effective Turns ratio
220W	245.3	12.9	84%	19
200W	242.8	12.8	84.4%	18.95
150W	237.3	12.7	85.3%	18.7
100W	231.8	12.5	86.4%	18.5
50W	223.8	12.2	87%	18.4
40W	222.2	12.1	87.2%	18.35
30W	220.3	12.05	87.5%	18.3
20W	217.9	12	87.6%	18.2

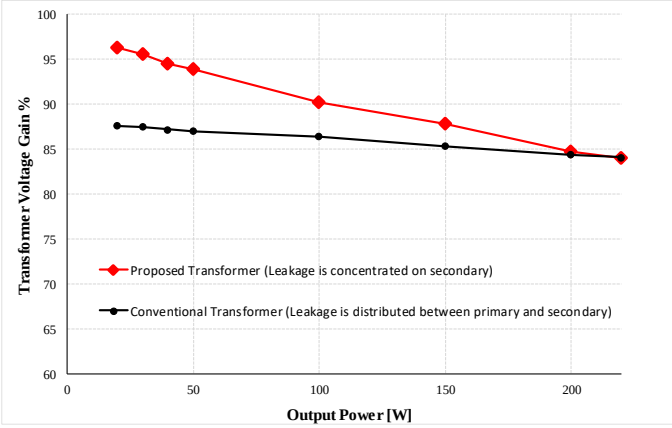

Fig.5.16 A voltage gain comparison between the proposed transformer and the conventional transformer.

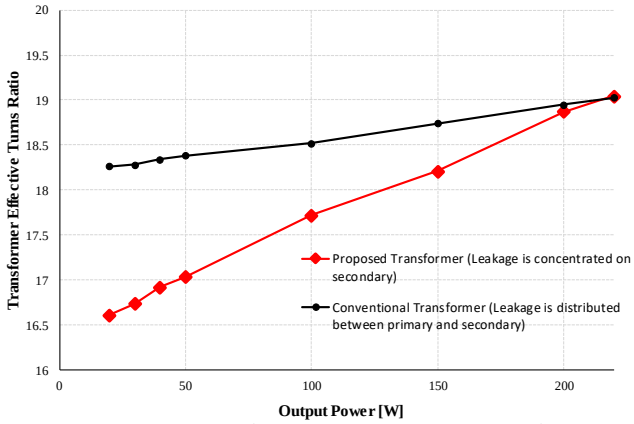

Fig.5.17 Effective turns ratio comparison between the proposed transformer and the conventional transformer.

measurements are tabulated in Tables 5.X and 5.XI. The efficiency of the LLC utilizing the proposed transformer design exhibits a

TABLE 5.X Efficiency measurements for the LLC resonant converter utilizing the proposed transformer (Leakage inductance concentrated on secondary)									
	Input Power	Switching Frequency	Input Voltage	Input current	Output Power	Output Voltage	Output current	Power Losses	Efficiency
P_o = 220W	246.3W	217 kHz	390V	0.631A	220.1W	12.04V	18.3A	26.2W	89.4%
P_o = 200W	222.3W	220 kHz	390V	0.57A	199.1W	11.98V	16.61A	23.3W	89.5%
P_o = 150W	167.7W	229 kHz	390V	0.43A	149.8W	12.03V	12.44A	17.85W	89.4%
P_o = 100W	110.9W	250 kHz	390V	0.28A	99.3W	11.99V	8.28A	11.7W	89.3%
P_o = 50W	57.9W	285 kHz	390V	0.15A	49.6W	12.05V	4.1A	8.3W	85.6%
P_o = 40W	47.1W	299 kHz	390V	0.12A	39.5W	12.03V	3.3A	7.6W	83.8%
P_o = 30W	36.3W	315 kHz	390V	0.093A	29.4W	12.03V	2.4A	6.9W	81%
P_o = 20W	27W	339 kHz	390V	0.07A	20.3W	12.05V	1.7A	6.6W	75.5%

* This evaluation has been done using HIOKI PW6001 Power Analyzer and the electronic load was current controlled.

TABLE 5.XI Efficiency measurements for the LLC resonant converter utilizing a transformer with Leakage inductance distributed between primary and secondary									
	Input Power	Switching Frequency	Input Voltage	Input current	Output Power	Output Voltage	Output current	Power Losses	Efficiency
P_o = 220W	246W	203 kHz	390V	0.63A	219.5W	12.01V	18.3A	26.3W	89.3%
P_o = 200W	222.7W	204.5 kHz	390V	0.57A	199.2W	11.99V	16.61A	23.6W	89.4%
P_o = 150W	167.9W	208 kHz	390V	0.43A	149.4W	12V	12.44A	18.6W	88.9%
P_o = 100W	113.7W	213 kHz	390V	0.29A	99.7W	12.05V	8.28A	13.95W	87.7%
P_o = 50W	59.2W	223 kHz	390V	0.15A	49.4W	12.01V	4.1A	9.8W	83.4%
P_o = 40W	48W	227.5 kHz	390V	0.12A	39.2W	11.97V	3.3A	8.8W	81.6%
P_o = 30W	37.4W	232 kHz	390V	0.095A	29.2W	11.96V	2.4A	8.24W	78%
P_o = 20W	27.7W	236 kHz	390V	0.071A	20.2W	11.98V	1.7A	7.5W	72.9%

* This evaluation has been done using HIOKI PW6001 Power Analyzer and the electronic load was current controlled.

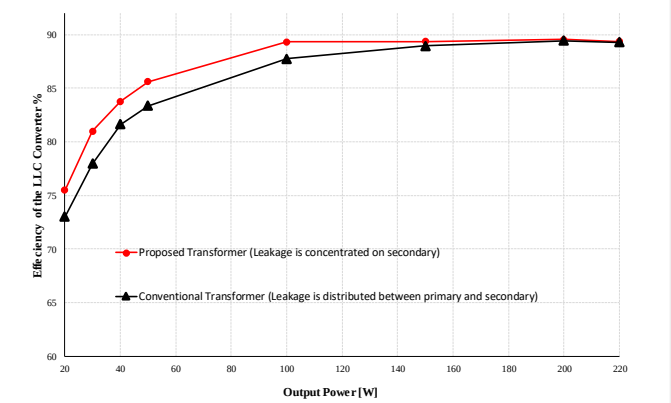

Fig.5.18 Efficiency measurements for the proposed transformer with a concentrated secondary leakage inductance and the conventional transformer with distributed leakage inductance on the primary and secondary.

higher efficiency than the conventional transformer, at light load condition. The efficiency comparison is presented in Fig.5.18. The major power loss is originated in the secondary rectifiers and the transformer copper loss due to the high value of output current. The conduction loss of secondary rectifiers is estimated based on:

$$P_{diode} = V_F . I_{D-rms} \qquad (5.26)$$

The secondary rectifiers are Schottky diodes VS-100BGQ100 with a V_f = 0.6. The total rectifier losses are calculated as 17.1W, which contributes to 64% of the total power loss of 26.2W shown in Table 5.VII. The copper loss of the transformer is calculated based on:

$$P_{copp-T} = I_{pri-rms}^2 R_{pri-ac} + I_{\sec-rms}^2 R_{\sec-ac} \qquad (5.27)$$

The *ac* resistance of the transformers primary winding was measured as 0.8Ω and for the secondary winding is 0.1Ω. Leading to total copper losses of 4W, which contributes to 15% of the total power loss. Other kinds of power losses such as conduction and switching loss of the primary switches, transformer core losses, other circuit parasitics have less effect. The core loss is estimated using the improved generalized Steinmetz equation iGSE [32]

$$P_{core} = \frac{1}{T_s}\int_0^{T_s} k_i \left|\frac{dB}{dt}\right|^{\alpha} (\Delta B)^{\beta-\alpha}\, dt \qquad (5.28)$$

$$k_i = \frac{k}{2^{\beta+1}\pi^{\alpha-1}\left(0.2761+\frac{1.7061}{\alpha+1.354}\right)} \qquad (5.29)$$

The core loss is calculated as 52454.5 W/m3. The PC44PQ40/40-Z core volume is 20500mm^3. Therefore, the core losses contributed by the transformer is 1.1W. The MOSFETs utilized in our prototype are Toshiba, TK20E60W, with a drain-source resistance of 0.13Ω. The total conduction loss of the MOSFETs due to the on-resistance is around 0.5W. The power loss breakdown is depicted in Fig.5.19. It is clear that the conduction loss on the rectifiers contributes with the major power loss components due to the high current of the secondary side. In the future work, it is recommended to implement synchronous rectification to improve the efficiency of the converter.

5.6.4 Maximum flux density

The efficiency improvement at light load condition is because the maximum flux density (B_m) of the proposed transformer structure becomes far less than in the conventional transformer, during light load condition. Therefore, the core loss of the proposed transformer is lower than the conventional transformer, at light load condition. However, the core losses of the transformers are quite nearly the same at the full load condition.

According to [33], the maximum flux density (B_m) in the transformer core is function of the transformer input voltage and the frequency. It can be calculated as

$$B_m = \frac{V_{in-T}}{8 f_s N_p A} \qquad (5.30)$$

The maximum flux density and the core losses are lower in the proposed transformer during the light load condition due to the following reasons:

1- At light load condition, the frequency is higher in the proposed transformer (due to a lower value of input impedance). Therefore, the maximum flux density (B_m) becomes lower. According to Steinmetz equation the effect of (ΔB^{β}) is higher than (f^{α}), because the Steinmetz parameters for PC40: α=1 and β=2.

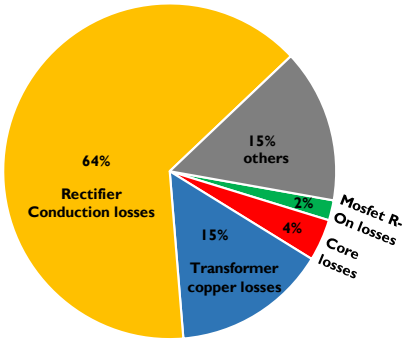

Fig.5.19 Pie chart of the power loss distribution in the LLC converter.

TABLE 5.XII Maximum Flux Density (B_m) at Light Load condition (P_{out} = 20W)	
Proposed Transformer with concentrated leakage inductance on secondary side	Transformer with leakage inductance distributed on primary and secondary sides
Switching Frequency = 339kHz	Switching Frequency = 236kHz
V_{in-T} = 200.2V (refer to Table.VIII)	V_{in-T} = 217.9V (refer to Table.IX)
$B_m = \frac{V_{in-T}}{8 f_s N_p A} = \frac{200.2}{8x339x10^3 x16x201x10^{-6}} = 22.95mT$	$B_m = \frac{V_{in-T}}{8 f_s N_p A} = \frac{217.9}{8x236x10^3 x16x201x10^{-6}} = 35.9mT$

TABLE 5.XIII Maximum Flux Density (B_m) at Full Load condition (P_{out} = 220W)	
Proposed Transformer with concentrated leakage inductance on secondary side	Transformer with leakage inductance distributed on primary and secondary sides
Switching Frequency = 217kHz	Switching Frequency = 203kHz
V_{in-T} = 248.5V (refer to Table.VIII)	V_{in-T} = 245.3V (refer to Table.IX)
$B_m = \frac{V_{in-T}}{8 f_s N_p A} = \frac{248.5}{8x217x10^3 x16x201x10^{-6}} = 44.5mT$	$B_m = \frac{V_{in-T}}{8 f_s N_p A} = \frac{245.3}{8x203x10^3 x16x201x10^{-6}} = 46.9mT$

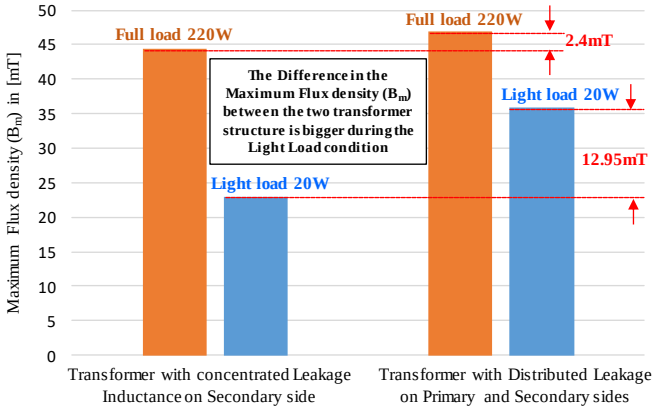

Fig.5.20 Comparison between the maximum flux denisty [mT] in the two transformer prototypes during full and light load conditions.

2- Furthermore, as per the theoretical discussion shown in section 5.4, it has been expected that the transformer input voltage of the proposed transformer will be lower than in the conventional transformer. This has been experimentally proven as shown in Tables 5.VIII and 5.IX. The proposed transformer input voltage (V_{in-T} = 200.2V) is lower than the conventional

transformer input voltage ($V_{in\text{-}T}$ = 217.9V), at light load condition (20W). According to Faraday's law shown in (5.19), the maximum flux value (φ_m) in the proposed core will be lower than in the conventional transformer. Accordingly, the proposed transformer has a lower value of maximum flux density (B_m), resulting in lower core loss.

The calculated values of the maximum flux density are depicted in Tables 5.XII and 5.XIII. A comparison is provided in Fig.5.20 to highlight the difference between the two transformer prototypes.

5.6.5 Frequency Control Bandwidth- experimental waveforms

The experimental waveforms are shown in this section to show the proper operation of the power converter and the operating frequency. The two transformer structures have been examined under different load conditions. For the transformer with concentrated leakage inductance in the secondary side, Fig.5.21 (a) shows the experimental waveforms of resonant current with and drain-source voltage, where the converter operates at full load condition (i.e P_o=220W, V_o=12V, I_o=18.3A, and f_s =217kHz). In Fig.5.21 (b) the waveforms during light load condition (P_o=20W, V_o=12V, I_o=1.7A, and f_s =339kHz).

The rms value of the resonant current is the sum of two current components: (1) magnetizing current (2) load current, and it can be expressed by the following equation [9]

$$i_r = \sqrt{\frac{n^2 V_o^2 T_r^2 (2T_s - T_r)}{32 L_m^2 T_s} + \frac{\pi^2 I_o^2 T_s^2}{8 n^2 T_r^2}} \qquad (5.31)$$

The magnetizing current term is load independent. In other words, it is not function of the load, but instead it is dependent on the frequency, magnetizing inductance and voltage. In Fig. 5.21 (a) and Fig5.22 (a), the load current is high and the switching frequency is close to the resonant frequency therefore, the current waveform is almost sinusoidal. As for Fig. 5.21 (b) and Fig. 5.22 (b), the load current (I_o) goes to zero and the resonant current is almost equal the magnetizing current, that is the reason why the waveform is a triangle at light load condition, as reported in page 7 of [34]. Furthermore, simulation tests had been carried out to evaluate the operation proposed transformer, using PLECS (Plexim) software tool. The simulation waveforms of the proposed transformer are presented in Fig.5.23. The simulation waveforms are consistent with the experimental waveforms.

5.7 Summary

In this chapter, the effects of the secondary leakage inductance on the operation of the LLC converter is investigated. The unbalanced magnetic leakage distribution in the transformer primary and secondary sides can be realized by allocating the primary winding in the vicinity of the air gap and placing the secondary winding in a close contact with the magnetic core to minimize the magnetic leakage flux originated from the primary winding and maximize the leakage flux originated from the secondary. Noise absorber can be used to slightly alter the leakage inductance value. It has been reported that a transformer structure with a

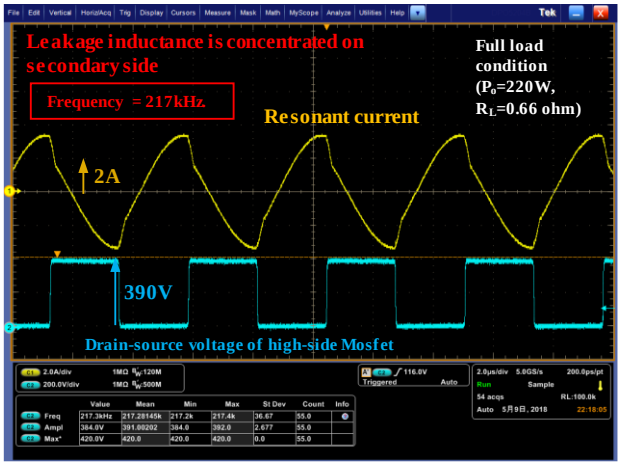

(a)

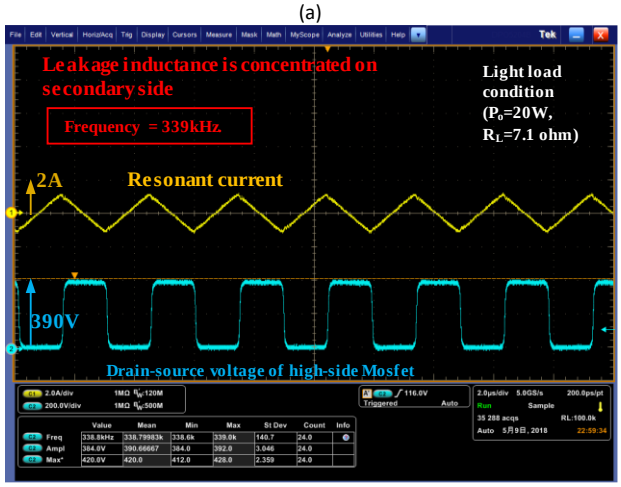

(b)

Fig.5.21 Experimental results when the leakage inductance is concentrated on secondary side. (a)Full load condition. (b) Light load condition.

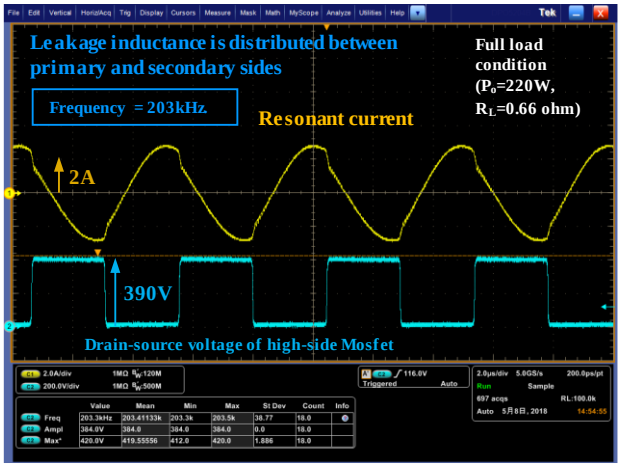

(a)

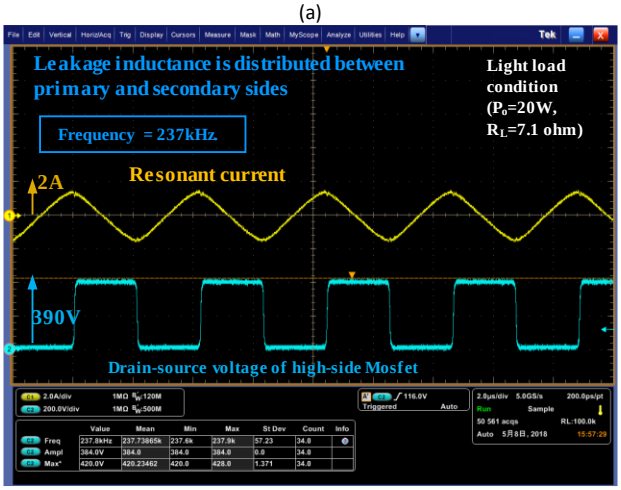

(b)

Fig.5.22 Experimental results when the leakage is distributed between the primary and secondary sides.(a)Full load condition.(b) Light load condition.

concentrated value of leakage inductance on secondary side realizes a higher transformer voltage gain and efficiency. The theory behind realizing efficiency improvement is that the proposed structure eliminates the primary leakage inductance and it has a concentrated leakage on the secondary side. As a result, the voltage drop on the primary leakage inductance due to magnetizing current (i_m) could be eliminated. Furthermore, the secondary leakage inductance expands the voltage gain curve of the LLC converter which results in a higher frequency control bandwidth with respect to the load variation. In future work, it is recommended to implement synchronous rectification to further improve the efficiency of the converter. Furthermore, in-depth analysis related to the fringing effects on the primary windings shall be conducted, as in asymmetric core structure there will be a winding which is located in the vicinity of the air-gap.

5.8 Appendix

5.8.1 Interleaving and high frequency operations on leakage inductance

Interleaving the windings is often used to reduce the proximity effect and the ac resistance. Nonetheless, the leakage inductance would be dramatically reduced within an interleaved structure. This bring another challenge to the LLC resonant converter, where

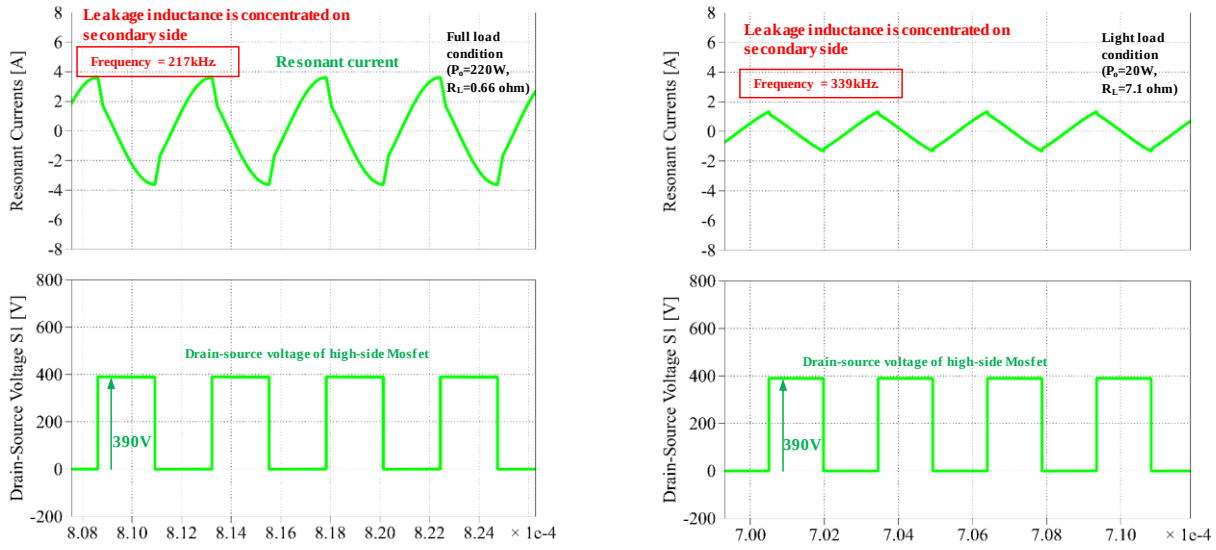

(a) (b)

Fig.5.23 Simulation waveforms of the LLC resonant converter using PLECS (Plexim). (a)full load condition. (b) light load condition.

the leakage inductance is utilized as a resonant inductance (with a relatively high value) to decrease the inductance ratio (L_m/L_r) and improve the frequency regulation characteristics of the LLC converter. Usually, the inductance ratio (L_m/L_r) is designed to be around 3~8 [35]. Therefore, the leakage inductance value should be relatively high. One of the best solutions to increase the value of the leakage inductance in an interleaved structure is to insert a magnetic shunt into the transformer [36]. However, this may complicate the transformer design when it comes to selecting the material permeability and the magnetic shunt thickness.

As for the effect of high frequency operation, it is expected that the current goes towards the surface of the conductors, and the equivalent cross-sectional area of the conductors in which the leakage energy is stored will be reduced. This means that leakage inductance is reduced with increasing frequency. The current is no longer homogeneously distributed within the conductors at high frequency because of the eddy current effect. The area of the mmf (magneto motive force) curve at high frequency is actually smaller than the one at low frequency, which means the stored leakage energy is smaller at high frequency [37].

It can be deduced that the effects of the interleaving and high frequency operation is reducing the leakage inductance value.

5.8.2 Effects of core size on the leakage inductance

The core size affects the leakage inductance value. A simple formula to calculate window inductance can be made on the basis of the model shown in Fig.5.3 as follow [30].

$$L = \frac{2\mu_o N^2 bc}{a} \qquad (31)$$

The window depth b = 28mm, window height h =30mm, and window width a =9mm. This equation implies that if b and c have been increased the leakage inductance is expected to increase as well.

5.8.3 Measurement of Self-Resonant Frequency (SRF) of the Primary Winding

The self-resonant frequency of the primary winding is measured to investigate the influence of the winding parasitic capacitance. The measurements had been obtained by using impedance analyzer (KEYSIGHT TECHNOLOGIES, Model: E4990A). Fig.5.24 shows that calculated value of parasitic capacitance is around 9.8 pF. Furthermore, the magnitude of impedance |Z| and the phase θ. The self-resonant frequency is around 4.25MHz which is 20 times of the operating frequency. The effects of the winding parasitic capacitance on the operation of the LLC resonant converter can be neglected.

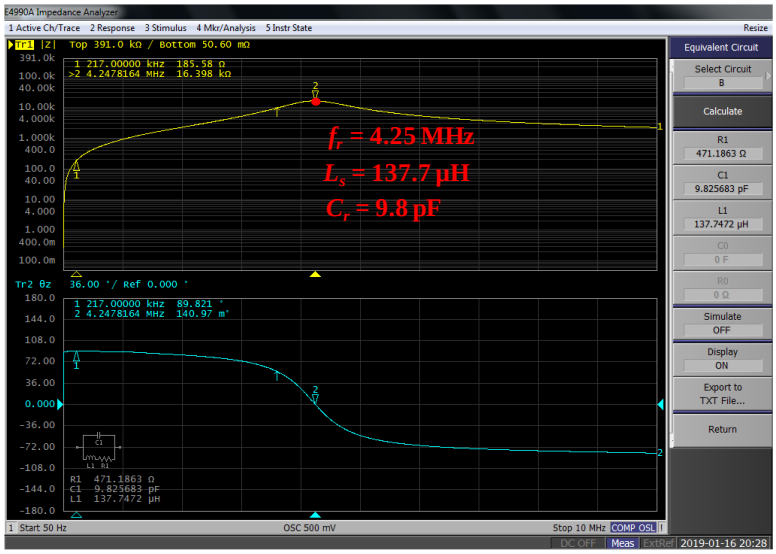

Fig.5.24 Impedance characteristics of the primary winding using *KEYSIGHT TECHNOLOGIES, Model: E4990A* Impedance Analyzer.

REFERENCES

[1] M. K. Kazimierczuk and D. Czarkowski, Resonant Power Converters. New York, NY, USA: Wiley, 1995.

[2] R. L. Steigerwald, "A comparison of half-bridge resonant converter topologies," IEEE Trans. Power Electron., vol. 3, no. 2, pp. 174-182, Apr. 1988.

[3] C. Chang, E. Chang, and H. Cheng, "A High-efficiency Solar Array Simulator Implemented by an LLC resonant DC-DC converter," IEEE Trans. Power Electron., vol. 28, no. 6, pp. 3039-3046, June, 2013.

[4] H. Hu, X. Fang, F. Chen, Z. Shen, and I. Batarseh, "A Modified high efficiency LLC converter with two transformers for wide input-voltage range applications," IEEE Trans. Power Electron., vol. 28, no. 4, pp.1946-1960, Apr. 2013.

[5] D. Kim, C. Kim, and G. Moon, "High-efficiency slim adapter with low profile transformer structure," IEEE Trans. Ind. Electron., vol. 59, no. 9, pp. 3445-3449, Sep. 2012.

[6] H. Choi, "Analysis and Design of LLC Resonant Converter with Integrated Transformer," in Proc. Appl. Power Electron. Conf. Expo, (APEC) 2007.

[7] H. Choi and FPS Application Group, Half-Bridge LLC Resonant Converter Design Using FSFR-Series Fairchild Power Switch, Fairchild Semiconductor Corporation, San Jose, CA, USA, Rev. 1.0.0 10/9/07, 2007.

[8] J. Zhang, W. G. Hurley, and W. H. Wolfle,"Gapped Transformer Design Methodology and Implementation for LLC Resonant Converters," in Proc. Appl. Power Electron. Conf. Expo, pp. 726-731, March, 2014.

[9] J. Zhang, W. Hurley and W. Wolfle, "Gapped Transformer Design Methodology and Implementation for LLC Resonant Converters," IEEE Transactions on Ind. App., Vol. 52, No. 1, pp. 342-351, January 2016.

[10] R. W. Erickson, D. Maksimovic, " Fundamentals of Power Electronics," 2nd Edition, 2001.

[11] Reusch, David, and Fred C. Lee. "High Frequency Bus Converter with Low Loss Integrated Matrix Transformer," in Proc. Applied Power Electronics Conference and Exposition (APEC), 2012 Twenty-Seventh Annual IEEE, March, 2012.

[12] C. Yan, F. Li, J. Zeng, T. Liu and J. Ying, "A Novel Transformer Structure for High power, High Frequency converter," 2007 IEEE Power Electronics Specialists Conference, Orlando, FL, pp. 214-218, March, 2007.

[13] H. Xiucheng, L. Zhengyang, L. Qiang, and F. Lee, "Evaluation and application of 600V GaN HEMT in Cascade structure," in Applied Power Electronics Conference and Exposition (APEC), 2013 Twenty-Eighth Annual IEEE, pp. 1279-1286, 17-21 March 2013.

[14] Daocheng Huang; Shu Ji; Lee, F.C., "LLC Resonant Converter with Matrix Transformer," IEEE Trans on Power Electron., vol.29, no.8, pp.4339-4347, Aug. 2014.

[15] B. H. Lee, M. Y. Kim, C. E. Kim, K. B. Park, and G. W.Moon, "Analysis of LLC resonant converter considering effects of parasitic components," in Proc. Int. Telecommun. Energy. Conf, pp. 1-6, 2009.

[16] J-H. Kim, C-E. Kim, J-K. Kim, and G-W. Moon, "Analysis for LLC Resonant Converter Considering Parasitic Components at Very Light Load Condition," in Proc. Power. Electron. and ECCE Asia (ICPE&ECCE), pp. 1863-1868, June, 2011.

[17] M. Pahlevaninezhad, D. Hamza, and P. K. Jain, "An improved layout strategy for common-mode EMI suppression applicable to high frequency planar transformers in high-power DC/DC converters used for electric vehicles," IEEE Trans. Power. Electron., vol. 29, no. 3, pp. 1211-1228, Mar. 2014

[18] M. Saket, N. Shafiei and M. Ordonez, "LLC Converters with Planar Transformers: Issues and Mitigation", IEEE Trans. on Power Electron., Vol. PP, No.99, 2017.

[19] N. Shafiei and M. Ordonez "Improving the Regulation Range of EV Battery Chargers with L3C2 Resonant Converters," IEEE Trans. Power Electron., Vol. 30, no. 6, pp. 31663184, Jun 2015.

[20] M. Noah et al., “Magnetic Design and Experimental Evaluation of a Commercially Available Single Integrated Transformer in Three-phase LLC Resonant Converter" IEEE Trans. on Ind. App., Vol. 54, Issue:6, Page:6190-6204, November/December 2018.

[21] Y. Liang, W. Liu, B.Lu, J. Wyk, " Design of integrated passive component for a 1 MHz 1 kW half-bridge LLC resonant converter", in Proc. Fourteenth IAS Annual Meeting. Conference Record of the Industry Applications Conference, pp. 2223-2228, 2005.

[22] B. Yang, F. Lee, M. Concannon,"Over current protection methods for LLC resonant converter" in Proc. Appl. Power Electron. Conf. Expo, APEC, pp. 605-609, March 2003.

[23] Y. Gu, Z. Lu, L. Hang, Z. Qian, G. Huang, "Three-level LLC series resonant DC/DC converter" IEEE Trans on Power Electron, Vol.20, pp.781 – 789, July 2005.

[24] B. Yang, F. Lee, A. Zhang, G. Huang, "LLC resonant converter for front end DC/DC conversion" in Proc. Appl. Power Electron. Conf. Expo, APEC , pp.1108-1112, March 2002.

[25] B. Lu, W. Liu, Y. Liang, F. Lee, D. Wyk, "Optimal design Methodology for LLC Resonant Converter," in Proc. Appl. Power Electron. Conf. Expo, APEC pp.533-538, March 2016.

[26] M. Noah, K. Umetani, J. Imaoka, and M. Yamamoto, "Winding orientation method to minimise the secondary leakage of a gapped transformer utilised in LLC resonant converter," IET Electron. Lett., vol. 54, no. 3, pp. 157-159, Feb. 2018.

[27] P. L Dowell, "Effects of eddy currents in transformer windings," In Proc. Of the IEEE, vol. 113, pp. 1378-1394, Aug. 1966.

[28] J. G. Hayes, N. O'Donovan, M. G. Egan, and T. O'Donnell, "Inductance characterization of high-leakage transformers," in Proc. Applied Power Electronics Conference and Exposition (APEC), vol. 2, pp. 1150-1156 vol.2, Feb 2003.

[29] C. Rim, and C. Mi, "Wireless Power Transfer for Electric Vehicles and Mobile Devices" Wiley-IEEE Press: Hoboken, NJ, USA, 2017.

[30] K. Venkatachalam, C. R. Sullivan, T. Abdallah, and H. Tacca, "Accurate prediction of ferrite core loss with nonsinusoidal waveforms using only Steinmetz parameters," in Proc. IEEE Workshop on computers in Power Electronics, pp. 36-41, June 2002.

[31] Y. Nakakohara, H. Otake, T. Evans, T. Yoshida, M. Tsuruya and K. Nakahara, "Three-phase LLC series resonant DC/DC converter using SiC MOSFETs to realize high-voltage and high-frequency operation," IEEE Transactions on Ind. Electron., Vol. 63, No. 4, pp. 2103-2110, April 2016.

[32] Online:https://www.infineon.com/dgdl/InfineonDesign_example_resonant_LLC_converter_operation_and_design-AN-v01_00 EN.pdf?fileId=db3a30433a047ba0013a4a60e3be64a1.

[33] Fairchild, "Half-Bridge LLC Resonant Converter Design Using FSFR-Series Fairchild Power Switch (FPS™)" Appl. Note AN-4151.

[34] M. Li, Z. Ouyang, and M. Andersen, "High Frequency LLC Resonant Converter with Magnetic Shunt Integrated Planar Transformer", IEEE Trans. on Power Electronics, May, 2018.

[35] Z. Ouyang, J. Zhang, and W. Hurley, "Calculation of Leakage Inductance for High Frequency Transformers", IEEE Trans. on Power Electron., Vol. 30, Issue: 10, Oct. 2015.

Chapter 6: Conclusion

6.1 Summary of each Chapter

In order to address the global environmental concerns, societies are now turning towards “transportation electrifications” to reduce the Co_2 emissions. The implementation of EV and MEA involves usage of several power electronics components. Specifically, DC-DC converters. In this kind of converters, it is necessary to keep high-power density and high-efficiency. The circuit topology under in this study is the LLC resonant converter which can guarantee high-efficiency at high frequency due to the soft switching operation. Furthermore, integrated magnetics was applied on the three-phase topology to downsize the passive components. The current unbalance in the three-phase topology was tackled as well. Furthermore, the effects of the secondary leakage inductance were investigated. The conclusion of each chapter is as follow:

In chapter 2 a Lagrangian dynamics based model of the integrated transformer incorporated in three-phase LLC converter is proposed. The Lagrangian formulation leads to an equivalent model of a three-discrete transformers, with three independent magnetic cores. The Lagrangian dynamics has been proven effective to simplify complicated magnetic structures.

In Chapter 3, a three-phase LLC resonant converter with a three-phase integrated transformer is proposed. The proposed magnetic core is commercially available and easy to be implemented. The integrated transformer attains a 43% volume reduction, 28% weight reduction and an approximate of 16% cost reduction, compared with the three-discrete transformer topology. Furthermore, it has been proven to be efficient and has a uniform thermal distribution along the magnetic core. The proposed integrated transformer topology would be highly beneficial in high-frequency applications, in which keeping the core loss at a minimal value is hard to realize. The FEA simulation and Experimental tests showed a proper operation of the integrated transformer. I believe that the merits of the integrated transformer reported in this study would promote the industrial applications of the three-phase LLC resonant converter topologies. Chapter 4 deals with the unbalanced current that arises in the three-phase topology. A balancing transformer has been proposed to compensate the unbalanced current, which arises from the uneven phase parameters. The basic principle of the balancing transformer is based on Ampere’s law, by forcing the sum of the three resonant currents to zero. Beside the leakage and magnetizing inductances, further unbalance evaluation has been performed under a harsh unbalancing conditions, considering uneven values of 1) Resonant capacitors. 2) Transistor on-resistance. 3) Propagation delay of the gate drivers. The proposed balancing transformer has been proved effective and the it is concluded that connecting the integrated transformer in a star provides the best current balance performance because it acts as an ideal balancing transformer. Nonetheless, utilizing a balance transformer might be a solution for other multi-phase topologies where realizing a star connection is not feasible.

Furthermore, utilizing a current balance transformer keeps the interleaving topology of the converter simple, and it allows the traditional phase-shedding to be easily implemented.

In chapter 5, the effects of the secondary leakage inductance on the operation of the LLC converter is investigated. The unbalanced magnetic leakage distribution in the transformer primary and secondary sides can be realized by allocating the primary winding in the vicinity of the air gap and placing the secondary winding in a close contact with the magnetic core to minimize the magnetic leakage flux originated from the primary winding and maximize the leakage flux originated from the secondary. Noise absorber can be used to slightly alter the leakage inductance value. It has been reported that a transformer structure with a concentrated value of leakage inductance on secondary side realizes a higher transformer voltage gain and efficiency. The theory behind realizing efficiency improvement is that the proposed structure eliminates the primary leakage inductance and it has a concentrated leakage on the secondary side. As a result, the voltage drop on the primary leakage inductance due to magnetizing current (i_m) could be eliminated. Furthermore, the secondary leakage inductance expands the voltage gain curve of the LLC converter which results in a higher frequency control bandwidth with respect to the load variation.

6.2 Overall Contribution of Thesis

Compared with the existing technology in the three-phase LLC resonant converter, for example in TESLA Model 3, the DC/DC converter implement three discrete transformers and a control based technique to counter the current unbalance. This thesis addresses the challenges of magnetics in the LLC resonant converter. With the academic contribution in this thesis, the cost and footprints of the magnetics can be reduced by applying the integrated transformer, and the proposed balancing transformer can replace the complicated control circuits to tackle the current unbalance in the three-phase topology. Furthermore, the efficiency can be improved with proper design of the secondary leakage inductance.

This thesis will help the industry engineers and power electronics researchers to design an LLC resonant converter with high-efficiency, high-power density and reduce the cost for the isolated converter used in EVs and MEA.

6.3 Future Challenges

The future trend in the isolated DC/DC converter is that higher power will be needed to satisfy the constant growth in the electric loads of the EV auxiliary systems. As shown in Fig. 6.1, the current output power for the isolated converter is around 1.6 kW. These loads are expected to be doubled with few decades to cater the constant increment in the electric loads. Nonetheless, it will be a future challenge to realize high-power density in these isolated DC/DC converters. Utilizing the magnetic integration methods proposed in this thesis will help to reduce the cost and footprints of the converter's magnetics in the future.

As for future works, it will be interested to investigate the effects of the secondary leakage inductance in a multi-phase integrated

magnetic structure. The effects of the secondary leakage inductance presented in this thesis was tested on a single phase circuit topology. However, it is very important to investigate the effects in different coupled magnetic component structures. Also it will be very beneficial to apply synchronous rectification to further improve the efficiency of the LLC resonant converter.

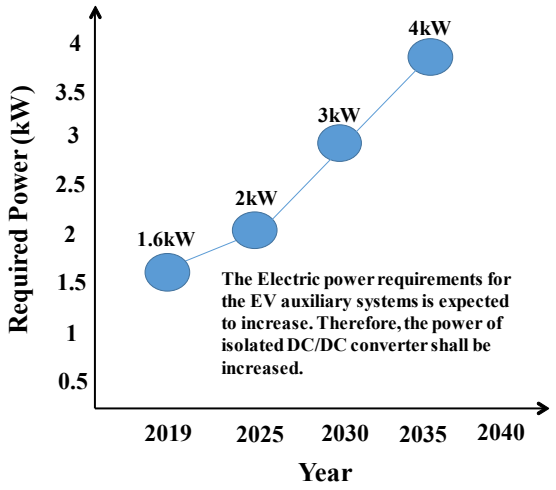

Fig. 6.1 Trend in the power requirement in Future isolated DC/DC converters for EVs

List of Publications

Peer Reviewed Journal Publications (First Author):

1. **Mostafa Noah,** Tomohide Shirakawa, Kazuhiro Umetani, Jun Imaoka, Masayoshi Yamamoto, and Eiji Hiraki "Effects of the Secondary Leakage Inductance on the LLC Resonant Converter", *IEEE Transactions on Power Electronics*, (*Accepted – Early access*).

2. **Mostafa Noah**, Shota Kimura, Jun Imaoka, Wilmar Martinez, Shun Endo, Masayoshi Yamamoto, and Kazuhiro Umetani, "Magnetic Design and Experimental Evaluation of a Commercially Available Single Integrated Transformer in Three-phase LLC Resonant Converter" *IEEE Transactions on Industry Applications, Volume: 54, Issue:6, Page:6190-6204, November/December 2018*.

3. **Mostafa Noah,** Shun Endo, Hiroki Ishibashi, Kimihiro Nanamori, Jun Imaoka, Kazuhiro Umetani, and Masayoshi Yamamoto, "A Current Sharing Method Utilizing Balancing Transformer for a Multiphase LLC Resonant Converter with Integrated Magnetics" *IEEE Journal of Emerging and Selected Topics on Power Electronics, Volume: 6, Issue:2, Page:977-992, June 2018*.

4. **Mostafa Noah,** Kazuhiro Umetani, Jun Imaoka, and Masayoshi Yamamoto, "Lagrangian Dynamics Model and Practical Implementation of an Integrated transformer in Multi-phase LLC Resonant Converter" *IET Power Electronics Volume:11, issue:2, Page:339-347, February 2018.*

5. **Mostafa Noah,** Kazuhiro Umetani, Jun Imaoka, and Masayoshi Yamamoto, "Winding Orientation Method to Minimise the Secondary Leakage of a Gapped Transformer Utilised in LLC Resonant Converter" *IET Electronics Letters, Volume:54, Issue:3, Page:157-159, February 2018.*

Peer Reviewed International Conference (First Author):

1. **Mostafa Noah,** Tomohide Shirakawa, Kazuhiro Umetani, Jun Imaoka, Masayoshi Yamamoto, and Eiji Hiraki, "Effects of Secondary Leakage Inductance on the LLC Resonant Converter-Part I: Transformer Voltage Gain and Efficiency", *34th Annual IEEE Applied Power Electronics Conference & Exposition (APEC 2019), Anaheim, California, USA, March 17-21, 2019.*

2. **Mostafa Noah,** Tomohide Shirakawa, Kazuhiro Umetani, Jun Imaoka, Masayoshi Yamamoto, and Eiji Hiraki, "Effects of Secondary Leakage Inductance on the LLC Resonant Converter-Part II: Frequency Control Bandwidth with respect to Load Variation", *34th Annual IEEE Applied Power Electronics Conference & Exposition (APEC 2019), Anaheim, California, USA, March 17-21, 2019.*

3. **Mostafa Noah,** Jun Imaoka, Yuki Ishikura, Kazuhiro Umetani, and Masayoshi Yamamoto, "Review of Current Balance Mechanism in Multiphase LLC Resonant Converters", *in Proc. IEEE International Symposium on Industrial Electronics (ISIE 2018), Cairns, Australia, June 2018*.

4. **Mostafa Noah,** Kazuhiro Umetani, Shun Endo, Hiroki Ishibashi, Masayoshi Yamamoto and Jun Imaoka, "A Lagrangian Dynamics Model of Integrated Transformer Incorporated in a Multi-phase LLC Resonant Converter", *in Proc. IEEE Energy Conversion Congress & Exposition (ECCE), Cincinnati, USA, Oct. 2017*.

5. **Mostafa Noah**, Shun Endo, Shota Kimura, Masayoshi Yamamoto, Jun Imaoka, Kazuhiro Umetani and Eiji Hiraki "An Investigation into a Slight-Variation of the Transformer Effective Permeability in LLC Resonant Converter" *Record of IEEE 19th Conference on Power Electronics and Applications, EPE'17-ECCE Europe, Warsaw, Poland, Sep. 2017*.

6. **Mostafa Noah**, Shota Kimura, Shun Endo, Masayoshi Yamamoto, Jun Imaoka, Kazuhiro Umetani and Wilmar Martinez, "A Novel Three-phase LLC Resonant Converter with Integrated Magnetics for Lower Turn-off Losses and Higher Power Density" *Proceedings of the IEEE Applied Power Electronics Conference and Exposition (APEC), Tampa, FL, USA, pp. 1-8,* March, 2017.

Peer Reviewed Journal Publications (Co-author):

1. Jun Imaoka, Kenkichiro Okamoto, Masahito Shoyama, Yuki Ishikura, **Mostafa Noah,** and Masayoshi Yamamoto, "Modelling, Magnetic Design, Simulation Methods, and Experimental Evaluation of Various Powder Cores Used in Power Converters Considering Their DC Superimposition Characteristics", IEEE Transactions on Power Electronics, Volume: 34, Issue:9, Page:9033-9051, Sep. 2019.

2. Yuki Ishikura, Jun Imaoka, **Mostafa Noah,** and Masayoshi Yamamoto, "An Improved Core Loss Calculation Method Considering the non-uniform Distribution of Magnetic Flux Density in Powder Cores" IET Power Electronics Volume:12, issue:6, Page:1393-1399, May 2019.

3. Yuki Ishikura, Jun Imaoka, **Mostafa Noah**, and Masayoshi Yamamoto, "Comparative Evaluation of Electrical and Calorimetric Methods to Estimate Core Loss in Powder Cores" *IEEJ Transactions on Industry Applications, Volume 8, Issue 3, Page: 386-393, May 2019.*

4. Jun Imaoka, Kenkichiro Okamoto, Shota Kimura, **Mostafa Noah,** Wilmar Martinez, Masayoshi Yamamoto, and Masahito Shoyama, "A Magnetic Design Method Considering DC Biased Magnetization for Integrated Magnetic Components Used in Multi-Phase Boost Converters" *IEEE Transactions on Power Electronics, Volume: 33, Issue:4, Page:3346-3362, April 2018.*

Peer Reviewed International Conference (Co-author):

1. Jun Imaoka, Yuki Ishikura, Koichiro Ito, Tatsuya Aoki, **Mostafa Noah**, and Masayoshi Yamamoto "Magnetic Design Method for Multi-Material Powder Core Inductor to Improve Efficiency of Bidirectional DC/DC Converter within Wide Load Range", *in Proc. 10th International Conference on Power Electronics ECCE Asia (ICPE2019), pp. 1-8, Busan, Korea, May 2019.*

2. Hongjing Zhang, Jun Imaoka, **Mostafa Noah**, Yuki Ishikura, and Masayoshi Yamamoto "Study on the Imbalanced Voltage of Series-Connected Active Power Semiconductor Devices in Power Conversion Systems", *in Proc. IEEE Workshop on Wide Bandgap Power Devices and Applications in Asia (WiPDA-Asia 2019), pp. 1-5, Taiwan, May, 2019.*

3. Yuki Ishikura, Jun Imaoka, **Mostafa Noah,** and Masayoshi Yamamoto "Bidirectional Converter with Balancing Capacitor using Multi-stage FET Driving Technique*", in Proc. the 3rd IEEE ICDCM 2019 International Conference on DC Microgrids, pp. 1-5, Shimane, Japan, May, 2019.*

4. Tengfei Ou, **Mostafa Noah,** Koichi Morita, Mamoru Tsuruya, Seiji Namiki, Jun Imaoka, and Masayoshi Yamamoto, "A Novel Transformer Structure used in 1.4 MHz LLC Resonant Converter with GaNFETS", *in 2nd IEEE International Power Electronics and Application Conference and Exposition (PEAC 2018), Shenzhen, China, November 4-7, 2018.*

5. Jun Imaoka, Kenkichiro Okamoto, Masahito Shoyama, Yuki Ishikura, **Mostafa Noah,** and Masayoshi Yamamoto, "Modelling, Magnetic Design, and Simulation Methods considering dc superimposition Characteristics of Powder Cores used in Power Converters", *in Proc. IEEE International Power Electronics Conference (IPEC 2018), Niigata, Japan, May. 2018.*

6. Yuki Ishikura, Jun Imaoka, **Mostafa Noah,** and Masayoshi Yamamoto, "Core Loss Evaluation in Powder Cores: A Comparative Comparison between Electrical and Calorimetric Methods", *in Proc. IEEE International Power Electronics Conference (IPEC 2018), Niigata, Japan, May. 2018.*

7. Daigoro Ebisumoto, Shota Kimura, Kimihiro Nanamori, **Mostafa Noah,** Jun Imaoka, Masataka Ishihara, and Masayoshi Yamamoto, "Analytical Investigation of Interleaved DC-DC Converter using Closed Coupled Inductor with Phase Drive Control", *in Proc. IEEE International Communication Energy Conference (INTELEC 2017), Gold Coast, Australia, Oct. 2017.*

8. Jun Imaoka, Kenkichiro Okamoto, Masahito Shoyama, **Mostafa Noah,** Shota Kimura, and Masayoshi Yamamoto, "A High-Reliable Magnetic Design Method for Three-Phase Coupled Inductor used in Interleaved Multi-Phase Boost Converter", *in Proc. IEEE Energy Conversion Congress & Exposition (ECCE), Cincinnati, USA, Oct. 2017.*

9. Thai Hoang Chuong, Shota Kimura, Daigoro Ebisumoto, **Mostafa Noah,** Masayoshi Yamamoto, Masataka Ishihara, and Jun Imaoka, "Magnetic Structure of Close-Coupled Inductors to Improve the Thermal Handling Capability in Interleaved DC-DC Converter", *in Proc. IEEE Energy Conversion Congress & Exposition (ECCE), Cincinnati, USA, Oct. 2017.*